HIGH-THROUGHPUT METHODS FOR PHENOTYPING EPICUTICULAR WAX AND GRAIN YIELD IN WHEAT

A Dissertation

by

FATIMA DEL ROSARIO CAMARILLO CASTILLO

Submitted to the Office of Graduate and Professional Studies of
Texas A&M University
in partial fulfillment of the requirements for the degree of

DOCTOR OF PHILOSOPHY

Chair of Committee,	Dirk B. Hays
Committee Members,	Matthew P. Reynolds
	Nithya Rajan
	Amir Ibrahim
Head of Department,	David Baltensperger

August 2017

Major Subject: Plant Breeding

ABSTRACT

The increasing demand of wheat and the incidence of extreme weather events demand the development of high yielding wheat cultivars with resilience to extreme heat events. Photoprotective traits, as cuticular waxes, support the plant to maintain the photosynthetic activity, decrease stomatal water loss and regulate the plant's internal temperature under extreme abiotic stress. The work described in this dissertation aims to develop new tools for phenotyping epicuticular wax and grain yields that can potentially contribute to accelerate the genetic gain of wheat to fulfill the demand of this economically important cereal by 2050. The objectives of this study were; i) to understand the role of leaf EW as a photoprotective mechanism for adaptation, ii) develop reliable and efficient indirect selection methodologies for the accurate estimation of EW content, and iii) define selection indices for indirect estimation of GG of GY under heat stress environments incorporating the spectral response of the plant.

For the first objective, a set of RIL's was evaluated under controlled conditions. The light reflectance of wavelength at the visible region were highly associated with EW. For the estimation of EW with a leaf clip spectroradiometer, three empirical spectral indices were developed: $EWI\text{-}1_{Blue/Red}$, $EWI\text{-}2_{Blue/NIR}$, $EWI\text{-}15_{625\ (1/736\ -\ 1/832)}$ and $EWI\text{-}16_{(625\text{-}736)\ /\ 832}$. Two additional linear models are also proposed, the *Model-10* and *Model-11*. For the second objective, a set of spring wheat landraces and product of interspecific hybridization was evaluated under severe heat stress conditions. The canopy reflectance of the NIR and SWIR was highly associated with the EW load of the

flag leaves. For field phenotyping, the spectral indices *DIB-2*, *DIB-3*, and the linear model *MB-DI-2* provided a reliable indirect estimation of the EW content in leaves. And for the last objective, the canopy reflectance obtained in the second study was evaluated for indirect selection of the GG of the wheat genotypes. Indirect selection with the Smith/Hazel index did not provide any additional GG when the components of GY were incorporated. The best parameters for indirect selection based on indices were BIO; the broadband vegetation indices ARI, ReCl, NDII, SAVI, GRVI and TDVI; and the narrow band vegetation index NDVI.

ACKNOWLEDGEMENTS

I would like to express my deepest gratitude to my advisor, Dr. Dirk B. Hays, for his guidance and encouragement for doing research. I would also like to thank Dr. Matthew P. Reynolds for letting me gain experience in plant physiology and breeding during my stay at CIMMYT-Mexico. To the members of my dissertation committee, Dr. Nithya Rajan and Dr. Amir Ibrahim, I thank you for your contributions and support during the development of this project.

To my friends and colleagues, Maria Tattaris, Suchismita Mondal, Trevis Hugging and Alfredo Delgado for being always willing to help and give me their best suggestions for this project. I appreciate the help and support that I received to conduct this study from the Wheat Physiology team at the CENEB research station in Ciudad Obregon, Sonora, Mexico. I would also like to thank my parents, family and friends who were always supporting and encouraging me to successfully conclude this project.

CONTRIBUTORS AND FUNDING SOURCES

Contributors

This dissertation was supervised by the committee chair, Dr. Dirk B. Hays, and the committee members Drs. Nithya Rajan and Amir Ibrahim from the Departments of Soil and Crop Sciences, as well as Dr. Matthew P. Reynolds from CIMMYT-Mexico.

The data presented in this dissertation were obtained independently by the student, under the supervision of the committee chair, Dr. Dirk B. Hays, in collaboration with the Wheat Physiology group at CIMMYT-Mexico, and the Aerial Application Technology department of USDA in College Station, Texas.

Founding Sources

This work was supported with the scholarship provided by the National Council of Science and Technology in Mexico. Additional funds were provided by CIMMYT-Mexico through the Sustainable Modernization of Traditional Agriculture Program (MasAgro) to partially cover the stipend of the student and expenses related to this research.

NOMENCLATURE

EW	Epicuticular wax
SRI	Spectral reflectance indices
VI	Vegetation index
NIR	Near infrared region
VIS	Visible region
SWIR	Short wave infrared region
PLSR	Partial leas square regression
SPLSR	Sparse partial least square regression
PAR	Photosynthetic active radiation
RMSE	Root mean square error
RMSEP	Root mean square error of the predictor
DER	Derivative response
GY	Grain yield
BIO	Biomass
SNO	Spikes number m^{-2}
GNO	Grain number m^{-2}
TKW	Thousand kernel weight
SR	Simple ratio
NDI	Normalized difference index
DI	Difference index

LOOCV	Leaving one out cross validation
SR’s	Spectral regions
VI’s	Vegetation indices
S/H	Smith-Hazel selection index
RIL’s	Recombinant inbreed lines
GG	Genetic gain
CIMMYT	International Maize and Wheat Improvement Center

TABLE OF CONTENTS

Page

LIST OF FIGURES

Page

LIST OF TABLES

Page

CHAPTER I

INTRODUCTION AND LITERATURE REVIEW

Wheat (*Triticumm aestivum* L.) is one of the most wide spread cereals in terms of area planted, with a global production of 753 million metric tons (FAO 2016). By 2050, the global wheat production will have to increase by 60-110% to fulfill the demand of the increasing population (Tilman et al. 2011). The actual increment of grain yield (GY) per year is not superior to 0.9%, but to ensure the necessary wheat production by 2050, GY must reach an annual gain of 2.4% (Ray et al. 2013). The scientific community agree that any advance of the current GY will secure a sustainable supply of wheat in the next few decades (Foley et al. 2011).

According to the Intergovernmental Panel on Climate Change (IPCC, 2013), the atmospheric CO_2 levels will double by the end of the century, rising the global temperature and significantly reducing precipitation. Climate change has a direct impact on crop production systems. These extreme events are already causing large reductions in the yield of cereals (Fontana et al. 2015). Temperatures superior to 34 ºC during the reproductive stage can decrease the production of wheat by 50% (Asseng, Foster, and Turner 2011). To cope these effects, it's necessary to develop wheat cultivars with resilience to climate change.

The increase of the productivity of wheat has been the result of the development of varieties with dwarf stature, increased yield and resistance to biotic and abiotic stress. Selection based on plant physiological and morphological traits associated to heat and

drought stress can increase the actual the genetic gain (Reynolds et al. 2011). Selection and strategic crossing of wheat genotypes with complementary physiological traits can enhance radiation use efficiency (RUE) and harvest index (HI), which are major drivers of GY (Reynolds and Langridge 2016). However, improvement base on these traits heavily depends on direct phenotyping. The new generation of plant phenotyping and molecular technologies promises to increase the genetic gain of grain yield, but the most recent advances in phenomics remain empirical rather than analytical compared to genomics. Proximal remote sensing provides a rapid and non-destructive estimations of plant characteristics (Araus and Cairns 2014) facilitating the screening of a large number of progeny from breeding populations and germplasm (Reynolds et al. 2015).

1.1 High temperature stress on crop development and grain yield

Extreme high temperatures limit the growth and productivity of major crops, including wheat. A typical increase of 10-15 °C above the optimum growth conditions is considered as heat stress (Porter and Gawith 1999). Extended periods of exposure to high temperatures during the reproductive stage directly affect the number of grains and dry weight (Wollenweber, Porter, and Schellberg 2003). It has been estimated that temperatures higher that 34 °C during grain filling can reduce ~0.2 ton of grain yield per every day of exposure to these conditions (Asseng, Foster, and Turner 2011).

Photosynthesis is the most sensitive physiological process to heat stress (Wardlaw 1994). The decrease in the photosynthetic rate is strongly associated with the increase in plant photorespiration (Ogren 1984) and the reduction of grain yield (Blum et al. 1994). At molecular level, heat stress affects the activity of Rubisco (Salvucci and Crafts-

Brandner 2004), decreases the efficiency of the photosystem II (Nash, Miyaio, and Murata 1985), and inhibits the biosynthesis of chlorophyll (Tewari and Tripathy 1998). During anthesis, heat stress induces pollen sterility leading to floral abortion and decreasing seeds number per plant (Wardlaw 1994).

1.2 Physiological and morphological traits associated to heat stress

Wheat is particularly sensitive to heat and drought stress. Plants respond to this genotype by environment interactions by modifying stress-adaptive traits for light interception, water uptake and use efficiency, and harvest index (Reynolds et al. 2007). This physiological response can be exploited to improve the tolerance of wheat cultivars, but these morphological and physiological traits must be highly heritable and strongly associated to grain yield (Edmeades et al. 2001). Some potential traits for screening are photosynthesis rate, membrane stability, leaf chlorophyll content, flag-leaf stomatal conductance (Reynolds et al. 1994), canopy temperature depression (Shanahan et al. 1990), (Blum, Klueva, and Nguyen 2001), early heading, stay-green, and cuticular waxes (Reynolds et al. 2015). Integrative traits that increase albedo or that reflects excess photosynthetic and infrared radiation directly contribute to an increased heat load and unnecessary evaporative cooling (i.e. water loss).

Leaf cuticular waxes coat the leaves and stems limiting water lost and reflecting excess photosynthetic and non-photosynthetic light. Epicuticular wax (EW) is the outer lipophilic structure deposited onto the side of epidermal cell (Shepherd and Wynne 2006), composed by long chain aliphatic molecules (hydrocarbons as esters, alcohols, fatty acids, and aldehydes) fixed to a layer of polymer cutin (Buschhaus and Jetter

2011). This cuticle is an adaptive response to water stress that prevents plants from desiccation. Stress-resilient plants, adapted to arid conditions, tend to have a ticker layer of wax compared to plants from more temperate locations. Through the optimization of this cuticle, plants prevent water loss by the cuticular route. Reflective leaf hairs and waxes maintain a temperate canopy and cellular environment, reducing unnecessary water loss, enzymatic denaturation and membrane oxidation (Shepherd and Wynne 2006). EW is critical to dissipate albedo/heat during high light intensity, regulating the plant temperature (Mondal et al. 2014) and evaporative cooling based water loss. It is estimated that the optimization of this cuticle can potentially reduce water loss as much as 31,000 liters/acre, or 1/3 inch of rain/irrigation water per day (Richards, Rawson, and Johnson 1986). At physiological level, the regulation in the excess of light by the epicuticular wax might reduce the risk of over-excitation of PSII and prevent photo oxidative damage (Robinson 1993).

1.3 The influence of epicuticular wax on plant-light interactions

As a photoprotective layer, EW is associated with an increase in light reflectance at the photosynthetic active radiation region (PAR) (Johnson, Richards, and Turner 1983), a decrease in the light transmitted through the mesophyll cells (Johnson, Richards, and Turner 1983) reduction in the absorbed light at the near-infrared region (NIR) (Cameron, 1970; Eller, 1979). Short wavelength energy is also highly affected by the presence of waxes, mutagenic UV light (~ 330 nm) and the PAR (680 nm) reflectance significantly increase in waxy leaves (Holmes and Keiller 2002). A reduction in reflectance by cuticular waxes for *E. cinerea* at the 270-500 nm, and for *E. gunni* at the PAR suggest

that light reflectance interactions are very specific to plant species (Johnson, Richards, and Turner 1983). EW has also a marked effect on total reflectance, strongly influencing reflectivity and dissipates albedo/heat during high light intensity. Significant increases in the percentage of light reflectance have been attributed to the only presence of EW (Johnson, Richards, and Turner 1983). Waxy leaves are normally very reflective of UV (330 nm) and photosynthetic (680 nm) light (Holmes and Keiller 2002), which protects against the damage by UV radiation. However, the key reflectance event by EW is at the near-infrared (NIR) wavelengths (Caldwell *et al.,* 1983; Ellen, 1979; Cameron, 1970). The reduction in energy abortion at this NIR decreases plant temperature (Richards, Rawson, and Johnson 1986), transpiration (Shepherd and Wynne 2006) and prevents nonphotochemical quenching by blocking the heat that would otherwise reach the tissue. Overall, waxy leaves reflect more energy that protects the photosynthetic machinery, and represent a selective advantage in environment where the solar radiation is intense or of long duration.

1.4 High-throughput phenotyping for crop improvement

The application of remote sensing approaches has enabled advances in plant phenotyping, facilitating plant characterization and indirect selection of complex traits**.** Spectral information enables the characterization of chlorophyll, carotenoids and water content in plants by detecting the light reflected across the whole electromagnetic spectrum. Structural, physiological and biochemical characteristics are phenotyped by transforming this spectral response into simple mathematical combination or vegetation indices. Through the integration of the plant spectral response under different water

regimens, it has been possible to predict 40% of the genetic variation of corn grain yield (Weber et al. 2012).

Although major advances in molecular breeding and statistical techniques have enabled selection base on genotypic data, there still a need for phenotypic information. The ultimate goal of phenotyping platforms is the rapid, accurate and simultaneous characterization of large numbers of genotypes at low cost. The acquisition of hyperspectral information enables the assessment of complex traits by obtain hundreds of spectral bands from the near-infrared (NIR), the visible (VIS), and the short-wave infrared region (SWIR) of the electromagnetic spectrum. Under natural sunlight conditions, hyperspectral sensors capture the light reflected by vegetation, a direct response of the plant physiology. The variation in the light reflected at the VIS region (400-700 nm) directly depends of the light absorbed by chlorophylls and carotenoids, and the NIR (700-1300 nm) is highly influenced by the scattering of the light in leaf tissue (Knippling 1970). Spectral vegetation indices combine reflectance information from the whole spectrum by using simple mathematical formulas to obtain a quantitative estimation of plant characteristics. The Normalized Difference Vegetation Index [NDVI=(NIR-VIS)/(NDVI+VIS)] (Rouse et al. 1974) is a common and widely used index to monitor the greenest of plants. Several other indices have also been developed to phenotype chlorophyll content (Maccioni, Agati, and Mazzinghi 2001, Yu et al. 2012), xanthophyll cycle and chlorophyll fluorescence (Gamon et al. 1990), pigments concentration (Panuelas, Baret, and Fillela 1995)(Blackburn 1998, Merzlyak et al. 1999), anthocyanins (Gitelson, Merzlyak, and Chivkunova 2001, Van den Berg and Perkins

2005, Gitelson, Keydan, and Merzlyak 2006), carotenoids content (Gitelson, Zur, et al. 2002), plant water status (Hunt and Rock 1989), lignin and cellulose (Daughtry 2001), nitrogen (Serrano, Penuelas, and Ustin 2002) and light use efficiency (Gamon, Serrano, and Surfus 1997).

The development of novel remote sensing methodologies for proximal sensing phenotyping promises to transform plant characterization, facilitating the dissection of the genetics of quantitative traits, particularly those related to yield and stress tolerance. Grain yield is a complex trait to be predicted using a single spectroradiometrical index. During the growth and development, the plant will intercept and reflect solar energy, which will provide an indicator of physiological traits that are directly related to grain yield. Integrating the spectral response at the NIR region, (Babar, van Ginkel, et al. 2006) was able to predict up to 75% of the variation of grain yield in wheat. Similarly, applying linear empirical models to predict grain yield using reflectance data collected during anthesis and grain filling, (Hernandez et al. 2015) also estimated grain yield with a prediction accuracy of 77% and 91%. Physiological traits as canopy temperature, water and pigment content, and biomass can be easily estimated using airborne imaging, but still necessary the development of phenotyping approaches for complex traits to screen genetic resources and breeding progeny at large scale.

1.5 Rationale and objectives of the project

High temperature stress causes changes in various physiological and biochemical processes and development of morphological and physiological adaptations. The cuticular waxes are a protective mechanism for heat stress avoidance. In water scarcity

and high temperature environments, this cuticle can provide resilience to maintain high GY. Advances in phenotyping methodologies of this cuticles will facilitate its introgression into elite background, and facilitate the understanding of the molecular and physiological basis of improved adaptation conferred by the presence of this cuticle.

Plants use a small proportion of the light intercepted in the photosynthetic process, and the cuticular waxes have an important role dissipating the excess of light. The central hypothesis of this project is that cuticular waxes on the leaf surface contribute to change the light reflected by the plant and these changes can be statistically associated with quantitative measurements of this cuticle. Additionally, we hypothesize that the spectral response of the plant is linked to major physiological process in the plant, which can be used as a proxy estimator of GY under heat stress environments. The main objective of this study is to advance technologies in precision phenotyping by developing indirect selection methodologies for stress adaptive traits and GY. To accomplish this objective, we have established the following specific objectives: 1) Understand the role of leaf EW as a photoprotective mechanism for adaptation, 2) Develop reliable and efficient indirect selection methodologies for the accurate estimation of EW content, and 3) Define selection indices for indirect estimation of the genetic gain of GY under heat stress environments.

CHAPTER II

NONDESTRUCTIVE METHOD TO ESTIMATE EPICUTICULAR WAX CONTENT IN LEAVES USING HIGH-RESOLUTION SPECTRAL INFORMATION

2.1 Introduction

Cuticular waxes are protective mechanisms that cover plant surfaces to avoid and overcome climatic extremes. This specialized structure plays a key role for adaptation to diverse and extreme environments. Waxes are an exterior lipid coating deposited onto the surface of the epidermal cells, composed of two main lipophilic structures, the cuticular wax and the cutin (Buschhaus and Jetter 2011). Cuticular waxes are a complex mixture of different hydrocarbon chains or ring structures (Walton 1990) embedded (intracuticular wax) and dispersed (epicuticular wax) on top of the polymer cutin. The total load of these two wax structures ranges from the 8 to 40 µg cm^{-2}, of which 20 to 90% corresponds to epicuticular wax (EW) (Buschhaus and Jetter 2011). As the main interface of the plant with the environment, EW prevents non-stomatal and stomatal water loss (Bengtson 1978) and avoids photo oxidative damage by reducing the risk of over-excitation of the PSII (Robinson 1993).

The presence of waxes and leaf hairs directly affects the reflectivity of leaves, modifying the optical characteristics of plant surfaces. In *Eucalyptus* and *Kalanchoe* waxy leaves reflect more light at the 0.33µm and 0.68µm, compared to non-waxy leaves (Holmes and Keiller 2002). However, these plant-light interactions are specific for every

species. For *E. cinereal* and *E.gunni,* the main changes in light reflectance were identified at the 0.27-0.5µm, and at the 0.4-0.5µm in leaves of *K.pumila.* (Shepherd and Wynne 2006). The light dispersed on the surface of the leaves is also affected by the presence of glaucousness, the greyish waxy visible coat of leaves. Glaucous lines of wheat tend to be more reflective at the PAR (photosynthetically active region), compared to non-glaucous lines, and simultaneously decrease ~12% of the light transmitted through the leaf (Johnson, Richards, and Turner 1983). EW dissipates light at the NIR (near infrared region) reducing plant temperatures(Mondal et al. 2014) and reducing unnecessary evaporative cooling (i.e. water loss) (Shepherd and Wynne 2006). If optimized, cuticular waxes can provide adaptability to water limited and high temperature environments and potentially decrease 1/3 inch of rain/irrigation water per day (Richards, Rawson, and Johnson 1986). EW is conventionally extracted by dipping the plant tissue into organic solvents for a short period of time, and quantify using colorimetric methodologies (Ebercon, Blum, and Jordan. 1977). This approach is impractical and costly for screening a large number of wheat genotypes and is limited in allowing multiple stage monitoring of EW during development. In this study, we evaluated the application of high-resolution spectral information as a proxy estimate of the EW load in leaves. Under the assumption that EW modifies the light reflected by the leaf, we aim to identify these specific changes and statistically incorporate them to develop predictors for indirect selection of EW. The results of this study will support ongoing research to understand the physiological and genetical mechanisms of these waxes as an adaptive response to heat and drought stress environments. For wheat

breeding programs, an indirect selection method will facilitate the selection and introgression to accelerate the development of high yielding resilient wheat cultivars to climate change.

2.2 Materials and methods

2.2.1 Plant material and culture

Twenty-four spring wheat recombinant inbred lines (RIL) derived from the cross of the heat tolerant cultivar 'Halberd' and the heat susceptible 'Len' were established under controlled conditions in a plant growth chamber as a completely randomized design with four replications. These genotypes were sown in nursery pots, 18.5 cm in height and 16.2 cm in diameter, filled with the substrate peat moss and fertilized twice during the plant growing period with the standard fertilized 20-20-20. The plants were established in a plant growth chamber programmed with intervals of twelve hours of light and twelve hours of dark. At flowering, plants were separated in two groups. Each group consisted of twenty-four genotypes including two replications, from now on referred as the EW-change and the EW-content group.

2.2.2 Quantification of EW

Samples from flag leaves were collected at 10 to 15 days after pollination (DAP) to quantify EW content. For the genotypes included in the EW-content group, the leaf samples were obtained right after the light reflectance from the adaxial and abaxial side of the leaf was captured. Two samples were obtained from the genotypes included in the EW-change group, one sample from half of the flag leaf before EW was extracted and an additional sample from the remaining half of the leaf after EW was extracted with

chloroform. Every sample consisted of six punches of 1 cm diameter and were collected in 2.0 milliliters (mlL) glass vials. The EW was extracted by emerging the leaf sample for 20 seconds in 1.5 ml of chloroform ($CHCl_3$) at room temperature, and quantified via the colorimetric technique described by (Ebercon, Blum, and Jordan. 1977). A standard curve was developed to transform the absorbance readings at the 590 nanometer (nm) to milligrams (mg) per square decimeter (dm^2) of EW.

2.2.3 Leaf radiometric measurements

All radiometric measurements were obtained with a CI-710 Miniature Leaf Spectrometer from CID Bio-Science. This spectroradiometer captures the spectral information from the 350 to 1050 micrometer (nm). The equipment was calibrated every ten minutes with an integrated BaSO4 reference disk. For the genotypes included in the EW-change group, ten reading of the light reflected, absorbed and transmitted through the leaf were captured from the abaxial and adaxial side before and after EW was removed with HPL chloroform. Light reflectance was the only light interaction recorded from the plants in the EW-content group. The range of all spectral measurements was restricted to 400 - 900 nm to eliminate the noise captured at the ends of the signals, and the spectral resolution was adjusted to 1 nm.

2.2.4 Identification of spectral features associated to EW

The spectral signatures collected after EW was removed were subtracted from the initial readings captured with EW in place. These differences are presented as percentage of change (Fig. 1 and 2). A two samples *t*-test was conducted to statistically assess the spectral response of the visible (400 to 748 nm), the red-edge (691 to 730) and the near

infrared (NIR 751 to 900) regions before and after extraction of EW. The analysis was conducted under the null hypothesis that the difference of the mean spectral response captured with EW in place and the mean spectral response after removal of EW is equal to zero (H_0: $\mu_1 - \mu_2 = 0$). The null hypothesis was tested with the assumption of similar standard deviations: $t = \frac{\overline{x_1} - \overline{x_2}}{s_p\sqrt{\frac{1}{n_1}+\frac{1}{n_2}}}$. In this equation, $\overline{x_1}$ and $\overline{x_2}$ represent the average spectral response with EW in place and after EW wax removed, respectively; s_p corresponds the pooled standard deviation; n_1 and n_2 are the number of observations included per sample. The pooled standard deviation was calculated with the follow equation: $s_p = \sqrt{\frac{(n_1-1)s_1^2+(n_1-1)s_2^2}{n_1+n_2-2}}$, where s_1^2 and s_2^2 are the standard deviation of the sample 1 and 2, n_1 and n_2 are the number of observations included in the mean of every sample. All results were confirmed with the *t.test* function, and the confidence interval estimated with *conf.int* in the statistical software R (R Development Core Team, 2012).

The first derivative of the spectrum was computed to enhanced important spectral feature of the reflectance signatures collected in the EW-content group. This derivative approach estimates the rate of change of the reflectance, absorbance or transmittance with respect to the wavelength and projects the changes in the curvature of the spectrum for a specific interval of the signal. All the spectral derivatives were calculated within a window size of 11 nm using the *savitszkyGolay* function. This function is included in the package *prospect* (Stevens 2014) and applies the Savitzy-Golay filter (Bromba and Ziegler 1981) before the derivative is estimated:

$$x_j * = \frac{1}{N} \sum_{h=-k}^{k} c_h x_j + h$$

In this equation, the x_j* represents the new value obtained after the first derivative was estimated, *N* is a normalizing coefficient, *k* is the number of neighbor values at each side of *j*, and c_h are pre-computed coefficients that depend of the polynomial order and degree. Pearson correlation coefficients were calculated with the *corr* function for the first derivative of the reflectance and EW content.

2.2.5 Partial Least Square (PLSR)

A supervised multivariate model for a training data set was built to predict the variation of EW (*Y*) with the Partial Least Square Regression (PLSR) approach. PLSR is an statistical method that combines the theoritical principles of multiple linear regression and principal component analysis (PCA) to confront situations where there exist several highly correlated predictor variables and relative few samples. This approach decomposes the response variables (*X*) into orthogonal scores (*T)* and loadings (*P*) (Geladi and Kowalski 1986), simultaneously incorporating the information from both variables.

$$\boldsymbol{X = TP' + E}$$

In this study, two hundred spectral bands with 3 nm resolution were incorporated in the analysis to find the set of components that best estimates EW. The RMSE (Root Mean Square Error) was calculated with a leave-one-out cross validation analysis (LOOCV) in a subset of the data that included 66.7% of the observations collected from the EW-

content group. This analysis was performed with the *plsr* function in the package *pls*. EW was estimated for the remaining 33% of the observations (validation set) using the optimum number of factors detected included the PLSR model that were selected based on minimum RMSE values.

2.2.6 Stepwise Regression (SWR)

The spectral bands selected with the derivative analysis and the PLSR were incorporated to build a multivariate model with a semiautomatic proces in which the spectral bands were included and/or removed based on the significance of the partial F-values. The final models were defined when the inclusion of more predictors was not justifiable. All the models were built with the PROC REG statement in the statistical analysis software SAS (Inc. 2011)in a random training data set (60% of the observations). The best models were selected based on their lowest values of the Mallows' Cp estimator and higher coefficient of determination (R^2). In the validation data set (the remaining 40% of the observations), the selection was base on their lowest RMSE.

2.2.7 Narrow and broad empirical spectral indices to estimate EW

All pairwise combinations incorporating the two hundred spectral bands at 3 nm resolution collected in the EW-content data set were estimated for spectral indices as simple ratio ($SR = \frac{R_i}{R_j}$), difference ($DI = R_i - R_j$) and normalized difference ($NDI = \frac{R_i - R_j}{R_j + R_j}$). In these indices, R_i and R_j represent the reflectance values at *i* and *j* nm, respectively. A leaving one out cross validation (LOOCV) analysis was conducted to define the significance of the linear model and estimate the coefficients of determination

(R^2) for EW as independent variable and the spectral indices as dependent variable (*X)*: $y_i = \beta_0 + \beta_1(x_j)$**.** In this equation, y_i corresponds to EW, x_i to the estimated spectral indices, and β_0 and β_1 are the intercept and the slope of the model, respectively. The spectral indices with the highest R^2 values were selected to fit an additional set of linear models for a defined training data set (66% of the observations) to predict every individual spectral index based on EW. These models followed the same linear function, $y_i = \beta_0 + \beta_1(x_i)$, but in this case y_i represents the spectral index and x_i corresponds to the EW content. In order to estimate the ability of the index predicting EW when selection is based on the index per se, the EW variable was solved for the linear models defined in the training data set as follow: $X_i = \frac{y_i - \beta_0}{\beta_i}$. An estimator for the Root Mean Square Error (RMSE) was bootstrapped in the validation data set (34% of the individuals) 1000 times with the function *boot*. The same statistical approach was applied to define narrow band indices associated to EW with the red, green and blue (RGB), near infrared (NIR) and short-wave infrared (SWIR) spectral bands.

2.3 Results

2.3.1 The effect of EW on the plant-light interactions

The variations of the light reflected, transmitted and absorbed by EW are presented in Fig. 1 and 2. These changes are represented as the difference in the spectral response with EW in place minus the spectral response collected after EW was removed with HPTS chloroform ($CHCl_3$). Overall, differences observed for all three light interactions were similar for the abaxial and the adaxial side of the leaf. An increase on the light

reflectance with EW in place was detected, along with a decline of the light transmitted and absorbed through the leaf.

The decrease in the percentage of light reflectance at the photosynthetic active radiation (PAR) when EW is in place enhances the importance of these waxes as a photo protective mechanism under high light intensity conditions. A minimum change in the reflectance at the 710 nm was detected, with an evident increase on the light absorbed and reflected through the leaf. Unlike the rest of the spectrum, the absorbance at the NIR had a similar response to the reflectance. As the EW load increases, the light absorbed at the NIR increases, with a dramatic decline in the transmittance.

The extraction method with HPLC chloroform was validated with electron microscope scanners. In these scanners (Fig. 3) we can observe that a large proportion of the EW deposited on the leaf surface was removed with the chemical method using HPLC chloroform. In general, the chemical removal method resulted to be more efficient that the mechanical removal technique using the adhesive tack.

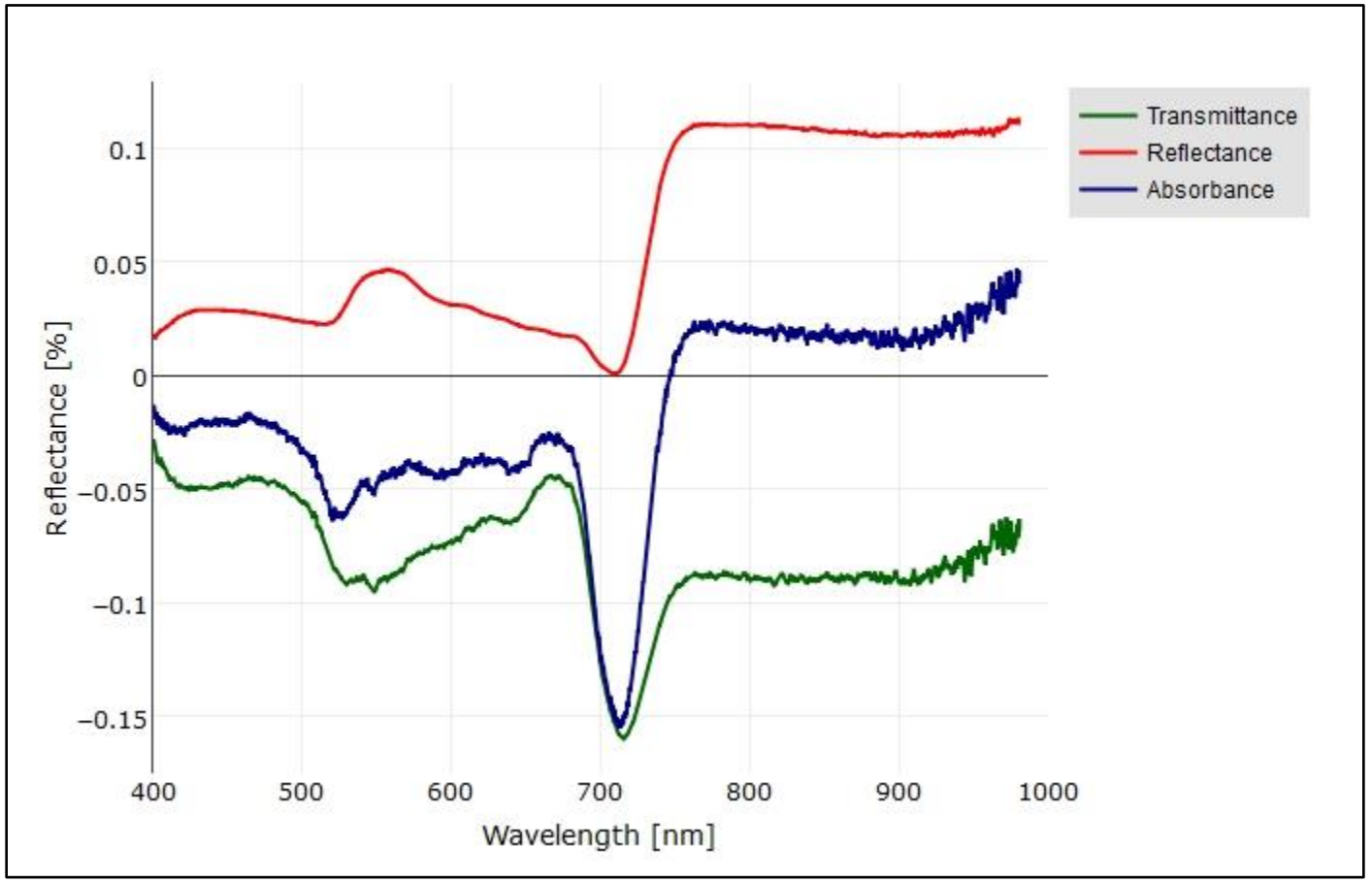

Fig. 1 Associated response of the light reflected, absorbed and transmitted with EW for the abaxial surface of the leaf. The change was estimated by subtracting the spectral response of the leaf with EW in place minus the spectral response after EW was extracted with HPTS chloroform.

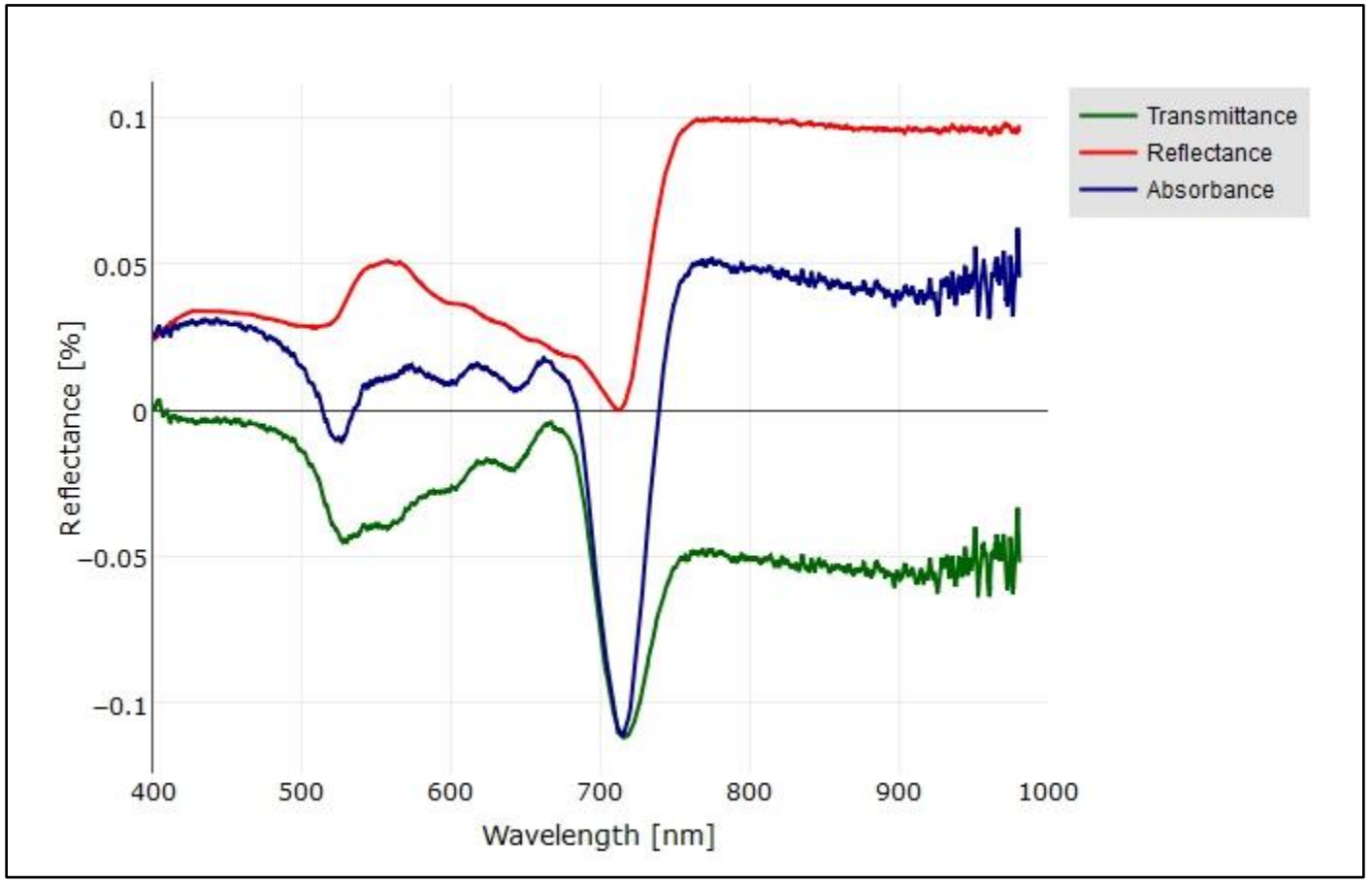

Fig. 2 Associated response of the light reflected, absorbed and transmitted with EW for the adaxial surface of the leaf. The change was estimated by subtracting the spectral response of the leaf with EW in place minus the spectral response after EW was extracted with HPTS chloroform.

Significant differences were detected between the means of the transmittance, reflectance and absorbance of the spectral signatures registered before and after the extraction of EW (Table 1). The response from the adaxial and the abaxial surface of the leaf were similar for all three light interactions. Statistically, the light transmitted through the leaf was affected by the presence of EW at all three main regions of the spectrum: the visible, the Red-edge and the NIR. However, the reflectance at the red-edge was completely insensitive to variations in EW change, while the visible and NIR reflectance decreased after EW was removed. The absorbance at the visible region of the spectrum was not sensitive to variations in EW, but the red-edge and the NIR were highly affected. As the EW is removed, a decrease of the absorbance at the red-edge and an increase at the NIR were detected.

(A) 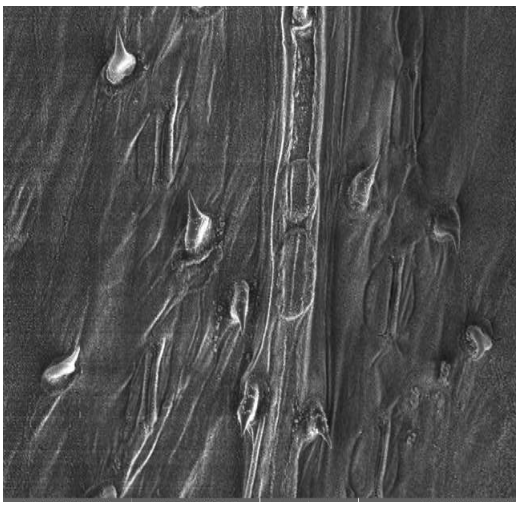 (B) 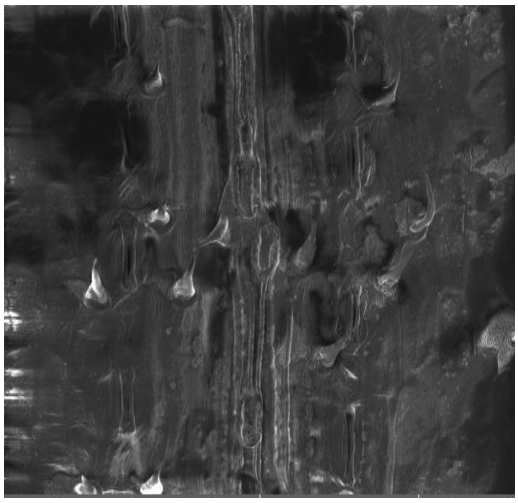

(C) 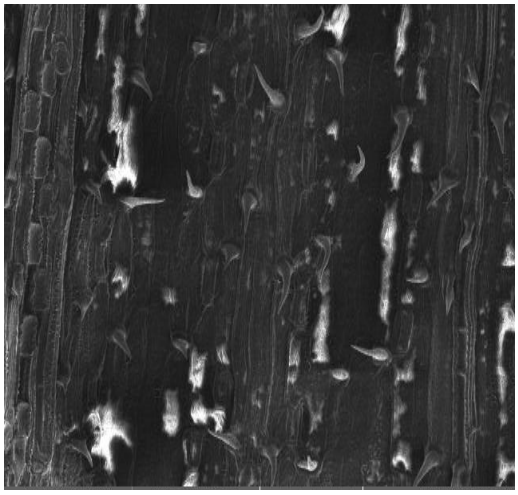

Fig. 3 Leaf surfaces observed with scanner electronic microscopy (SEM) (A) with wax in place, (B) after EW was removed with an adhesive tack, and (C) after EW was extracted with HPLC grade chloroform.

Table 1 Average response of the light reflected, absorbed and transmitted (%) for the visible (0.4 to 0.7 µm), red-edge (0.7-0.73µm) and the NIR (0.7 to 1.0 µm) regions of the spectrum and two samples t-test values comparing the mean of the spectral response before and after extraction of EW for the abaxial and adaxial surface of the leaf.

	Average response (%)					
	Surface of the leaf	Region of the spectrum	SRWEW	SRAEEW	95% CI	p-value
Transmittance	AB	Visible	0.085	0.116	0.006/0.054	0.014
		Red-edge	0.194	0.285	0.037/0.145	<0.001
		NIR	0.482	0.536	0.011/0.095	0.016
	BE	Visible	0.094	0.169	-0.11/0.159	0.085
		Red-edge	0.187	0.325	0.059/0.218	0.002
		NIR	0.467	0.553	0.035/0.139	0.002
Reflectance	AB	Visible	0.103	0.07	-0.043/-0.024	<0.001
		Red-edge	0.187	0.171	-0.033/0.005	0.142
		NIR	0.446	0.347	-0.131/-0.063	<0.001
	BE	Visible	0.093	0.064	-0.039/-0.021	<0.001
		Red-edge	0.173	0.162	-0.033/0.011	0.2908
		NIR	0.429	0.323	-0.151/-0.061	<0.001
Absorbance	AB	Visible	0.812	0.814	-0.023/0.27	0.8655
		Red-edge	0.621	0.551	-0.129/-0.009	0.025
		NIR	0.072	0.114	0.001/0.081	0.045
	BE	Visible	0.811	0.767	-0.129/0.041	0.281
		Red-edge	0.637	0.513	-0.202/-0.047	0.003
		NIR	0.104	0.124	-0.259/0.066	0.378

SRWEW- Spectral response with EW in place SRAEEW- Spectral response after the extraction of EW

2.3.2 Associated response of the light reflectance and EW content

Some of the spectral signatures of light reflectance collected from the EW-content group are presented in Fig. 4. As can be observed, the light reflectance from the adaxial surface of the leaves tends to be higher that the reflectance from the abaxial side. According to their EW content, there are differences between the light reflectance from leaves with high (3.18 and 3.11 mg dm^{-2}) and low (0.94 and 1.28 mg dm^{-2}) content of EW, and these differences are consistent across the entire electromagnetic spectrum.

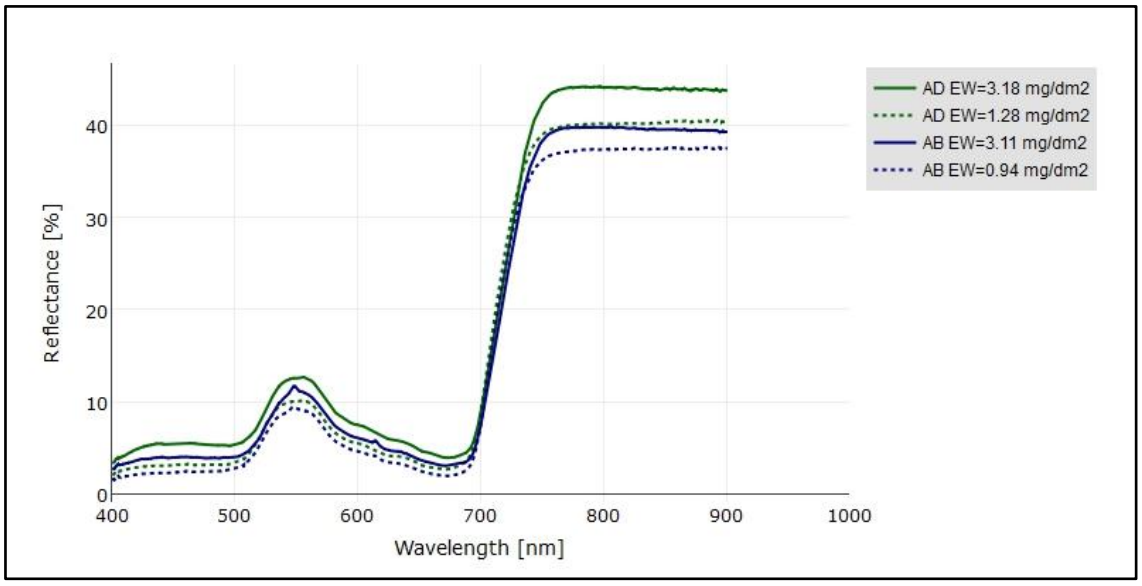

Fig. 4 Percentage of light reflectance for the adaxial (AD) and abaxial (AB) surfaces of the flag leaf and the EW content of the leaf (mg/dm^2).

The Fig. 4 presents the slope of the linear regressions models for the reflectance and EW content (mg dm^{-2}). The estimated rate of change of the light reflected for every unit of EW accumulated in the surface of the leaf varied across the spectrum. For the

visible and NIR, a positive slope is observed with an increase in the light reflectance of 1% and 1.5%, respectively. A large decrease in reflectance of almost 1% by every unit of increase in the EW load occurs at the red-edge.

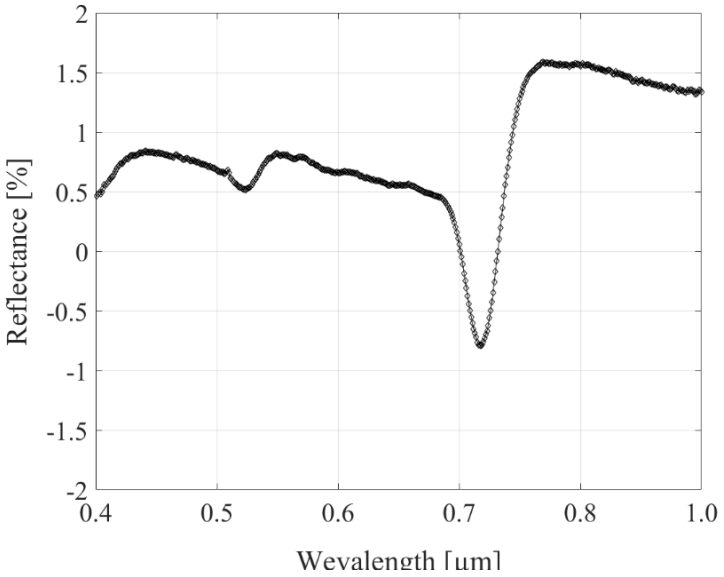

Fig. 5 Slope of the linear regression models for the light reflectance at 1nm resolution and EW content (mg dm^{-2}).

2.3.3 Derivative analysis and partial least square regression (PLSR)

The first derivative of the reflectance effectively enhanced specific changes in the spectral signature, separating the peaks from the overlapping bands. Four main peaks were identified to be highly associated with EW content. The first peak is located at the 480 nm; a second peak at the 560 nm, where the reflectance reached the maximum absorption for the green color; a third peak at the 640 nm, directly associated with the absorption of chlorophyll; and at the NIR region the peak was centered at the 750 nm,

which corresponds to the spectral change where the reflectance starts to increase from the visible to the NIR.

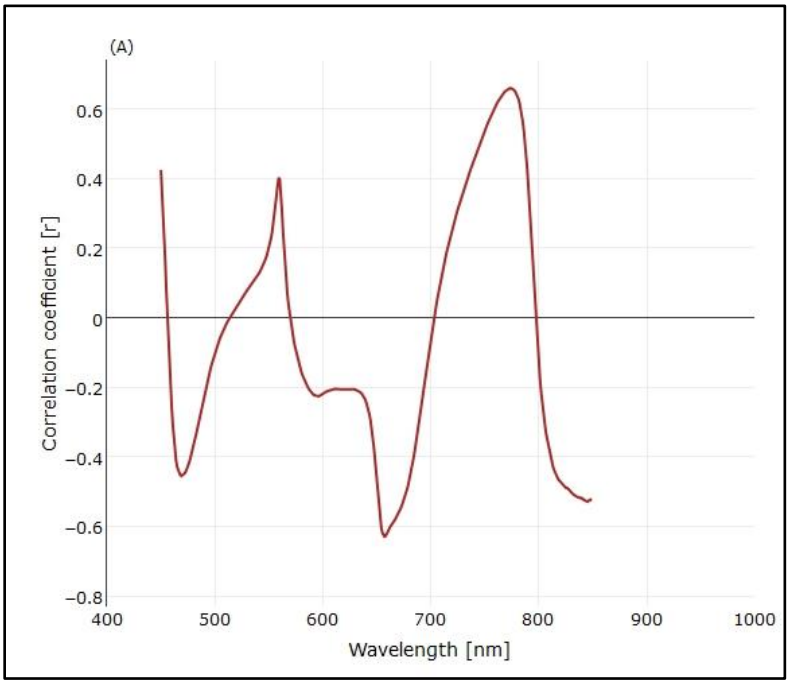

Fig. 6 Pearson correlation coefficients of the first derivative of the reflectance with the content of EW (mg/dm^2).

According to the results obtained from the PLSR analysis, the three main components explain 97.34% of the variability of EW. These components were also selected based on their lowest value of the root mean square error of the prediction (RMSEP). The coefficients included in the model are shown in Fig. 7-A. These coefficients can be directly applied to select relevant predictors according to the magnitude of the absolute value. The EW values for the training data set were predicted by integrating the selected components and the value of the coefficients. A linear relationship between the estimated and predicted values of EW was found (Fig. 7-B).

(A)

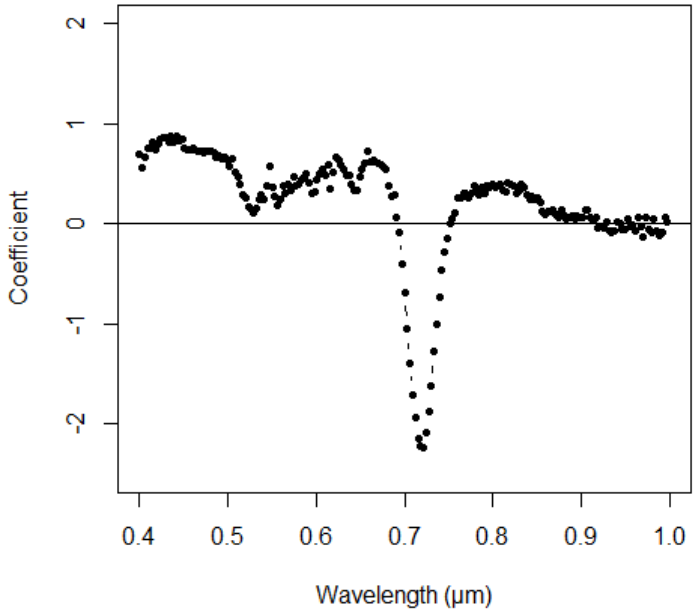

(B)

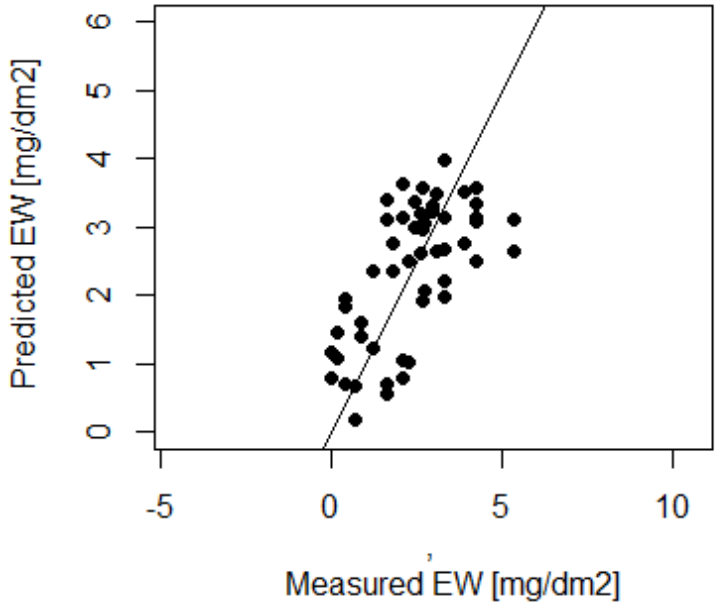

Fig. 7 PLSR coefficients for the three main components that explain 97.34 % of the variability of the EW (A), and estimated values of EW in the training data set incorporating the three main components (B).

2.3.4 Stepwise regression (SWR) for prediction of EW

The spectral bands selected from the derivative and the PLSR analysis were used as explanatory variables to select a set of spectral bands the best predict EW. The spectral bands included are the follow (nm): 520 to 550, 619 to 640, 652 to 670 and 760 to 751. Twelve linear models were statistically associated with EW variation at 1% of probability. According to the R^2 values estimated in the training data set, the developed linear models can predict up to 73% of the EW variation including six spectral bands. The root means square errors (RMSE) estimated in the validation data set were similar, which limited the selection of the models based on this estimator. Overall, the *Model-10* and *Model-11* seems to accurately estimate of the EW load in leaves.

Table 2 Summary of the estimators of the prediction models developed with the stepwise multiple regression (SWR) analysis for the estimation of EW load in leaves.

Model-1	Intercept	670							RMSE	R^2	C(p)
	-0.632	95.37							0.79	0.48	14.62
Model-2	**Intercept**	**670**	**715**								
	1.37	99.49	-9.88						0.75	0.53	10.06
Model-3	**Intercept**	**658**	**670**	**715**							
	1.69	48.18	48.43	-11.78					0.71	0.56	8.39
Model-4	**Intercept**	**658**	**670**	**715**	**751**						
	0.61	56.18	24.13	-16.11	6.09				0.69	0.57	7.54
Model-5	**Intercept**	**658**	**715**	**751**							
	0.59	72.73	-17.39	7.26					0.79	0.57	6.08
Model-6	**Intercept**	**658**	**715**	**721**	**751**						
	1.23	33.54	178.36	-211.93	42.73				0.74	0.67	-2.43
Model-7	**Intercept**	**652**	**658**	**715**	**721**	**751**					
	1.12	-76.29	100.53	220.21	-256.6	50.98			0.72	0.69	-4.68
Model-8	**Intercept**	**652**	**658**	**715**	**721**	**742**	**751**				
	0.91	-110.95	119.26	276.39	-345.22	140.64	-53.26		0.69	0.71	-5.48
Model-9	**Intercept**	**652**	**658**	**715**	**721**	**742**					
	1.001	-95.84	109.77	258.46	-312.18	71.38			0.78	0.71	-6.77
Model-10	**Intercept**	**652**	**658**	**715**	**721**	**742**	**745**				
	0.91	-111.64	123.444	259.35	-324.86	178.09	-96.12		0.74	0.73	-6.48
Model-11	**Intercept**	**523**	**652**	**658**	**715**	**721**	**742**	**745**			
	0.58	-28.63	-85.62	131.39	295.23	-356.80	190.83	-103.51	0.71	0.73	-5.55

2.3.5 Empirical spectral indices for phenotyping EW

Approximately 65% of the EW variation can be estimated with empirical spectral indices. All sixteen narrow band indices reported in Table 3 were selected as candidate indices to estimate EW content based on their RMSE and R^2 values. These indices involved combinations of spectral bands located at the 650, 700 and 830 nm. Most of these bands were previously associated to EW in the derivative analysis and the PLSR. Thus, the first derivative and the PLSR analysis can be an effective approach to eliminate unassociated spectral information to a response variable. Two indices combining the spectral bands at the 625, 736 and 832 nm were identified as best predictors for EW. Incorporating the blue and red bands of the spectrum, broad indices estimate as much as 44% of the EW variation. The NIR region was also associated to EW, but an index that involves this spectral band will be highly sensitive to differences in leaf area when applied for canopy reflectance.

The Figure 8 shows the relationship of three narrow and one broad band index with EW. These indices were selected when light reflectance was captured with an active sensor, and non-additional factors as canopy architecture or light scattering are considered. When the indices were calculated in the validation data set, the values of the indices simultaneously increase with the increase of EW.

Table 3 Spectral indices from the cluster analysis. For the cluster with the higher R2 for the narrow band indices 2sd + mean was used to select the top performance indices. Results from the cross-validation k=10.

Index	Number of clusters		Number of indices in the selected cluster		Values of the R^2	
	N	B	N	B	N	B
$\mathbf{R_i}$	5	3	44	1	0.34-0.47	0.39
$\frac{\mathbf{R_i}}{\mathbf{R_j}}$	5	4	121	2	0.50-0.56	0.34-0.36
$\mathbf{R_r - R_j}$	6	3	58	4	0.38-0.45	0.14-0.16
$\frac{\mathbf{R_i - R_j}}{\mathbf{R_i + R_j}}$	6	5	112	1	0.51-0.54	0.38
$\frac{\mathbf{R_i - R_j}}{(\mathbf{R_i + R_j})^2}$	5	3	144	3	0.48-0.54	0.24-0.4
$\left(\frac{\mathbf{1}}{\mathbf{R_j}}\right) - \left(\frac{\mathbf{1}}{\mathbf{R_j}}\right)$	5	3	195	6	0.48-0.53	0.35-0.39
$\mathbf{R_k}\left[\left(\frac{\mathbf{1}}{\mathbf{R_i}}\right) - \left(\frac{\mathbf{1}}{\mathbf{R_j}}\right)\right]$	6	4	5683	24	0.41-0.65	0.24-0.37
$\frac{\mathbf{R_i - R_j}}{\mathbf{R_k}}$	6	3	3624	18	0.41-0.62	0.33-0.36
$\frac{\mathbf{R_i}}{\mathbf{R_j}^2}$	5	4	142	3	0.47-0.52	0.38-0.4
$\left(\frac{\mathbf{R_i}}{\mathbf{R_j}}\right) - \mathbf{1}$	5	3	80	2	0.51-0.56	0.14-0.16
$\frac{\mathbf{R_i}^2 - \mathbf{R_j}}{\mathbf{R_i} + \mathbf{R_j}^2}$	6	5	44	2	0.50-0.54	0.20-0.23
All the indices were highly significant with p-values <0.0001 N-narrow band indices B-broadband indices						

Table 4 Narrow and broad band indices selected based on their higher R^2 values from the validations data set in the LOOCV and lowest RMSE in the validation set for the bootstrapping analysis.

Bests fitted model parameters						
Index	**a**	**B**	**R^2**	**RMSE (mg/dm^2)**	**95% CI**	**p-value**
Broad indices with two RGB and NIR spectral bands						
EWI-1 $_{Blue/Red}$	0.213	0.04	0.44	1.19	1.037-2.17	<0.0001
EWI-2 $_{Blue/NIR}$	0.07	0.13	0.39	1.18	0.98-1.98	<0.0001
EWI-3 $_{(NIR-Red)/Blue}$	-0.93	0.01	0.31	1.19	1.04-1.97	<0.0001
EWI-4 $_{(Red^2-Blue)/(Red-Blue^2)}$	-0.09	-0.03	0.32	1.19	1.09-2.55	<0.0001
Narrow indices involving one and two spectral bands						
EWI-5 $_{676}$	0.019	0.005	0.45	0.97	0.75-1.21	<0.0001
EWI-6 $_{658/712}$	0.12	0.03	0.52	1.02	0.70-1.36	<0.0001
EWI-7 $_{625/706}$	0.22	0.05	0.50	0.96	0.67-1.28	<0.0001
EWI-8 $_{694/625}$	-0.006	-0.002	0.42	1.08	0.96-1.55	<0.0001
EWI-9 $_{(670-718) / (670+718)}$	-0.85	0.03	0.51	1.04	0.61-1.54	<0.0001
EWI-10 $_{(691-661) / (691+661)^2}$	4.92	-1.03	0.51	0.99	0.74-1.27	<0.0001
EWI-11 $_{(1/661) - (1/694)}$	29.13	-5.73	0.48	1.01	0.71-1.35	<0.0001
EWI-13 $_{(622/718)-1}$	0.62	0.12	0.51	0.99	0.74-1.28	<0.0001
Narrow indices involving three spectral bands						
EWI-15 $_{625\ (1/736\ –\ 1/832)}$	0.008	0.004	0.65	1.01	0.622-1.426	<0.0001
EWI-16 $_{(625-736) / 832}$	0.02	0.007	0.62	0.98	0.65-1.35	<0.0001

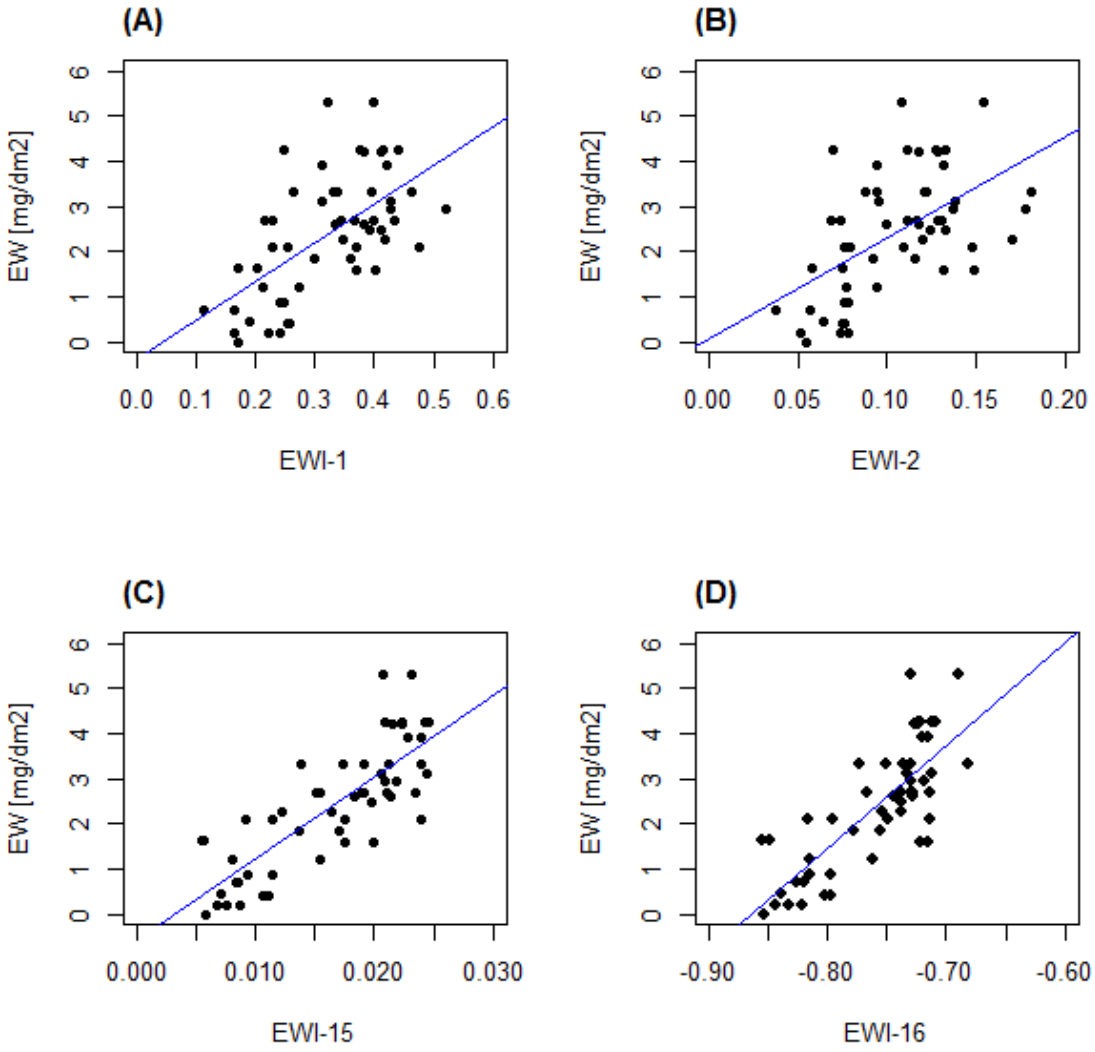

Fig. 8 Relationship between EW and EWI-16 (A), EWI-15 (B), EWI-8 (C) and EWI-4 (D). The solid line indicates the best fitted line in the validation data set.

2.4 Discussion

An increase of the light reflected along with a decrease on the absorbance and transmittance at the PAR was detected with EW in place. The decrease of the absorbance at the PAR is the main impact of this adaptive photoprotective mechanism in the plant. The reduction of the absorbance wavelength longer than 700 nm prevents overheating of the leaf and the possible damage of the tissue. This decline of the light absorbed at the NIR is also linked to a decrease of the vapor pressure differences between the tissue and the air, which can potentially reduce transpiration water lost. The insensitivity of the reflectance at the red edge when EW was extracted was different to the associated response detected with the slopes of the linear models derived from the spectral bands and the EW content. Thus, for every unit of EW (mg/dm^2) accumulated, there was a decrease of ~1% on the light reflected at the red edge region. Light reflectance at the visible and NIR both increase 1% and 2% by every unit of EW ($mg/dm^{2)}$ accumulated, respectively. A similar decrease on the absorbance at the PAR was also linked to the effect of waxes in Scots Pine (*Pinus sylvestris* L.) needles (Olascoaga et al. 2014).

The main peaks detected by the derivative analysis were highly associated with physiological processes and characteristics of plants; carotenoids absorption at the 470 nm, reflectance of the green light at the 550 nm, chlorophyll absorption at the 640 nm and internal heat dissipation at the 780 nm. The linear models developed with the PLSR approach were able to accurately predict EW. However, the large number of spectral bands included as predictors in these models made it difficult for interpretation. The predicted and observed values of EW had a very strong linear relationship, which

demonstrate the power of the PLSR analysis for prediction of morpho-physiological traits integrating the spectral response of the plant. The SWR was implemented to facilitate the interpretation and application for further prediction of EW. With the application of both statistical approaches, the PLSR and SWR, the risk of overfitting the prediction models was minimized. According to the accuracy of the linear models, two linear combinations of spectral bands are proposed, the *Model-10* and the *Model-11*. These models independently estimate ~74 % of the variability of EW with the spectral bands at the 523, 652, 658, 715, 721, 742 and 745 nm.

For the development of the spectral indices, the two hundred spectral bands were incorporated in the analysis. With this approach, approximately 65% of the EW variability can be explained. The best indices incorporate the majority of the spectral band that were already identified by the derivative analysis and the PLSR. The narrow band indices had a higher coefficient of determination, compared to the broadband indices. The broad band spectral index $EWI = \frac{\rho_{Blue}}{\rho_{Red}}$, was the best predictor with a coefficient of determination of 0.44. If the cost of hyperspectral sensors is considered, the *EWI-1* index offers a reliable estimation of EW for applications with multiband sensors. The $EWI - 5 = 676$ with only one spectral band offer an estimation of 45% of the EW variability, this spectral band is mainly associated with chlorophyll absorption. Two narrow indices that integrate three spectral bands had the highest coefficient of determination. All four proposed indices; *EWI-1*, *EWI-2*, *EWI-15* and *EWI-16* are linearly associated with EW. As the value of these index increases, the EW load simultaneously increases.

2.5 Conclusions

EW is the outermost cuticle of leaves and is strongly associated to major physiological process and characteristics of the plant. The presence of these waxes on leaf surfaces provides photoprotective protection, support the regulations of water loss through the stomatal route, and dissipate excess heat wavelengths. The selection of genotypes with high EW can provide adaptation to high temperatures and water scarcity environments.

The spectral bands in the visible region of the spectrum are highly associated to EW content, and variations in these specific bands provide a reliable estimation of EW. Considering the results of this study, four novel empirical based indices are proposed for phenotyping EW with a leaf clip spectroradiometer: $EWI\text{-}1_{Blue/Red}$, $EWI\text{-}2_{Blue/NIR}$, $EWI\text{-}15_{625\ (1/736\ -\ 1/832)}$ and $EWI\text{-}16_{(625\text{-}736)\ /\ 832}$. Two linear models are also proposed, the *Model-10* and *Model-11*. Further this study, it is necessary to gain more insights into the prediction of the proposed indices under field conditions and with canopy reflectance.

CHAPTER III

FIELD-BASED PHENOTYPING OF EPICUTICULAR WAX USING HYPERSPECTRAL INFORMATION

3.1 Introduction

Wheat is the second most important source of calories in the diets of developing countries (FAO 2013), and the first source of protein for 2.5 billion consumers who live on less than 2 USD per day. To overcome the demand of wheat by 2050, the global wheat production (GWP) will have to increase by 110 percent at a rate of 2.4% per year (Ray et al. 2013). Nonetheless, any substantial increase in grain yield (GY) will be limited by an estimated reduction of 6% by every °C of increase in the global mean temperature (Asseng et al. 2014). Along with heat stress, drought prone environments also contribute to the reduction of harvestable yield of wheat. Climate change has already impacted the productivity of wheat and other cereals (Fontana et al. 2015). There are approximately 64 million ha of wheat around the world directly affected by drought and heat stress (FAO 2013), which has raised the concern for food security for the next decades (Easterling 2005).

Wheat is particularly sensitive to high temperatures. Temperatures above the 34ºC triggers the senescence of leaves, accelerating the rate of grain filling (Tewari and Tripathy 1998) and reducing the transport of assimilates from leaves to the grain (Wardlaw 1994). Heat shock during grain filling can potentially lead to a reduction of ~0.02 t/ha of the grain yield (Asseng, Foster, and Turner 2011). Under limited soil

moisture and high temperature conditions, plants regulate water loss through transpiration by closing stomata. The stomatal closure not only restrict evapotranspiration, it also decreases CO_2 uptake, drastically reducing the plant photosynthetic rate (Mittler 2002, Blum et al. 1994). In order to cope the negative impacts of heat and drought stress, plants modify morphophysiological and metabolic mechanisms (Semenov and Halford 2009). These mechanisms, or traits, work synergically to adapt the genotype to the environment and increase its resilience to extreme weather conditions. Screening and selection based on these stress-related characteristics can not only facilitate the dissection of the physiology and genetics of heat and drought stress in wheat, but can directly contribute to expedite the development of resilient superior wheat lines to climate change.

Integrative traits that increase the reflectance of excess photosynthetic and infrared radiation directly contribute to decrease heat load and unnecessary evaporative cooling of the plants (Reynolds 2005). As a photo-protective trait, cuticular waxes and trichomes enhance the dissipation of albedo/heat during high light intensity environments. Cuticular waxes are lipophilic structures composed by long chain aliphatic molecules (Buschhaus and Jetter 2011) fixed to a layer of polymer cutin on the epidermal cells. Through the optimization of this cuticle, plants prevent water loss via the cuticular route. The presence of these cuticular waxes also affect the plant-light interactions. Absorbance of ultraviolet (0.33µm) wavelengths are most affected by epicuticular waxes (Holmes and Keiller 2002), but an increase in reflectance along with a decrease in the transmitted light trough the mesophyll cells at the photosynthetic active

radiation region (0.68μm) has been reported in wheat (Johnson, Richards, and Turner 1983)and *Sorghum bicolor* (Grant 2003). The effect of EW regulating the plant temperature (Mondal et al. 2014) concurs with the decrease of the energy absorbed at the near-infrared region (NIR) (Cameron, 1970; Eller, 1979). Overall, cuticular waxes represents an adaptive mechanism that protects the photosynthetic machinery and are a selective advantage for environments with high temperatures and light intensity. The introgression of this trait will contribute insight into ways to improve the environmental stability of wheat cultivars.

The breeding of new wheat cultivars has heavily relied on the direct selection of phenotypes, and although major advances in molecular breeding and statistics have enable selection based on genotypic data, there is still a need for phenotypic information. The application of high-throughput technologies has provided a new opportunity to breach the current yield barrier through the application of cost-efficient phenotyping systems that facilitate the simultaneous characterization of a large number of genotypes. Hyperspectral information enables the assessment of complex traits by capturing hundreds of spectral bands from the near-infrared (NIR), the visible (VIS), and the short-wave infrared region (SWIR) of the electromagnetic spectrum. Under natural sunlight conditions, these sensors accurately capture the canopy reflectance. Variations of the light reflected by vegetation at the VIS range directly depends of the light absorbed by chlorophylls and carotenoids, while the NIR is highly influenced by the scattering of the light on leaf tissue (Knippling 1970), and at the SWIR most of the water absorption

bands are located. The use of spectral information for plant characterization can enable the simultaneous screening of complex traits in real time and at low cost.

Phenotyping of EW with current methods is slow and inefficient. The development of an indirect method for phenotyping EW will provide clarity and direction to combine this adaptive trait into new drought and heat tolerant wheat cultivars that work synergistically to enhance grain yield by facilitating the screening of large breeding populations and its introgression into wheat elite background. The focus of this study is to estimate the prediction accuracy of spectral radiometric information to phenotype EW, and to evaluate its indirect selection under agronomic field conditions. To test this hypothesis, we evaluate a diverse panel of spring wheat lines and combine powerful spectroscopy methods to quantitatively estimate the variation of EW with the support of advance statistical tools.

3.2 Introduction

3.2.1 Plant material and experimental sites

Four panels of spring wheat landraces and products of interspecific hybridization with wild ancestors were evaluated during the years 2013, 2014 and 2015 at the Norman E. Borlaug Experimental Station (CENEB), Ciudad Obregon, Sonora in Northwest Mexico (27.20°N, 109.54°W, 38 masl). The genotypes were established approximately 80 days late from the normal planting date in the Yaqui Valley, Mexico to expose the plants to average daily temperatures of 28°C and maximum temperatures of 39°C during heading and anthesis. The experimental design was an alpha-lattice with two replications, established under the raised bed system with two rows per bed, an inter-row spacing

within each bed of 10 centimeters (cm), and a space between beds of 80 cm. In 2016, an additional panel of synthetic derived wheat lines (SDLs) was evaluated in College Station, Texas under non-irrigated conditions as an alpha-lattice design. The plot size was 3.0 x 1.5 meter (m) seeded at 100 grams (g).

3.2.2 Leaf wax quantification

Samples of flag leaves were obtained at 10 to 15 days after pollination (DAP) to quantify EW. Each sample consisted of twelve leaf disks of 1 cm diameter obtained from four randomly chosen flag leaves per plot collected in 2.0 ml glass vials. EW was extracted by emerging the samples in HPLC chloroform ($CHCl_3$) at room temperature for 20 sec. After extraction, EW was dried and quantified via the colorimetric technique described by (Ebercon, Blum, and Jordan. 1977).

3.2.3 Ground base radiometric measurements

Canopy reflectance per plot was collected from 11AM to 1PM by placing the optic fiber of the spectroradiometer 40 centimeters (cm) above the canopy. The spectral information was captured with a FieldSpec 4 Hi-Res spectroradiometer. This spectroradiometer captures the light reflected in 2151 continuous bands with a spectral resolution of 3 nanometers (nm) from the 0.35 to 0.7 µm, and 8 nm from the 1.4 to 2.1 µm. The sensor was radiometrically calibrated with a white BaSO4 reference card for 100% of reflectance, and by blocking the light intercepted by the optic fiber for 0% of reflectance. Ten readings were captured along the plot, but only the average response of these signatures was used for further analysis.

3.2.4 Airborne hyperspectral information

Aerial hyperspectral images from the SDL's evaluated in College Station, Texas were captured with an Aisa KESTREL-10 hyperspectral camera by SPECIM® mounted in a Cessna 355 II aircraft. A flight height of 5000 feet (ft) altitude and speed of 192 kilometers per hour (Km/h) were maintained through the flight. The camera captured 120 spectral bands with a spectral and spatial resolution of 5 nm and 0.25 meter (m), respectively. Four 8 m by 8 m ground tarps with nominal reflectance values of 8%, 16%, 32% and 48% were laid out in the field to calibrate the hyperspectral images. The reflectance from the tarps was captured using a Hand-held 2 spectroradiometer with a spectral range from the 0.325 to 1.075 µm, and 3 nm spectral resolution. The hyperspectral images were georeferenced and ensembled using the image analysis software ERDAS®. Digital counts (DCs) were extracted individually for the tarps and plots using the software ENVI®. Linear regression models were derived incorporating the ground base reflectance captured with the spectroradiometer and the DCs from the calibration tarps obtained with the aerial sensor. The derived linear equations were used to estimate the total canopy reflectance of the two hundred spectral bands for every plot.

3.2.5 Spectral features associated to EW content

Pearson correlation (PC), derivative analysis (DA) and sparse partial least square regression (SPLSR) were conducted to define the association of the canopy reflectance with the EW content. The average spectral range of the visible (0.4 to 0.7µm), the NIR (0.7 to 0.9µm), the SWIR (0.9 to 1.8µm) and the red-edge region (0.691 to 0.73µm) were incorporated in the PC analysis with the EW content. The correlation coefficients

and significance of the correlation were estimated with the *corr* function in the statistical analysis software R (R Development Core Team, 2012).

The first derivative of the spectrum was calculated to enhance important spectral features, estimating the rate of change of the reflectance respect to the wavelength by projecting the changes in the curvature of the spectrum in the specific interval of the signal. All the spectral derivatives were calculated within a window size of 11 nm using the *savitszkyGolay* function. This function is included in the package *prospect* (Stevens 2014), which applies the Savitzy-Golay filter (Bromba and Ziegler 1981) before the derivatives are estimated using the follow equation:

$$\boldsymbol{x_j *= \frac{1}{N} \sum_{h=-k}^{k} c_h x_j + h}$$

In this equation, the x_j* represents the new value obtained after the first or second derivative was estimated, N is a normalizing coefficient, k is the number of neighbor values at each side of j, and c_h are pre-computed coefficients that depend of the polynomial order and degree. Correlation coefficients were estimated for the first derivative of the spectrum with the EW content to identify the spectral features associated to EW.

The SPLSR is a supervised multivariate technique based on the principle of partial least square regression (PLSR) and relies on dimentionally reduction and multiple regression to confront situations where there exist highly correlated predictor variables and relative few samples. Although the PLSR is able to achieve good predictive performance, the linear combinations are complex and dificult to be interpreted. In this

study we conduct the SPLSR incorporating two hundred spectral bands with a resolution of 3 nm as dependent variables (X') for prediction of EW. The analysis was conducted with the *spls* function, the sparcity tuning parameter *'eta'* and *'K'* were assigned according the specifications in the *spls* package version 1.0 (Chung 2012).

3.2.6 Narrow and broad empirical spectral indices to estimate EW

All pairwise combinations incorporating one hundred and sixty-three spectral bands at 6 nm resolution were estimated for spectral indices as simple ratio ($SR = \frac{R_i}{R_j}$), difference ($DI = R_i - R_j$) and normalized difference ($NDI = \frac{R_i - R_j}{R_j + R_j}$). In these indices, R_i and R_j represent the reflectance values at *i* and *j* nm, respectively. A leaving one out cross validation (LOOCV) analysis was conducted to define the significance of the linear model and estimate the coefficients of determination (R^2) for EW as independent variable and the spectral indices as dependent variable (*X*): $y_i = \beta_0 + \beta_1(x_j)$**.** In this equation, y_i corresponds to EW, x_i is the estimated spectral index, and β_0 and β_1 are the intercept and the slope of the model, respectively. The spectral indices with the highest R^2 values were selected to fit an additional set of linear models for a defined training data set (66% of the observations) to predict every individual spectral index based on the variation of EW. These models followed the same linear function, $y_i = \beta_0 + \beta_1(x_i)$, but in this case y_i represents the spectral index and x_i corresponds to the EW content. In order to estimate the ability of the index predicting EW when selection is based on the index per se, the EW variable was solved in the second set of linear models as follow: $X_i = \frac{y_i - \beta_0}{\beta_i}$. An estimator for the Root Mean Square Error (RMSE) was bootstrapping in

the validation data set (34% of the individuals) 1000 times with the function *boot* in the software R. The same statistical approach was applied to define narrow band indices associated to EW with the red, green, blue (RGB), near infrared (NIR) and short-wave infrared (SWIR) spectral bands.

3.2.7 Stepwise Regression (SWR)

The selected cobinations of spectral bands for the SR, DI and NDI were incorporated in a stepwise regression analyis (SWR). SWR built a multivariate models with a semiautomatic proces in which the band combinations were included and/or removed based on the significance of the partial F-values. The final models were defined when the inclusion of more predictors was not justifiable. All the models were built with the PROC REG statement in the statistical analysis software SAS (Inc. 2011)for a defined training data set (60% of the observations). The best models were selected based on the lowest values for the Mallows' Cp estimator. For the validation data set (the remaining 40% of the observations), the selection was base on their lowest RMSE and higher coefficient of determination (R^2).

3.2.8 Vegetation indices

Narrow and broad vegetation indices associated to leaf pigments, light use efficiency, leaf area, plant greenest and water content, as well as spectral indices that include the red-region of the spectrum (Table 6 throught) were estimated. The association of these common vegetation indices with the EW content was tested with the Pearson correlation analysis.

3.2.9 Efficiency of indirect selection of EW with spectral based methods

The spectral indices and linear models were subject to an analysis of variance (ANOVA) for an alpha-lattice design to test the variation among the genotypes for every indirect selection approach and the conventional colorimetric method. The ANOVA was calculated with the PROC GLM procedure using the Statistical Analysis System (SAS) software version 9.2 (SAS, 2008). The phenotypic (σ_p^2) and genotypic σ_g^2 variance were estimated as follow: $\sigma_g^2 = \frac{[(msg)-(mse)]}{r}$ and $\sigma_p^2 = \sigma_g^2 + \frac{\sigma_e^2}{r}$ where *msg* and *mse* corresponds to the mean square of the genotypes and the error, respectively, σ_g^2 is the genetic variance, σ_p^2 the phenotypic variance, σ_e^2 the error variance, and *r* is the number of replications. The reported estimates of the heritability in broad sense (h^2) were calculated according to the formula describes by (Allard 1960): $h^2 = \frac{\sigma_g^2}{\sigma_p^2}\ x\ 100$.

Phenotypic correlations and the covariance matrix of the selected spectral indices and prediction models for EW were calculated using the PROC CORR procedure including the COV option in the statement in SAS. The genotypic correlations (σ_g), the expected response to selection (*R*), the correlated response to selection (*CR*) and the relative efficiency of indirect selection (*RE*) were all estimated according to (Falconer 1989), and the estimated genetic advance by selection (GA) as described by (Johnson, Robinson, and Comstock 1955).

$\sigma_g = \frac{COV_{XY}}{\sqrt{Var_x Var_y}}$ where COV_{XY} corresponds to the covariance estimate of the vegetation index and EW, Var_x corresponds to the variance of the spectral index, and Var_y is the variance of the EW.

$R = h_x\sigma_x$ where h_x is the square root of the heritability and σ_x the genotypic standard deviation.

$CR = h_x r_{gx}\sigma_{gy}$ where the h_x is the square root of the heritability for the trait *X* (spectral index), r_{gx} is the genetic correlation of the spectral index and EW, and σ_{gy} is the genotypic standard deviation of the trait *Y* (EW).

$RE = \frac{CR}{R}$ where *CR* is the correlated response to selection and *R* is the expected response to selection of the trait.

$GA = K(\sigma_p)h^2$ where *K* is the selection differential, $\sigma_p$is the phenotypic standard deviation of every spectral index or prediction model, and h^2 corresponds to the broad sense heritability. The *k* was estimated for 10% selection intensity as $k = \overline{x_p} - \overline{x_s}$, where $\overline{x_p}$ and $\overline{x_s}$, are the population mean and the mean of the selected individuals, respectively.

$GAM\ (\%) = \frac{GA}{\overline{x}}\ x\ 100$ where *GAM* is the genetic advance as percentage of the mean, and $\overline{x}$ is the grand mean of the specific character.

3.2.10 Phenotyping of EW using airborne hyperspectral information

The selected epicuticular wax indices (EWI) and the linear models that best estimate EW load were calculated using the spectral information collected with the aerial sensor. Pearson correlation analysis was conducted to estimate the association of the proposed indices and models to estimate EW with aerial hyperspectral imagery.

Table 5 Narrow band spectral indices for leaf pigments and light use efficiency.

NAME		FORMULA	REFERENCE
	LEAF PIGMENTS		
Carotenoid Reflectance Index-1	CRI-1	$\frac{1}{\rho_{510}} - \frac{1}{\rho_{550}}$	(Gitelson, Zur, et al. 2002)
Carotenoid Reflectance Index-2	CRI-2	$\frac{1}{\rho_{510}} - \frac{1}{\rho_{700}}$	(Gitelson, Zur, et al. 2002)
Anthocyanin Reflectance Index	ARI	$\frac{1}{\rho_{550}} - \frac{1}{\rho_{700}}$	(Gitelson, Merzlyak, and Chivkunova 2001)
Blue Green Pigment Index	BGPI	$\frac{\rho_{450}}{\rho_{550}}$	(Zarco-Tejada et al. 2005)
Blue Red Pigment Index	BRPI	$\frac{\rho_{450}}{\rho_{690}}$	(Zarco-Tejada et al. 2005)
Normalized Phaeophytinization Index	NPI	$\frac{\rho_{415} - \rho_{435}}{\rho_{415} + \rho_{435}}$	(Barnes et al. 1992)
	LIGHT USE EFFICIENCY		
Photochemical Reflectance Index	PRI	$\frac{\rho_{531} - \rho_{570}}{\rho_{531} + \rho_{570}}$	(Gamon, Serrano, and Surfus 1997)
Structure Insensitive Pigment Index	SIPI	$\frac{\rho_{800} - \rho_{450}}{\rho_{800} + \rho_{650}}$	(Panuelas et al. 1995)
Red Green Ratio Index	RGRI	$\frac{\sum_{i=600}^{699} R_i}{\sum_{i=500}^{599} R_j}$	(Gamon and Surfus 1999)

Table 6 Narrow band vegetation indices for leaf area, red-edge, and plant water content.

NAME	FORMULA		REFERENCE
	LEAF AREA		
Modified Triangular Vegetation Index	MTVI	$1.2[1.2(\rho_{800}-\rho_{550})-2.5(\rho_{670}-\rho_{550})]$	(Haboudane et al. 2004)
	RED-EDGE INDICES		
Red-edge position	ReP	$700+40\left[\frac{\rho_{670}+\rho_{780}}{2}-\rho_{700}\right]/(\rho_{740}-\rho_{700})$	(Gayout, Baret, and Major 1988)
Vogelmann Index-1	VGI-1	$^{740}/_{720}$	(Vogelmann, Rock, and Moss 1993)
Vogelmann Index-2	VGI-2	$\frac{\rho_{734}-\rho_{747}}{\rho_{715}-\rho_{726}}$	(Zarco-Tejada et al. 2003)
Vegetation Stress Ratio	VSR	$^{725}/_{702}$	(White, Williams, and Barr 2008)
Modified Red-edge Normalized Difference Vegetation Index	MRENDVI	$\frac{\rho_{750}-\rho_{705}}{\rho_{750}+\rho_{705}-2*\rho_{455}}$	(Datt 1999)
	PLANT WATER CONTENT		
Water Index	WI	$^{970}/_{900}$	(Penuelas et al. 1993)
Moisture Stress Index	MSI	$\frac{\rho_{1599}}{\rho_{819}}$	(Hunt and Rock 1989)
Simple Ratio Water Index	SRWI	$\frac{\rho_{860}}{\rho_{1240}}$	(Zarco-Tejada, Rueda, and Ustin 2003)

Table 7 Narrow band vegetation indices for plant greenest.

NAME	FORMULA		REFERENCE
	PLANT GREENEST		
Normalized Difference Vegetation Index	NDVI	$\frac{\rho_{800} - \rho_{640}}{\rho_{800} + \rho_{640}}$	(Rouse et al. 1974)
Plant Scenecense Reflectance Index	PSRI	$\frac{\rho_{680} - \rho_{500}}{\rho_{750}}$	(Merzlyak et al. 1999)
Reg-green Ratio Index	RGI	$\frac{\rho_{690}}{\rho_{550}}$	(Gamon and Surfus 1999)
Greenest Index	GI	$\frac{\rho_{554}}{\rho_{677}}$	(Zarco-Tejada et al. 2005)
Normalize Difference Nitrogen Index	NDNI	$\frac{\log\left(\frac{1}{\rho_{1510}}\right) - \log(\frac{1}{\rho_{1680}})}{\log\left(\frac{1}{\rho_{1510}}\right) + \log(\frac{1}{\rho_{1680}})}$	(Serrano, Penuelas, and Ustin 2002)
Normalized Pigment Chlorophyll Index	NPCI	$\frac{\rho_{680} - \rho_{430}}{\rho_{680} + \rho_{430}}$	(Penuelas et al. 1994)
Pigment Specific Simple Ratio for Chlorophyll *a*	PSI-*a*	$\frac{\rho_{800}}{\rho_{675}}$	(Blackburn 1998)
Pigment Specific Simple Ratio for Chlorophyll *b*	PSI-*b*	$\frac{\rho_{800}}{\rho_{650}}$	(Blackburn 1998)
Transformed Chlorophyll Absorption Ratio Index	TCARI	$3[(\rho_{700} - \rho_{670}) - 0.2(\rho_{700} - \rho_{550})(\rho_{700}/\rho_{670})]$	(Haboudane et al. 2002)

Table 8 Broad spectral indices to characterize pigments, leaf area, and plant water content.

NAME		FORMULA	REFERENCE
	LEAF PIGMENTS		
Modified Anthocyanin Reflectance Index	mARI	$\left[\left(\frac{1}{\rho_{\text{Green}}}\right) - \left(\frac{1}{\rho_{\text{Red edge}}}\right)\right] * \rho_{\text{NIR}}$	(Gitelson, Keydan, and Merzlyak 2006)
Anthocyanin Reflectance Index	ARI	$\frac{\rho_{\text{GREEN}}}{\rho_{\text{NIR}}}$	(Berg and Perkins 2005)
	LEAF AREA		
Enhanced Vegetation Index	EVI	$2.5 * \frac{(\rho_{NIR} - \rho_{Red})}{(\rho_{NIR} + 6\rho_{Red} - 7.5\rho_{Blue} + 1)}$	(Huete et al. 1997)
Leaf Area Index	LAI	$3.618 * EVI - 0.118$	(Boegh and Soe 2002)
	PLANT WATER CONTENT		
Normalized Difference Infrared Index	NDII	$\frac{(\rho_{\text{NIR}} - \rho_{\text{SWIR}})}{(\rho_{\text{NIR}} + \rho_{\text{SWIR}})}$	(Kim et al. 2015)
Moisture Stress Index	MSI	$\frac{\rho_{\text{SWIR}}}{\rho_{\text{NIR}}}$	(Kim et al. 2015)

Table 9 Broad band vegetation indices for plant greenest.

NAME	FORMULA		REFERENCE
	PLANT GREENEST		
Soil Adjusted Vegetation Index	SAVI	$\frac{(\rho_{NIR} - \rho_{Red})}{(\rho_{NIR} + \rho_{Red} + L)} * (1 + L)$	(Huete 1988)
Normalized Difference Vegetation index	NDVI	$\frac{(\rho_{NIR} - \rho_{Red})}{(\rho_{NIR} + \rho_{Red})}$	(White, Williams, and Barr 2008)
Simple Ratio	SR	$\frac{\rho_{NIR}}{\rho_{Red}}$	(Birth and McVey 1968)
Green Normalized Difference Vegetation Index	GNDVI	$\frac{(\rho_{NIR} - \rho_{Green})}{(\rho_{NIR} + \rho_{Green})}$	(Gitelson, Kaufman, and Merzlyak 1996)
Green Difference Vegetation Index	GDVI	$\rho_{NIR} - \rho_{Green}$	(Sripada et al. 2006)
Difference Vegetation Index	DVI	$\rho_{NIR} - \rho_{Red}$	(Tucker 1979)
Red Green Ratio Index	RGRI	$\rho_{Red} - \rho_{Green}$	(Gamon and Surfus 1999)
Green Ratio Vegetation Index	GRVI	$\frac{\rho_{NIR}}{\rho_{Green}}$	(Sripada et al. 2006)
Transformed Difference Vegetation Index	TDVI	$\sqrt{0.5 + \frac{(\rho_{NIR} - \rho_{Reed})}{(\rho_{NIR} + \rho_{Reed})}}$	(Bannari, Asalhi, and Teillet 2002)
Visible Atmospherically Resistant Index	VARI	$\frac{\rho_{Green} - \rho_{Reed}}{\rho_{Green} + \rho_{Reed} - \rho_{Blue}}$	(Gitelson, Stark, et al. 2002)

3.3 Results

3.3.1 Descriptive statistics

The mean values of EW for the genotypes evaluated in 2013 and 2014 are presented in Table 8. The average of the EW load of the genotypes included in 2013 were 3.02 mg/dm^2 for the HS-I and 2.96 mg/dm^2 for the HS-II. In 2014, the mean values of the EW were 7.61 mg/dm^2 for the HS-III, and 6.74 mg/dm^2 for the HS-IV. The estimates of the h^2 were highly affected by the environment. The largest estimate of $h^2$was obtained for the trial HS-II, which also had a low CV. The other three estimated of the h^2 were low, but acceptable for a physiological trait greatly affected by the genotype by environment interaction. For all the four trials, EW was statistically different among the genotypes evaluated at 1% and 5% probability.

Table 10 Wheat trials evaluated under heat stress (HS) in 2013 and 2014 at the CENEB experimental station in Ciudad Obregon (OB), Sonora, Mexico. The h^2 corresponds to the broad sense heritability estimate, V_g is the genotypic variance, and CV the coefficient of determination of the epicuticular wax (EW).

ID	Year	Environment	No. of genotypes	Mean EW (mg/dm^2)	V_g	h^2	CV
HS-I	2013	OB-HS	114	3.02	0.011*	0.13	23.22
HS-II	2013	OB-HS	216	2.96	0.014**	0.66	6.97
HS-III	2014	OB-HS	266	7.61	0.21*	0.13	21.18
HS-IV	2014	OB-HS/D	266	6.74	0.02*	0.26	13.29

The boxplot of the EW content for all four trials evaluated in 2013 and 2014 is presented in Fig. 9. Overall, the distribution of the EW content of the genotypes included in the trial HS-III and HS-IV was larger than the distribution of the genotypes evaluated in 2013.

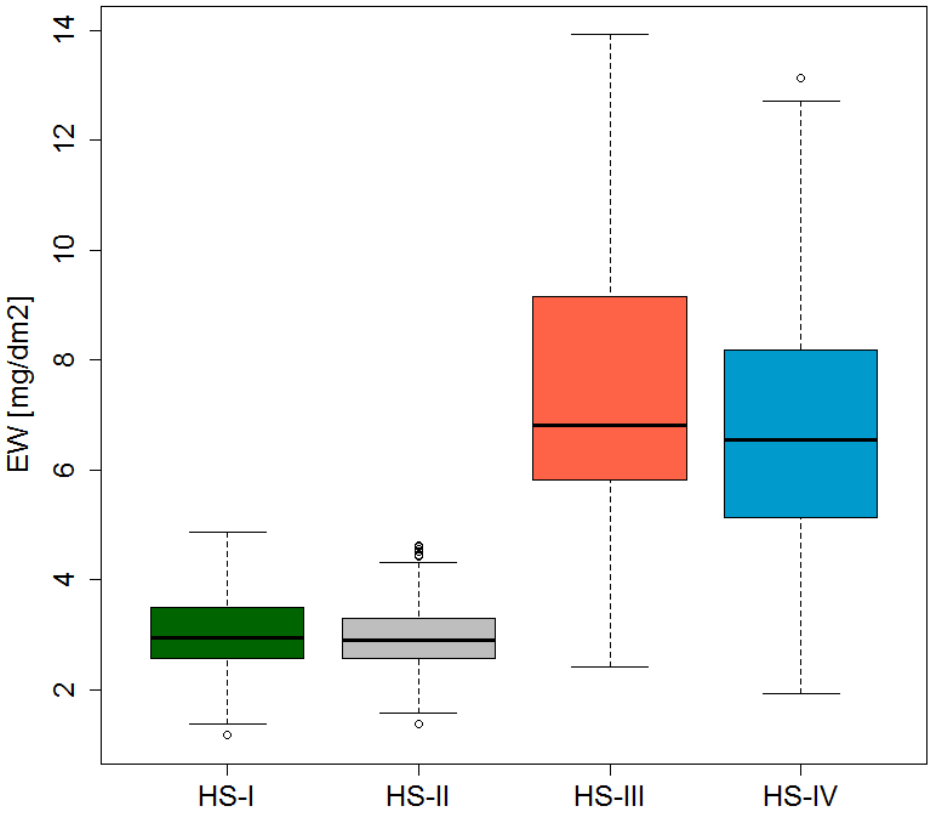

Fig. 9 Boxplot of EW content (mg/dm^2) for the four trials evaluated in 2013 and 2014 under severe heat stress (HS) at the CENEB, in Ciudad Obregon, Sonora, Mexico.

The canopy reflectance of the two groups that included the genotypes with the highest and the lowest content of EW, respectively, are shown in Fig.10. Overall, the percentage of light reflected by the canopy of the genotypes with the highest EW content was considerable lower that the canopy reflectance from the genotypes included in the group with genotypes with the lowest EW load. As can be observed, this difference is mainly detected at the NIR and SWIR. Minimum variations were observed in the visible region of the spectrum, except for the trial HS-III, where a slight change on the reflectance was observed.

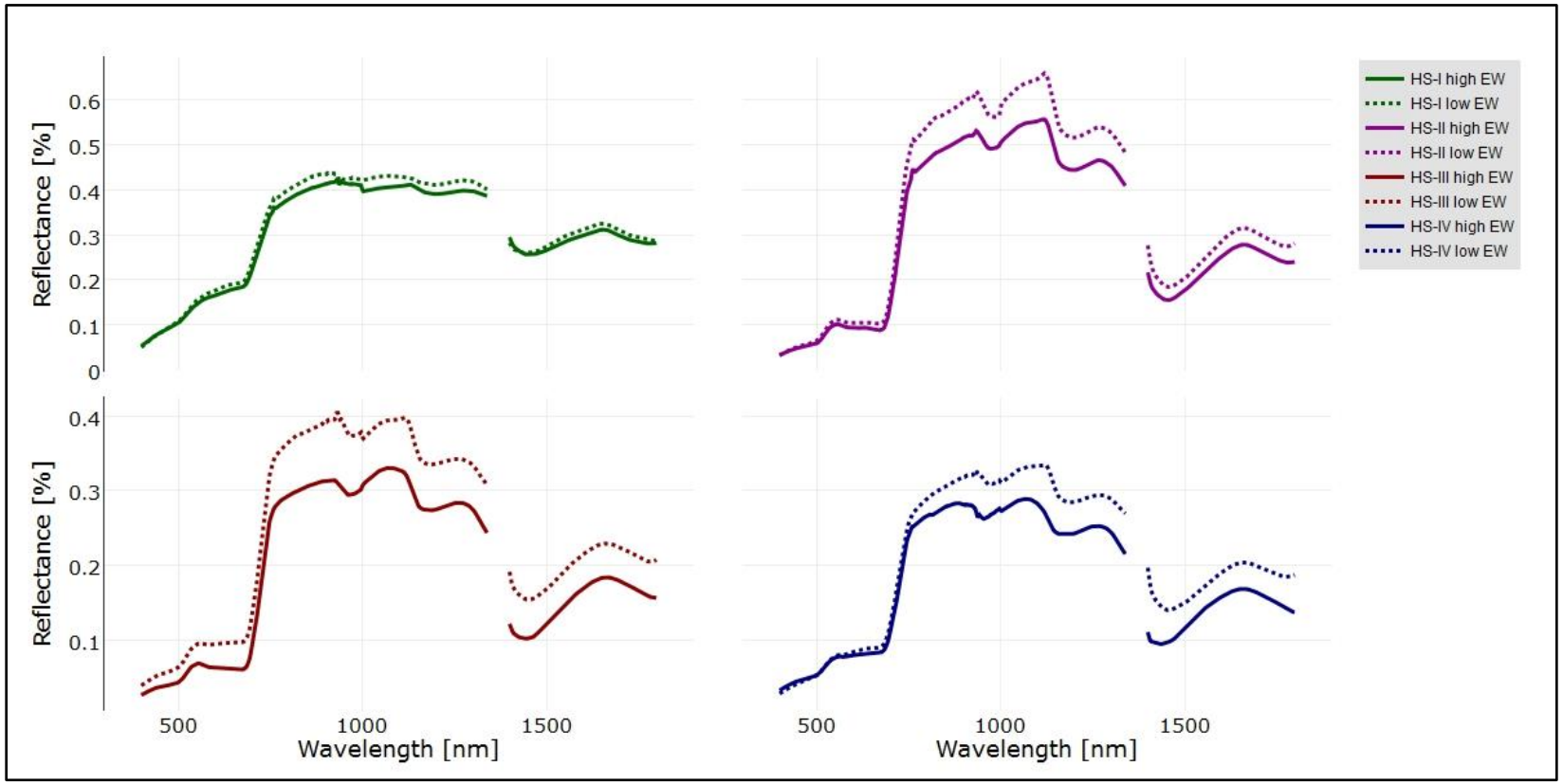

Fig. 10 Average spectral response of genotypes with the highest and lowest EW content evaluated under heat stress (HS) in Ciudad Obregon, Sonora, Mexico. For HI-I, the range of the lowest to highest EW (mg/dm^2) content were 4.05 to 4.86 and 1.16 to 2.01; for HI-II were 4.0 to 4.62 and 1.36 to 2.01; the HI-III were 12.01 to 14.79 and 2.4 to 4.9 5; and the HI-IV from 10.03 to 13.14 and 1.93 to 3.95.

3.3.2 Associated response of the canopy reflectance with EW

The Pearson correlation coefficients of the canopy reflectance for the main regions of the spectrum and EW content are presented in Fig. 11. The wavelengths of the spectrum were negatively associated with EW load, except for the violet wavelengths of the visible region. A positive association was detected at the violet region, with a correlation coefficient (r) of ~0.2. The results from the environments HS-I, HS-II and HS-IV were all consistent, with similar correlation coefficients, but the association of reflectance and EW was significantly higher for the trial HS-III.

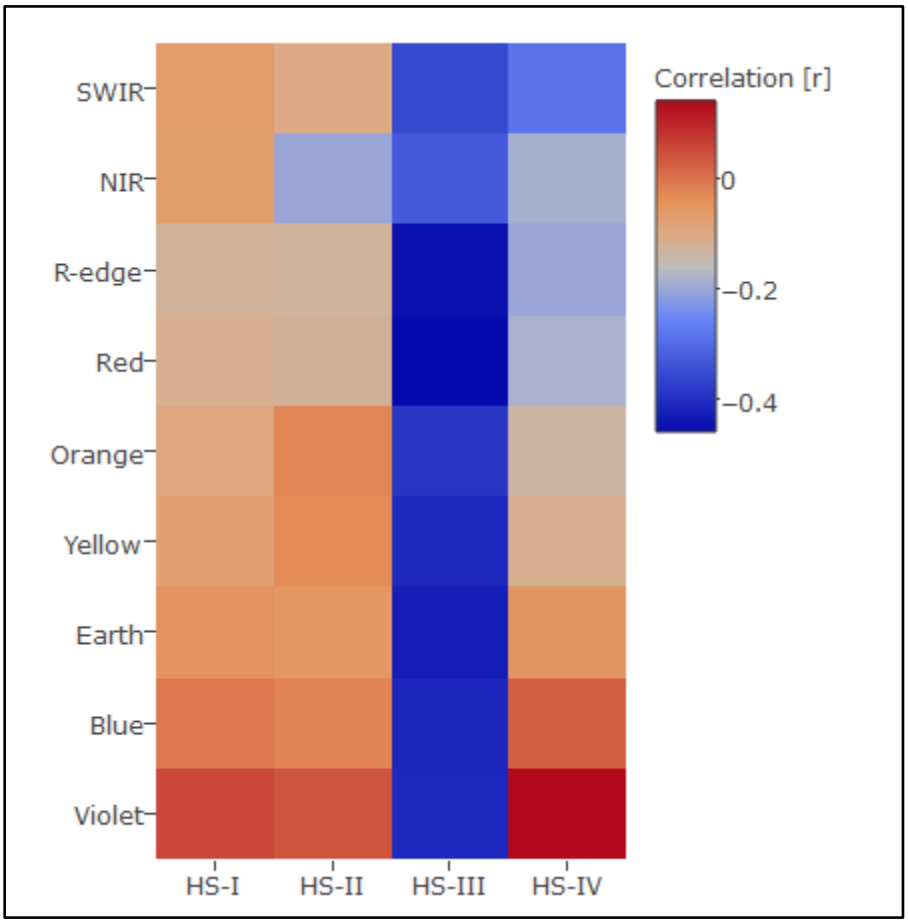

Fig. 11 Pearson correlation coefficients of the EW content (mg dm^{-2}) and the average response of canopy reflectance of the main regions of the electromagnetic spectrum.

The derivative analysis effectively enhanced the spectral changes, eliminating the small variations in the baseline of the spectrum. Correlation coefficients obtained with the derivative analysis are higher that the coefficients obtained by simply evaluating the canopy reflectance and EW. The peaks in the graphs represent where the highest association of EW with a specific change on the canopy reflectance occurs. Most of the peaks were located at the NIR and the SWIR. The results obtained in all four trials were compared to select the spectral regions consistently associated.

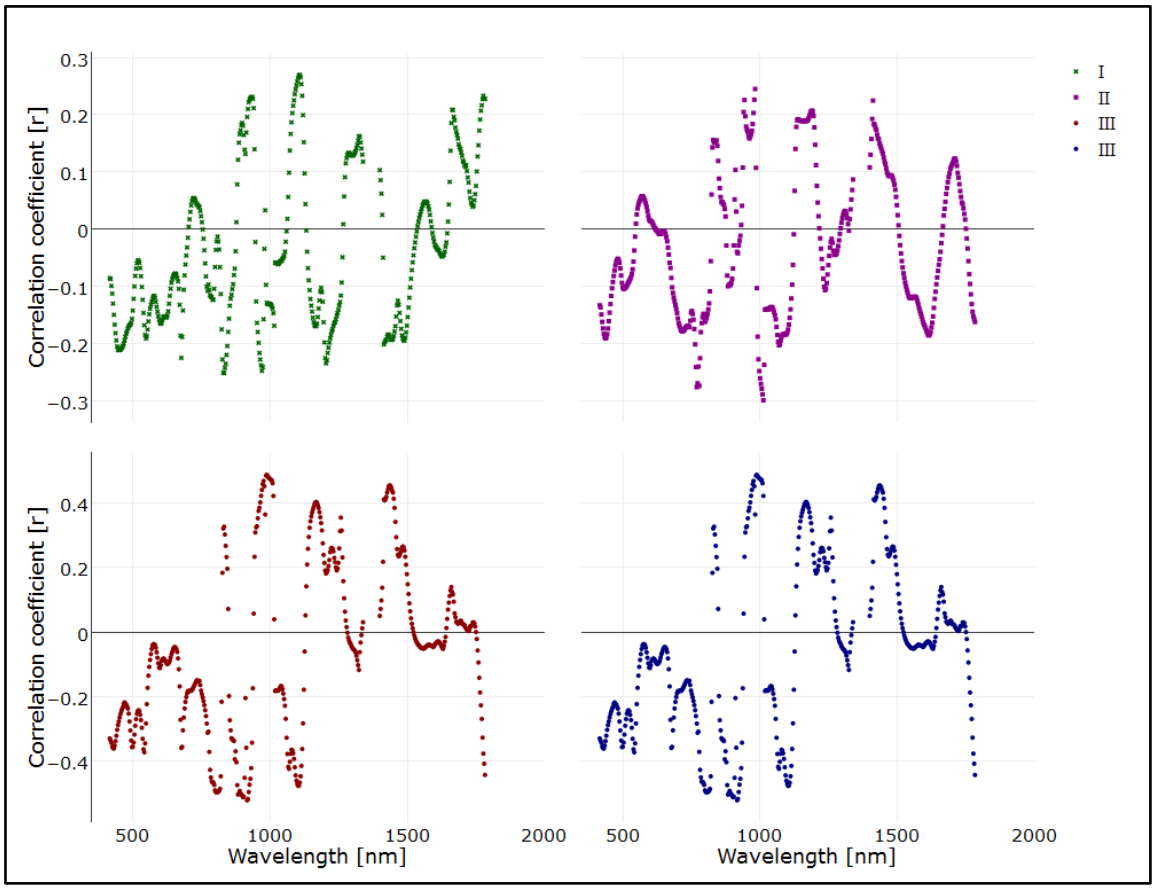

Fig. 12 Pearson correlation coefficients of the first derivative response and EW content (mg dm^{-2}) for the trial HS-I and HS-II in 2013, and HS-III and HS-IV in 2014. All genotypes were evaluated under severe heat stress during grain filling and anthesis.

In the Fig. 13 the sparse linear combinations of the original predictors are presented. The analysis simultaneously achieve good predictive performance and variable selection. A limited number of predictors were included in the trial HS-I, but most of these predictor were consistently associated in the other three enviroments. The spectral bands that were consistently associated in all three analysis and across the enviroments were automatically selected as predictos (Table 8).

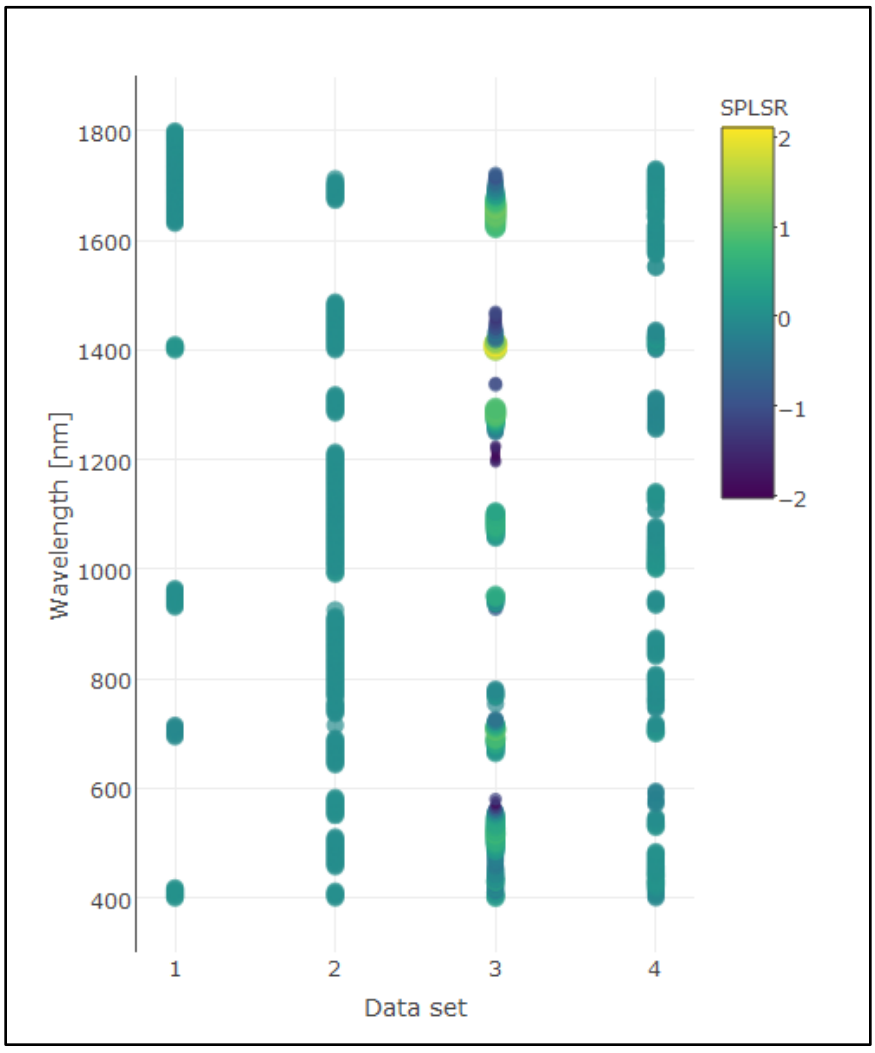

Fig. 13 Coefficients of the sparse partial least square regression (SPLSR) of the light reflectance and the EW content for the trials 1) HS-I, 2) HS-II, 3) HS-III, and 4) HS-IV.

Table 11 Spectral bands selected according to the results of the Pearson correlation analysis, the derivative response, and the sparse partial least square regression analysis.

Selection method	VIS (0.4-0.7 µm)	NIR (0.7-1.4 µm)	SWIR (1.4-1.7 µm)
Pearson correlation analysis of the light reflectance and EW	403-457	691-730	1321-1472
	520-574	706-928	1502-1733
		931-1000	
		1093-1183	
		1225-1339	
		1327-1415	
Pearson correlation of the first derivative of the reflectance and EW	430-466	787-802	1424-1451
	676-679	826-844	1766-1784
		889-913	
		961-1009	
		1099-1108	
		1150-1216	
Sparse Partial Least Square Regression (SPLS)	430-436	787-796	1424-1430
	676-679	961-970	
		1003-1009	

3.3.3 Broad and narrow band empirical indices for phenotyping EW

The wavelengths of the spectral reflectance were incorporated into simple combinations of spectral bands as indices. The simple ratio ($SR = \frac{R_i}{R_j}$), the difference index ($DI = R_i - R_j$) and the normalized difference index ($NDI = \frac{R_i - R_j}{R_i - R_j}$) were estimated and evaluated to define their association with EW. The coefficients of determination for every spectral combination are shown in Fig.14 for the SR, Fig.15 for the DI, and Fig. 16 for the NDI. For all indices, the maximum percentage of the EW variation that can be estimated with the canopy reflectance under field conditions is approximately 25%.

The prediction accuracy of the spectral indices varied across the environments. However, the highest R^2 values for the SR, DI and NDI were all obtained with similar spectral bands. The spectral combinations of the visible region were all consistently high in the HS-I, HS-II and HS-IV, but no association was detected in the HS-III environment. The indices that integrate the 1.4 to 1.8 µm spectral range with the visible wavelengths were also closely related to the EW load, but this association was only observed for the trial HS-IV. The combinations that were strongly associated with EW content across all four trials were estimated with the spectral bands around the 0.9 µm, 1.0 µm, 1.3 µm, from where163 indices were chosen for further analysis.

When the RGB, NIR and SWIR spectral bands were incorporated as indices, similar prediction accuracy to the narrow band indices were obtained, ~0.25 (Fig. 17). These higher R^2 values were reached when the DI was estimated with the Red and Blue, and the Red and Green wavelengths. Integrating the R-edge, the Blue and the Green band, good prediction estimates were obtained. However, an index that included the Red-edge not be useful for RGB multispectral sensors. The second set of indices selected was the NDI with the Red, Blue and Green bands.

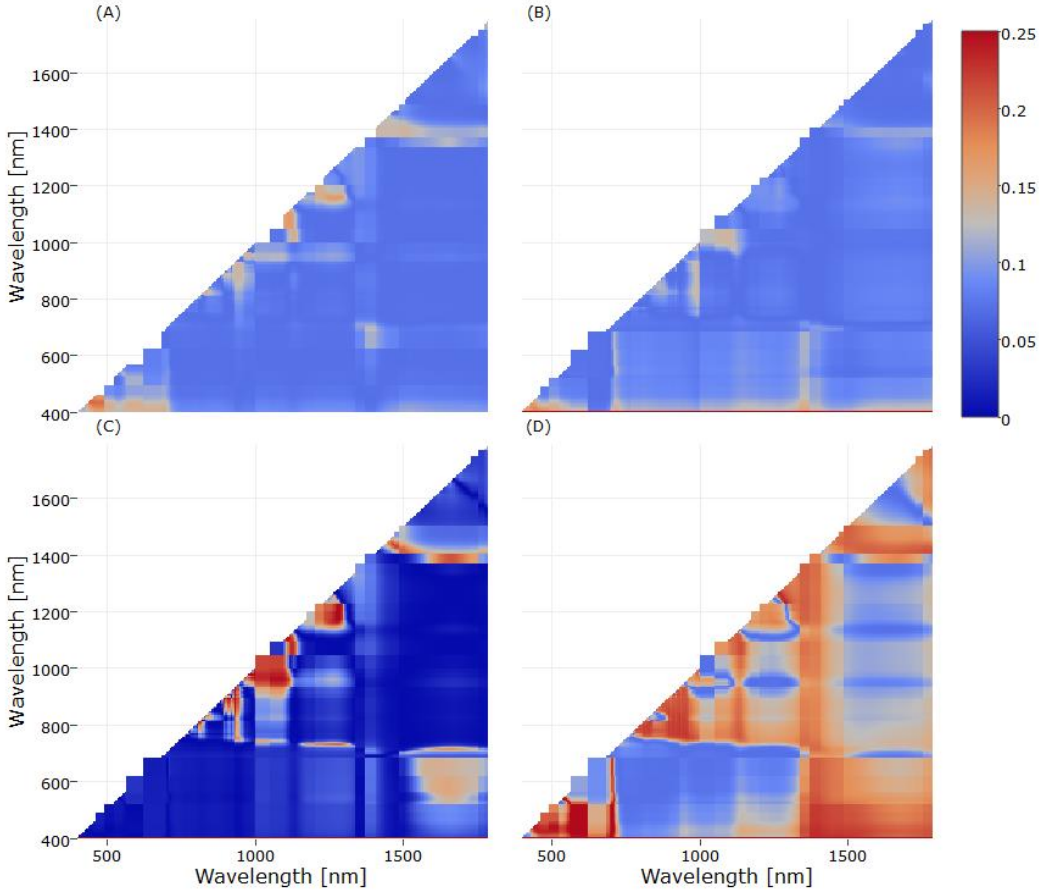

Fig. 14 Coefficients of determination from the LOOCV analysis between the simple ratio (SR) index incorporating the spectral bands from the 0.4 to 1.8 µm and EW content (mg dm^{-2}). (A) corresponds to the trial HS-I, (B) to the HS-II, (C) to the HS-III and (D) to the HS-IV.

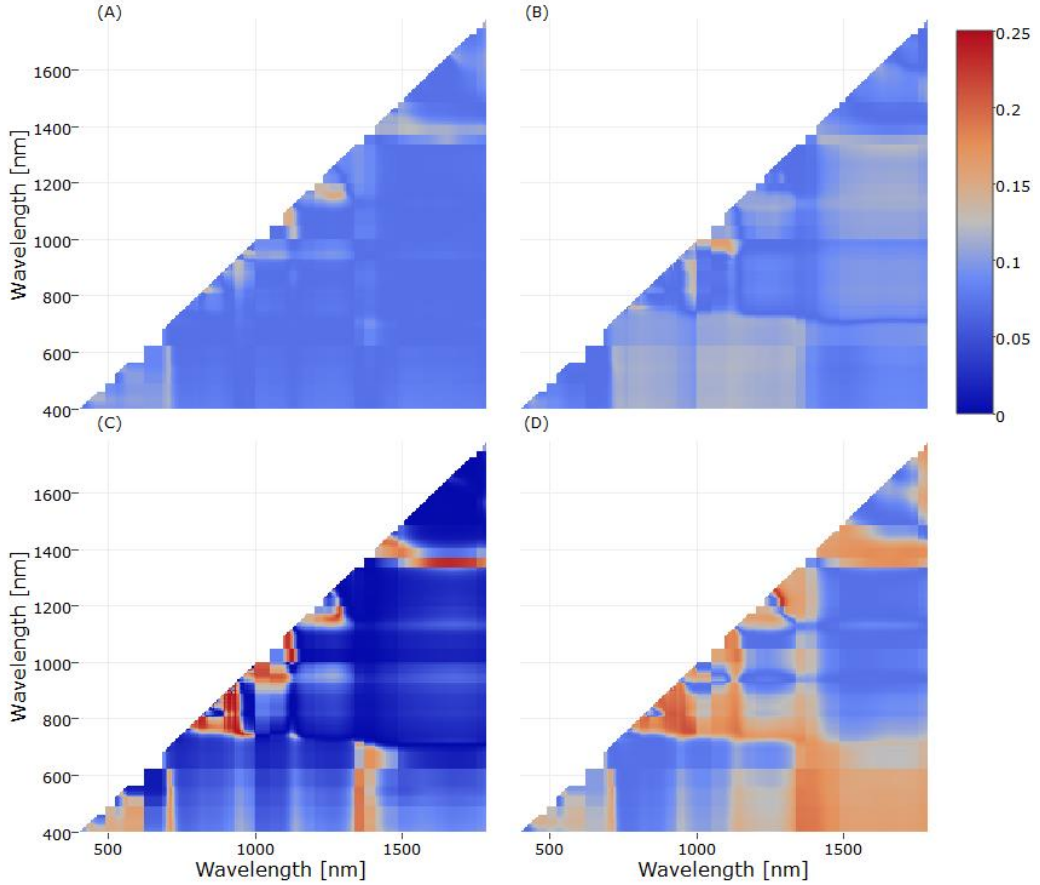

Fig. 15 Coefficients of determination from the LOOCV analysis between the different index (DI) incorporating the spectral bands from the 0.4 to 1.8 µm and EW content (mg dm^{-2}). (A) corresponds to the trial HS-I, (B) to the HS-II, (C) to the HS-III and (D) to the HS-IV.

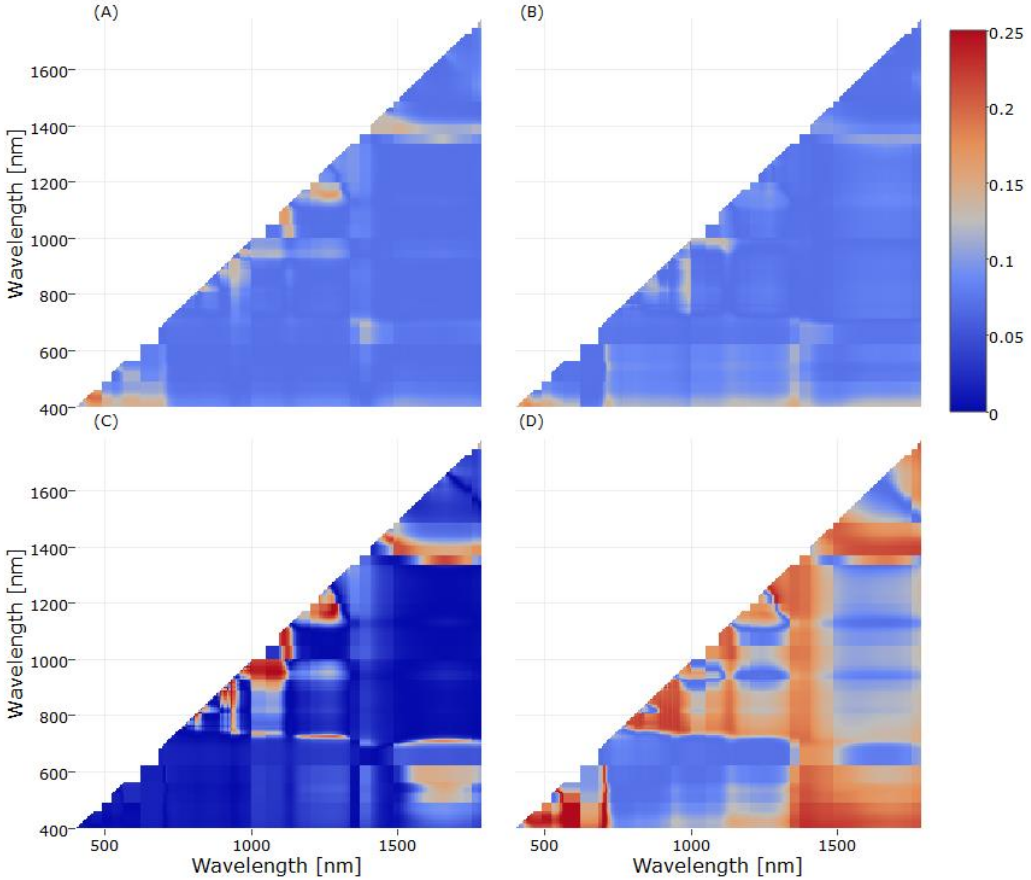

Fig. 16 Coefficients of determination from the LOOCV analysis between the normalized different index (NDI) incorporating the spectral bands from the 0.4 to 1.8 µm and EW content (mg dm^{-2}). (A) corresponds to the trial HS-I, (B) to the HS-II, (C) to the HS-III and (D) to the HS-IV.

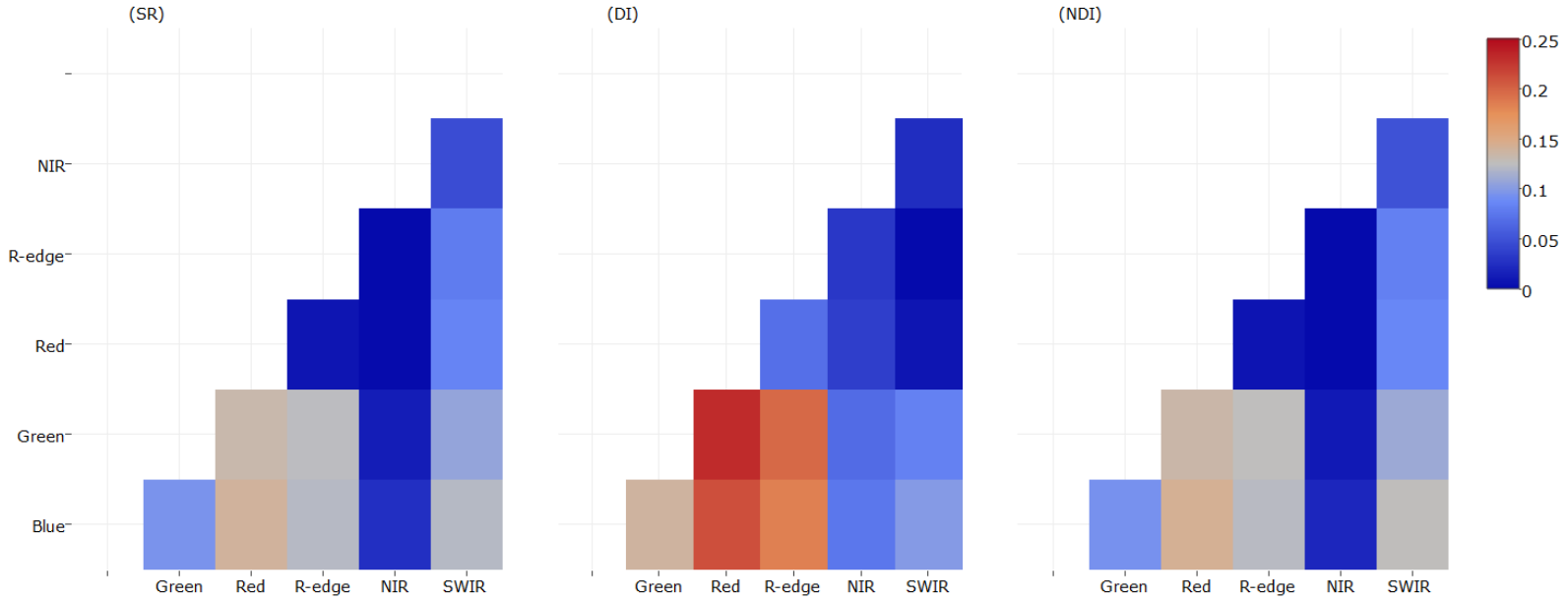

Fig. 17 Coefficients of determination (R^2) obtained with the LOOCV analysis between the EW content (mg/dm^2) and the estimated broad band indices. The spectral indices incorporated the main spectral bands from the 0.4 to 1.8 µm as the simple ratio (SR), the difference index (DI) and the normalized different index (NDI). The results obtained in every trait were very consistent and the presented R^2 are the average response for all four evaluated trials.

Table 12 Coefficients of determination (R^2) from the LOOCV analysis, and best fitted parameters estimated for the training data set and testes in the validation set by bootstrapping the estimator of the RMSE in (mg/dm^2) for the narrow and broad spectral indices. The h^2 is the estimate of the broad sense heritability.

	Bests fitted model parameters					
Index	**a**	**B**	**R^2**	**RMSE**	**h^2**	**p-value**
Broad band indices						
SRB-1 $\frac{\mathbf{Red}}{\mathbf{Green}}$	2.051	-0.088	0.14	0.47	0.42	<0.0001
DIB -2 Red-Blue	0.131	-0.062	0.22	0.36	0.42	<0.0001
DIB -3 Red-Green	0.095	-0.046	0.24	0.36	0.43	<0.0001
NDIN-1 $\frac{\mathbf{Red-Blue}}{\mathbf{Red+Blue}}$	-0.021	0.015	0.14	0.48	0.51	<0.0001
Narrow band indices						
SRN-1 $\frac{\mathbf{913}}{\mathbf{901}}$	1.033	-0.02	0.23	0.16	0	<0.0001
SRN-2 $\frac{\mathbf{1093}}{\mathbf{967\ to\ 979}}$	0.916	0.194	0.24	0.16	0	<0.0001
SRN-3 $\frac{\mathbf{1177}}{\mathbf{1273}}$	1.019	-0.046	0.22	0.15	0.14	<0.0001
DIN-1 **931 – 769 to 793**	0.127	-0.082	0.25	0.19	0	<0.0001
DIN-2 **931 – 811 to 817**	0.086	-0.064	0.24	0.19	0	<0.0001
DIN-3 **913 – 901**	0.011	-0.009	0.27	0.18	0	<0.0001
NDIN-1 $\frac{\mathbf{907-901}}{\mathbf{907+901}}$	0.009	-0.007	0.25	0.19	0	<0.0001
NDIN-2 $\frac{\mathbf{913-901}}{\mathbf{913+901}}$	0.012	-0.009	0.23	0.17	0	<0.0001
NDIN-3 $\frac{\mathbf{1279-1177}}{\mathbf{1279+1177}}$	-0.008	0.019	0.24	0.17	0	<0.0001

The results of the bootstrapping analysis for the narrow and broad spectral indices that were detected with the highest R^2 in the LOOCV are included in Table 9. The estimates of the RMSE were all calculated in the validation data set. According to their R^2, four broad band indices had the highest prediction accuracy, along with nine narrow band indices. For the broad indices, the *DIB -2 Red-Blue* and the *DIB -3 Red-Green* were both statistically associated with EW and had the lowest difference between

the predicted and actual EW values. The nine narrow indices had all similar R^2 and RMSE. However, extremely low heritability estimates were detected for these narrow indices, except for the *SRN-3* $\frac{1177}{1273}$ index. The h^2 estimates for the broad band indices were all similar and superior to the h^2 estimated for EW using the conventional chemical method.

3.3.4 Multiple linear regression for prediction of EW

The developed linear regression models incorporated the spectral combinations that were selected in the LOOCV analysis. The linear models were calculated in a randomly chosen training data set (66%) and the estimates of the prediction accuracy were calculated in the validation data set (44%). The proportion of the EW variance that was predictable with the linear models *MN-SR-1* and *MN-NDI-3* was 45%, and the RMSE values of ~0.08. The majority of the bands in these models are directly associated to water absorption. The indices calculated with the broad band combinations predict a smaller proportion of the EW variation, compared to the narrow band models. *The MB-DI-2* index had the higher R2 value, and lower RMSE. Heritability estimates for the broad band models were consistent and adequate to estimate the proportion of the variation of the phenotype EW that is due to genetic effect. The models proposed for indirect selection of EW are the follow: *MB-DI-2, MN-SR-1, MN-NDI-3* (Fig. 18).

Table 13 Linear regression models incorporating the broad and narrow bands for the estimation of EW load.

							RMSE	R^2	h^2	C(p)
Broad band combinations										
MB-SR-1	Intercept	$\frac{\text{Blue}}{\text{Red}}$	$\frac{\text{Blue}}{\text{NIR}}$	$\frac{\text{Green}}{\text{Red}}$	$\frac{\text{Redge}}{\text{NIR}}$	$\frac{\text{NIR}}{\text{Green}}$				
	-3.69	48.41	-89.48	-28.45	67.65	0.51	0.26	0.23	0.62	19.86
MB-DI-2	Intercept	$\text{Blue} - \text{SWIR}$	$\text{Red} - \text{Green}$	$\text{SWIR} - \text{NIR}$						
	1.12	-2.55	-10.74	-0.19			0.27	0.29	0.49	2.51
MB-NDI-3	Intercept	$\frac{\text{Blue} - \text{Red}}{\text{Blue} + \text{Red}}$	$\frac{\text{Blue} - \text{NIR}}{\text{Blue} + \text{NIR}}$	$\frac{\text{Red} - \text{Redge}}{\text{Red} + \text{Redge}}$	$\frac{\text{SWIR} - \text{Green}}{\text{SWIR} + \text{Green}}$					
	3.68	6.96	-4.22	10. 66	-0.51		0.33	0.21	0.53	10.86
Narrow band combinations										
MN-SR-1	Intercept	$\frac{895}{899}$	$\frac{913}{901}$	$\frac{1093}{961}$	$\frac{1093}{967}$	$\frac{997}{961}$				
	-22.11	46.22	-44.88	74.26	-74.82	-58.91	0.08	0.46	0	14.54
	$\frac{997}{967}$	$\frac{979}{973}$	$\frac{1165}{1273}$	$\frac{1165}{1279}$	$\frac{1165}{1285}$	$\frac{1171}{1273}$				
	62.89	18.19	104.21	-120.79	41.41	-24.76				
MN-NDI-3	Intercept	$\frac{895 - 899}{895 + 899}$	$\frac{907 - 901}{907 + 901}$	$\frac{913 - 901}{913 + 901}$	$\frac{1093 - 955}{1093 + 955}$	$\frac{997 - 961}{997 + 961}$				
	1.04	104.22	-68.41	-64.96	-6.44	25.03	0.07	0.45	0	38.44
	$\frac{1267 - 1165}{1276 + 1165}$	$\frac{1285 - 1165}{1285 + 1165}$	$\frac{1279 - 1171}{1279 + 1171}$	$\frac{1285 - 1171}{1285 + 1171}$						
	-165.53	155.61	319.95	-307.81						

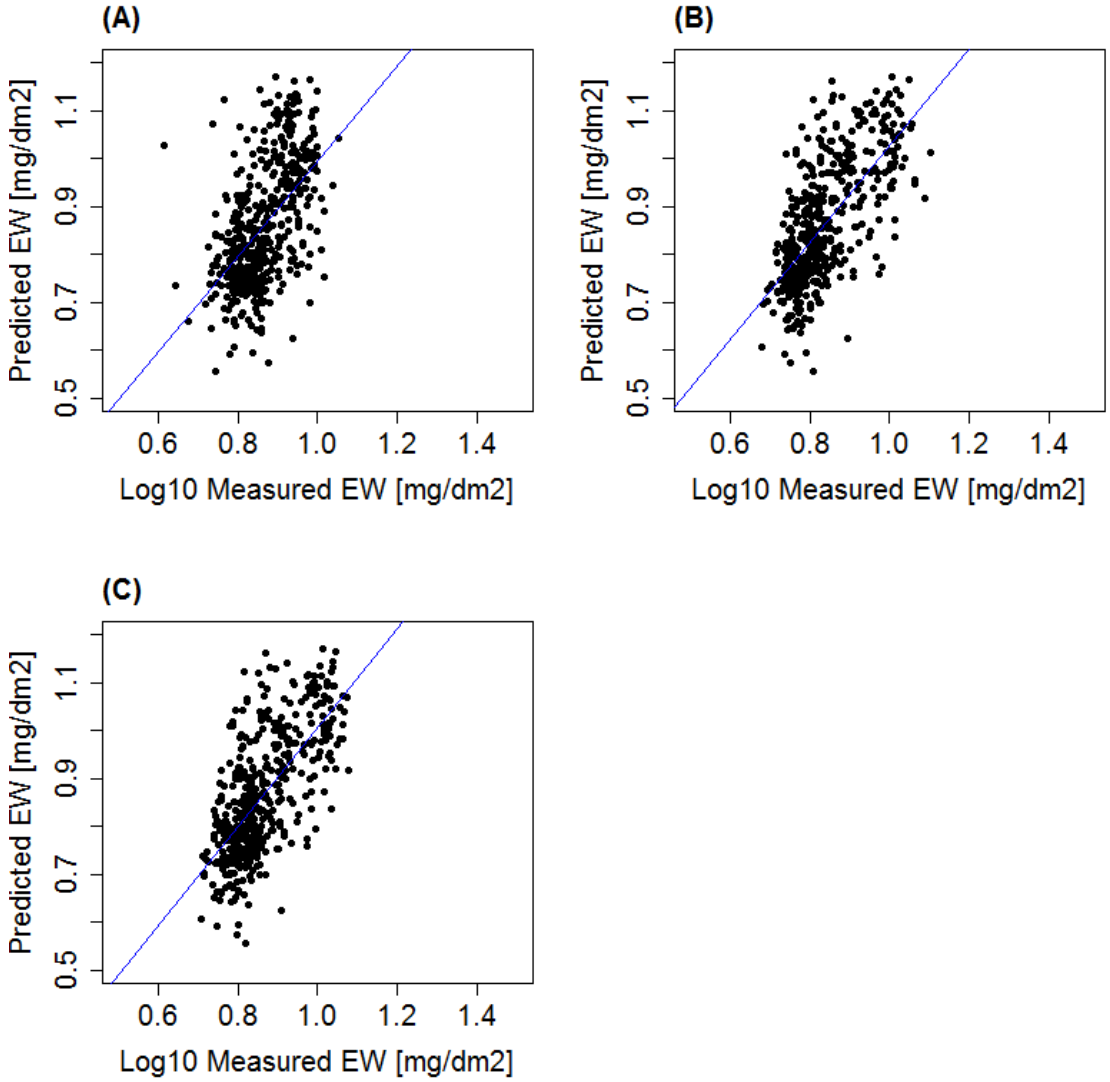

Fig. 18 Observed and estimated EW with the models A) *MB-DI-2*, B) *MN-SR-1*, and C) *MN-NDI-3*.

3.3.5 Association of EW content with common vegetation indices for plant characterization

The linear dependence of common vegetation indices (VI) with EW load is presented in Fig. 19. The narrow VI's that were most associated with EW load included spectral wavelengths at the VIS and SWIR spectral region. The correlation coefficients (r) ranged from 0.24 to 0.37 for the blue green pigment index ($BGPI = \frac{\rho_{450}}{\rho_{550}}$), the blue-red pigment index ($BRPI=\frac{\rho_{450}}{\rho_{690}}$), and the normalized phaeophytinization index ($NPI = \frac{\rho_{415}-\rho_{435}}{\rho_{415}+\rho_{435}}$). A negative association was found for the normalized difference nitrogen index ($NDNI = \frac{log\left(\frac{1}{\rho_{1510}}\right)-log(\frac{1}{\rho_{1680}})}{log\left(\frac{1}{\rho_{1510}}\right)+log(\frac{1}{\rho_{1680}})}$) and the normalized pigment chlorophyll index ($NPCI = \frac{\rho_{680}-\rho_{430}}{\rho_{680}+\rho_{430}}$).

The red-green index ($RGRI = \rho_{Red} - \rho_{Green}$) and the transformed difference vegetation index $TDVI = \sqrt{0.5 + \frac{(\rho_{NIR}-\rho_{Reed})}{(\rho_{NIR}+\rho_{Reed})}}$) were both negatively associated with EW, with correlation coefficients of -0.23 and -0.25, respectively. The visible atmospherically resistant index ($VARI = \frac{\rho_{Green}-\rho_{Reed}}{\rho_{Green}+\rho_{Reed}-\rho_{Blue}}$) was also strongly associated, but the correlated response was positive. The developed narrow and broad indices, and linear modeld for EW were superior in prediction, compared to the common VI's.

3.3.6 Selection of EW with indirect phenotyping methods

The efficiency of indirect selection of the developed spectral methodologies (ISM) is presented in Table 11. Compared to the EW quantified with the conventional colorimetric approach, the spectral indices and models had a significant lower CV. Heritability estimates of the ISM were superior in all cases to the heritability estimate for

EW. Phenotypic correlations were all within the same range, but the genotypic correlation of the *SRN-3*, the *MB-SR-1* and the *MD-NDI-3* were considerably higher, compared to the rest of the ISM. The RE of the indirect selection with the ISM using the *DIB-2*, *DIB-3*, the *SRN-3*, and *MB-NDI-3* was higher that selection of EW per se.

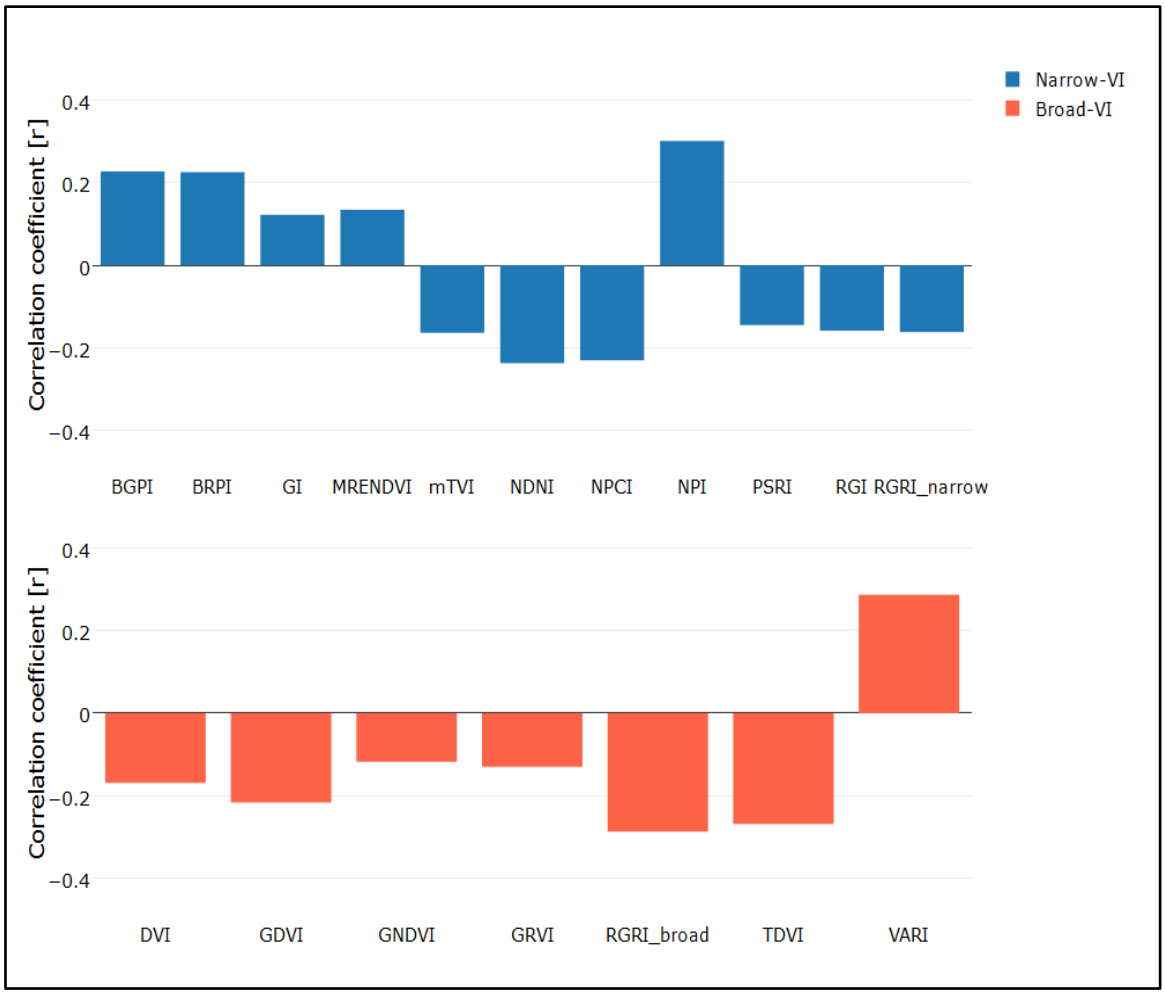

Fig. 19 Pearson correlation coefficients of the EW load and the narrow and broad vegetation indices (VI).

Table 14 Average response of the phenotypic and genotypic correlation of EW with the developed indirect selection methodologies (ISM), the response to selection (RS), correlated response (CR) and relative efficiency of selection (RE) of the trait for selection of EW, as well as the genetic advance respect to the mean (GAM). All parameters were estimated in the validation data sets of the four trials evaluated in 2013 and 2014.

Trait	**CV (%)**	**h^2**	r_p	r_g	**R**	**CR**	**RE**	**GAM**	**R^2**	**RMSE**
EW	21.33	0.29	-	-	1.31	-	-	23.29	-	
SRB-1 $\frac{\mathbf{Red}}{\mathbf{Green}}$	3.5	0.42	-0.43	-0.51	0.026	-0.037	-1.3	-5.01	0.14	0.47
DIB -2 Red-Blue	16.25	0.42	-0.43	-0.48	0.005	-0.15	-31.31	9.68	0.22	0.36
DIB -3 Red-Green	15.81	0.43	-0.45	-0.45	0.004	-0.14	-35.0	10.42	0.24	0.36
NDIN-1 $\frac{\mathbf{Red-Blue}}{\mathbf{Red+Blue}}$	4.83	0.51	-0.43	-0.55	0.012	-0.04	-3.33	5.56	0.14	0.48
SRN-3 $\frac{\mathbf{1177}}{\mathbf{1273}}$	0.84	0.14	-0.44	-0.69	0.003	-0.13	-43.33	2.8	0.22	0.15
MB-SR-1	4.77	0.62	0.51	0.83	0.087	0.08	0.92	8.53	0.23	0.26
MB-DI-2	4.87	0.49	0.48	0.55	0.021	0.19	9.05	11.89	0.29	0.27
MB-NDI-3	4.35	0.53	0.51	0.75	0.062	0.07	1.13	6.37	0.21	0.33

3.3.7 Efficiency of indirect phenotyping of EW with aerial hyperspectral imagery

The spectral bands captured with the aerial sensor and EW load had a similar association to the ground base spectral information and EW. With the aerial sensor, a negative response of the reflectance was found as the EW content increases. However, this spectral response was stronger at the visible range, and minimum change was detected at the NIR. The indices *DIB -2* $_{Red-Blue}$, *DIB -3* $_{Red-Green}$, and *MB-DI-2* were calculated using the airborne spectral information, and the correlation coefficients were 0.18, -0.18, -0.18 and -0.05, respectively.

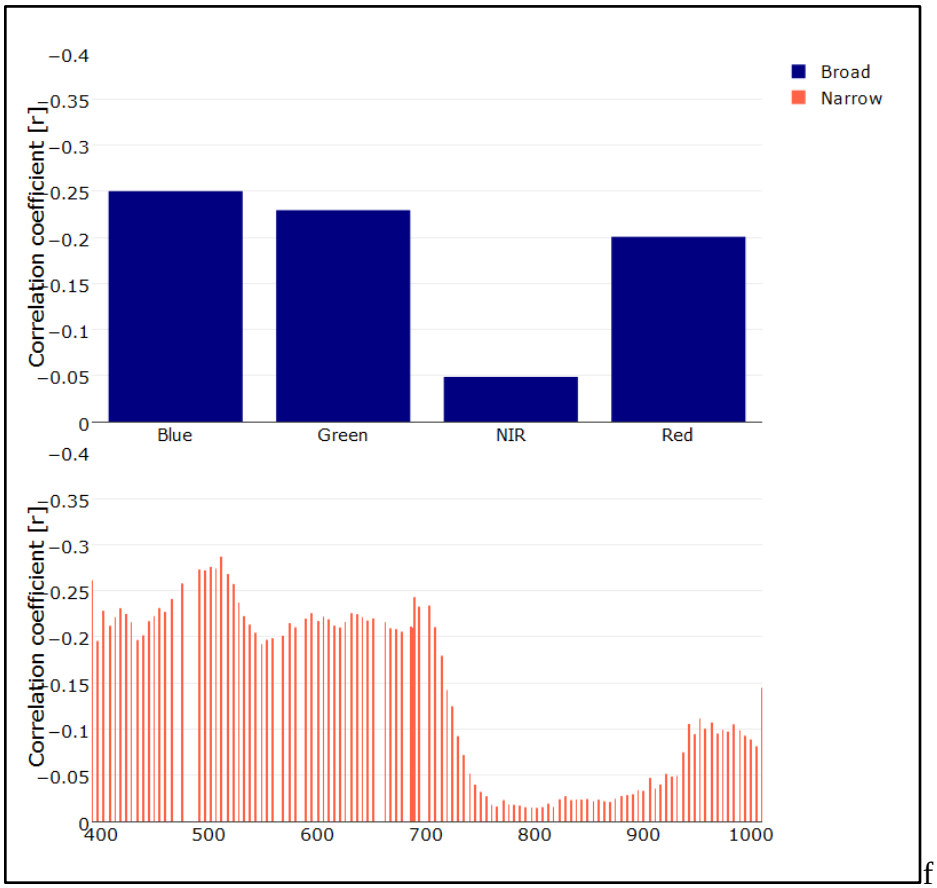

Fig. 20 Pearson correlation coefficients of the EW content in leaves and the hyperspectral information acquired with the aerial sensor.

3.4 Discussion

Epicuticular wax is a product of not only the genetic effect, but is also influenced by the environment. In the present study, the mean values of the genotypes evaluated ranged from the 3.02 to 7.61 mg/dm^2. One of the main goals in selection is to capture a large proportion of the genetic variability through phenotyping. In the case of EW, the average estimate of the h^2 across the four trials was 0.29, relatively low compared to other agronomic traits such are height and grain yield. However, the h^2 of the trial HS-II was 0.66, with a coefficient of variation (CV) of 6.97. The development of a high-throughput method for EW will provide a more accurate estimation of the genetic variation by increasing the number of replications for evaluation and the decreasing the experimental error.

3.4.1 Associated response of the canopy reflectance with EW

The wavelength at the NIR and SWIR were strongly associated to the EW load. As the EW content increased, the light reflectance decreased. The response of the visible region differed to the rest of the spectrum, where the violet region was positively associated to EW. The spectral bands selected with the derivative analysis and the SPLSR overlap with absorption bands for carotenoids, chlorophyll and water, and with spectral bands that are highly influenced by the light scattering of the mesophyll cells. Thus, it is reasonable to think that the EW load has a direct impact of main physiological process of the plant.

3.4.2 Empirical indices and linear models for phenotyping EW

The narrow band indices that best estimate EW combined water absorption bands at the 0.9 μm, 1.1 μm and 1.2 μm, and the broad band indices integrated the red, green and blue wavelengths of the visible range. The broad bands are directly associated with absorption and reflectance of the photosynthetic light. Heritability of the broad band indices was superior, compared to the estimated with the colorimetric method. Although nine of the narrow band indices were statistically associated to EW, these indices were not able to capture any additive genetic variation, except for the *SRN-3* index. The integration of the significant associated band ratios, as a function of the EW, increased the accuracy of the prediction up to 46%. The linear models that had the highest h^2 estimates are the *MN-SR-1*, *MB-DI-2*, and *MN-NDI-3* with 0.62, 0.49 and 0.53, respectively.

The moderate to strong genetic correlation of the indices/model and EW indicates the potential use of these indirect selection approaches to identify wheat genotypes with high EW load. Compared to the direct selection with the colorimetric method, the indirect selection with the *DIB-2*, *DIB-3* and the *SRN-3* is 31, 35 and 43 more efficient. The percentage of genetic advance was not superior to the genetic gains with the conventional methods. Through indirect selection, the *DIB-2*, *DIB-3,* and *MB-DI-2* had the highest genetic gain.

3.5 Conclusions

Consistent results suggest the possibility of using these spectral indices/models as proxy measurements to understand the genetic and physiological basis of EW. The relative higher heritability and the moderated to strong genetic correlation of the *DIB-2*, *DIB-3,* and *MB-DI-2* provides a reliable estimation of EW for selection under field conditions. The application of these indirect selection methods will facilitate the acquisition of multiple measurements throughout the growing season and accurately capture the variation of EW. In this study, we state that spectral reflectance can be used in plant breeding platforms not only for indirect selection, but as a component in an integrative selection in the breeding pipeline.

CHAPTER IV

SELECTION INDICES FOR HEAT STRESS IMPROVEMENT IN WHEAT

4.1 Introduction

Wheat is the most important source of calories in developing countries, and contributes to approximately 19% of the global dietary energy (Ray et al. 2013). The projected increase of the population to 9.1 billion by 2050 will require an increase in the wheat production by 60% worldwide (Rosegrant and Agcaoili 2010). In order to fulfill this demand, grain yield has to increase 2.4% annually (Ray et al. 2013). Nonetheless, the rise of the global mean temperature and changes on the frequency and intensity of rainfall will directly impact the productivity of wheat (Wheeler and von Braun 2013), undermining the future of global food security. To ensure the stability of the whole food system, it is necessary to develop superior wheat lines with resilience to climate change.

Advances in the genetic gain of GY have been mainly achieved using classical empirical approaches. The development of high-throughput genomic and phenomic methods may transform conventional breeding methodologies and facilitate the dissection of polygenic and complex traits. Methods such as genomic selection (GS) have enabled the identification of superior genotypes based on the merit of genetic markers, but phenotypic information is still required for the calibration of training sets. Compare to genomics, advances on phenomics is still limited. The development of novel methodologies for proximal sensing phenotyping promises to transform plant

characterization and facilitate the improvement of quantitative traits, particularly those related to yield and stress tolerance.

Proximal remote sensing provides a rapid and non-destructive characterization of plants (Araus and Cairns 2014), facilitating the screening of large breeding populations and germplasm (Reynolds et al. 2015). The most recent and intensify efforts in phenotyping have adapted machinery and electronic sensors for field-based plant characterization. These integrate systems collect information of the normalized difference index (NDVI), the leaf area (LAI) and hyper and multispectral imagery (Lan et al. 2009); as well as canopy height, and plant temperature (Andrade-Sanchez et al. 2014). Additional traits such as chlorophyll, carotenoids and water content can also be estimated by detecting variations of the canopy reflectance at specific wavelengths of the electromagnetic spectrum. This spectral response indicates the plant physiological status, and can potentially be used as a proxy estimator of grain yield (GY).

GY is a complex polygenic trait that is driven by the intercept of the solar radiation, the efficiency converting the solar energy into chemical energy, and the harvest index (Hay and Walker 1989). (Reynolds, Dreccer, and Trethowan 2007) defined specific conceptual models for GY according to main drivers that simultaneously group physiological and morphological adaptive traits for high temperature and water-limited environments. Under heat stress, the main drivers of GY are light interception (LI), radiation use efficiency (RUE) and harvest index (HI) (Cossani and Reynolds 2012). In terms of phenotyping, physiological and morphological from LI and RUE can be remotely estimated with radiometric approaches. In 2006,

(Babar, Reynolds, et al. 2006) reported one of the first efforts to associate GY and plant canopy reflectance. A clear response of the spectral bands related to water content and GY was found during heading and grain filling under irrigated and reduced irrigation conditions (Babar, van Ginkel, et al. 2006).

Genetic gains of GY in wheat have been achieved with selection based on multiple highly correlated morphological traits. However, little attention has had the selection based on multiple physiological traits for the LI and RUE. The goal of this study is to define the link of canopy reflectance with GY and components of GY, and evaluate the potential of multiple-trait selection with canopy reflectance. Through the development of selection indices, we aim to better understand the physiological response of wheat under heat stress and break through the application of high-throughput phenotyping technologies for indirect selection of GY. The results of this study will facilitate the selection of superior genotypes in early generations, and reduce the confounding effect of environmental drift.

4.2 Materials and methods

4.2.1 Plant material and experimental sites

Three panels of spring wheat landraces and products of interspecific hybridization with wild ancestors were grown during the 2012-2013 and 2013-2014 crop season at the Norman E. Borlaug Experimental Station (CENEB), Ciudad Obregon, Sonora in Northwest Mexico (27.20°N, 109.54°W, 38 masl). A total of 216 genotypes were grouped in 2013 (trial I), and 266 in 2014 (trial II and III). The trials were arranged as an alpha-lattice design with two replications under the raised bed system with two rows per

bed, an inter-row spacing within each bed of 10 centimeters (cm), and a space between beds of 80 cm. All traits were established the last week of February, approximately 90 days after the optimal planting date in the Yaqui Valley, Mexico. This delay on the planting date exposed the plants to average daily temperatures of 28°C and maximum temperatures of 39°C during heading and anthesis. Reduced irrigation was also provided for the trial II,

4.2.2 Grain yield and yield component

Samples of 1 m^2, using a quadrant as reference, were collected soon after physiological maturity (GS87). Fresh weight was recorded and the samples were dried in an oven 75ºC for 48 hours. A sub-sample of 50 fertile culms was separated and the number of spikes m^{-2} (SNO), grain number m^{-2} (GNO), thousand grain weight (TGW), biomass (BIO) and harvest index (HI) were estimated as described by (Pietragalla and Pasl 2012).

4.2.3 Radiometric measurements

Canopy reflectance was collected from 11AM to 1PM by placing the optic fiber of a spectroradiometer 40 centimeters (cm) above the canopy. The spectral information was captured with a FieldSpec 4 Hi-Res spectroradiometer in 2151 continuous bands with a spectral resolution of 3 nanometers (nm) from 0.35 to 0.7 µm, and 8 nm from 1.4 to 2.1 µm. The equipment was radiometrically calibrated with a white BaSO4 reference card for the 100% of reflectance, and by blocking the light intercepted by the optic fiber for 0% of reflectance. Ten readings were obtained along the plots. The mean of the spectral signatures captured per plot was calculated, and only the average response was considered for further analysis.

4.2.4 Analysis of variance (ANOVA) and correlation

The GY, SNO, GNO, TGW, HI and BIO were subject to an analysis of variance (ANOVA). The ANOVA was calculated with the PROC GLM procedure using the Statistical Analysis System (SAS) software version 9.2 (SAS, Cary, NC). The statistical model was established for an alpha-lattice experimental design:

$$\boldsymbol{Y_{ijk} = \mu + G_i + R_j + \beta_k(R_j) + \varepsilon_{ijk}} \begin{pmatrix} \boldsymbol{i = 1 \ldots 266} \\ \boldsymbol{j = 1 \ldots 2} \\ \boldsymbol{k = 1 \ldots 12} \end{pmatrix}$$

In this model, Y_{ijk} is the response variable that represents the genotype *i*, observed in the replication *j*, and in the *kl* block; μ is the general overall mean; G_i is the additive effect of the i^{th} genotype; R_j is the effect of the j^{th} replication; $\beta_k(R_j)$ is the effect of the k^{th} block within the j^{th} replication; and ε_{ijk} is the random error effect for the i^{th} genotype, in the j^{th} replication and the k^{th} block within the j^{th} replication. The phenotypic (σ_p^2) and genotypic σ_g^2 variance were estimated as follow: $\sigma_g^2 = \frac{[(msg)-(mse)]}{r}$ and $\sigma_p^2 = \sigma_g^2 + \frac{\sigma_e^2}{r}$, where *msg* and *mse* correspond to the mean square of the genotypes and the error, respectively, σ_g^2 is the genetic variance, σ_p^2 the phenotypic variance, σ_e^2 the error variance, and *r* is the number of replications. The reported estimates of the heritability in broad sense (h^2) were calculated according to the formula describes by (Allard 1960): $h^2 = \frac{\sigma_g^2}{\sigma_p^2}$. Phenotypic correlations and the covariance matrix of all parameters were calculated using the PROC CORR procedure including the COV option in the statement in SAS. The genotypic correlations (σ_g) were estimated as follow: $\sigma_g = \frac{COV_{XY}}{\sqrt{Var_x Var_y}}$,

where COV_{XY} corresponds to the covariance estimate of the GY components, BIO and HI with GY, Var_x is the variance of GY component, BIO or HI, and Var_y is the variance of the GY. The genotypic correlations (σ_g), the expected response to selection (*R*), the correlated response to selection (*CR*) the relative efficiency of indirect selection (*RE*) were all estimated according to (Falconer 1989).

$\sigma_g = \frac{COV_{XY}}{\sqrt{Var_x Var_y}}$, where COV_{XY} corresponds to the covariance estimate of the vegetation index and GY, Var_x corresponds to the variance of the spectral index, and Var_y is the variance of the GY.

$R = h_x \sigma_x$, where h_x is the square root of the heritability and σ_x the genotypic standard deviation.

$CR = h_x r_{gx} \sigma_{gy}$, where the h_x is the square root of the heritability for the trait *X* (spectral index), r_{gx} is the genetic correlation of the spectral index and GY, and σ_{gy} is the genotypic standard deviation of the trait *Y* (GY).

$RE = \frac{CR}{R}$, where *CR* is the correlated response to selection and *R* is the expected response to selection of the trait.

4.2.5 Two samples t-test

The narrow bands of the spectral signatures were averaged into three main spectral regions: the visible (0.4 to 0.748 µm), the red-edge (0.691 to 0.730 µm), the near infrared (NIR 0.751 to 1.399 µm) and the short-wave infrared (1.4 to 2.398 µm). These signatures were grouped into two sets. These sets contained the spectral signatures within 1+/- the standard deviation (SD) from the mean of GY, respectively. A two

samples *t*-test was conducted under the null hypothesis that the difference of the spectral response of these two sets is equal to cero (H_0: $\mu_1 - \mu_2 = 0$). This null hypothesis was tested under the assumption of similar standard deviations: $t = \frac{\overline{x_1} - \overline{x_2}}{s_p\sqrt{\frac{1}{n_1}+\frac{1}{n_2}}}$. In this equation, $\overline{x_1}$ and $\overline{x_2}$ correspond to the average reflectance of the high and low GY genotypes, respectively, s_p is the pooled SD, and n_1 and n_2 are the number of observations included in every sample. The pooled SD was calculated with the follow equation: $s_p = \sqrt{\frac{(n_1-1)s_1^2+(n_1-1)s_2^2}{n_1+n_2-2}}$, where s_1^2 and s_2^2 are the SD of the group 1 and 2. All results were confirmed with the *t.test* function, and the confidence interval to the specific alternative hypothesis estimated with the *conf.int* in the software R.

4.2.6 First derivative of the spectrum

The first derivative of the spectral response was calculated to enhance important spectral features. The analysis estimates the rate of change of the reflectance respect to the wavelength by calculating the changes in the curvature of the spectrum at the specific interval of the signal. The derivatives were computed within a window size of 11 nm using the *savitszkyGolay* function included in the package *prospect* (Stevens 2014). This function applies the Savitzy-Golay filter (Bromba and Ziegler 1981)before the derivative is estimated.

$$x_j * = \frac{1}{N}\sum_{h=-k}^{k} c_h x_j + h$$

In this equation, the x_j* represents the new value obtained after the first or second derivative was estimated, *N* is a normalizing coefficient, *k* is the number of neighbor values at each side of *j*, and c_h are pre-computed coefficients that depend of the polynomial order and degree. Pearson correlation coefficients were estimated with the *corr* function to identify the associated derivate regions of the spectrum with GY.

4.2.7 Sparse partial least square regression (SPLSR)

SPLSR is a supervised multivariate technique that is based on the principle of partial least square regression (PLSR) and lies in the dimentionally reduction and multiple regression to confront situations where there exist highly correlated predictor variables and relative few samples. Although the PLSR is able to achieve good predictive performance, the linear combinations are complex and dificult to be interpreted. In this study the SPLSR was conducted for three hundred and twenty six spectral bands with a resolution of 3 nm were integrated as the matrix with the dependent variables (X') for prediction of EW. The analysis was conducted with the *spls* function in the software R, the sparcity tuning parameter *'eta'* and *'K'* were assigned according the specifications in the *spls* package version 1.0 (Chung 2012).

4.2.8 Spectral vegetation indices

Broad and narrow spectral vegetation indices (SVI) associated to leaf pigments, light use efficiency, leaf area, red-edge, plant water content and plant greeness were estimated to evaluate the physiological response of the plant (Table 12 and Table13). SVI's combine the spectral information at specific wavelength using simple mathematical formulas to

obtain an estimator of the plant characteristic. All SVI's were calculated in the R statistical package version 2.15.2 (Team 2008).

4.2.9 Selection indices

Selection indices are linear combinations of variables to simultaneously select multiple traits while achieving maximum advance on genetic gain (GG). In this study, the first set of indices was developed with the components of GY, BIO and the HI. The second set of indices incorporated regions of the electromagnetic spectrum selected with the derivative and the PLSR analysis. The selection indices integrating the narrow and broad vegetation indices were analyzed separated for every index and by combining them. The selection theory based on indices was first proposed by (Smith 1936)considering the phenotypic information, the heritability estimates and the genetic correlation of the traits. The selection indices are derived as simple linear combinations: $Y = \beta' p$ and $Z = \theta' g$ where Y corresponds to the selection index, $\beta' = [b_1, \ldots\ldots, b_n]$ is the vector with the coefficients of the index, $p' = [p_1, \ldots\ldots, p_2]$ is the vector with the phenotypic values of y; Z represents the breeding values, and $\theta' = [w_1, \ldots\ldots, w_n]$ is the vector of economic weights. The Smith method is defined as S^{-1}, which is the inverse of the variance-covariance matrix, used to define the coefficients assigned to every genotype, $\beta_s = S^{-1} \sum \theta$. To define the specific relationship between the phenotypic values, and the estimated genotypic values, (Smith 1936) establish a model for phenotypic information: $P_j = g_j + \epsilon_j$. In this model P_j is the phenotypic information, g_j is the genotypic value at the *jth* observation with additive effects, and ϵ_j the random error and it was assumed that interaction of both factors was random. The selection coefficients with the Smith's

method were estimated in the SI-R Coded for Computing Selection Indices in R (Alvarado, Perez-Elizalde, and Ceron 2015) The genetic gain (ΔG) per cycle of selection for the 5% of the selected genotypes was estimated as follow: $\Delta G = h^2\ SED$. In this formula, the SED is the selection differential of the population mean and the mean of the selected individuals, $SED = \overline{x_p} - \overline{x_s}$, where $\overline{x_p}$ is the mean of the population before selection, and the $\overline{x_s}$ is the mean of the selected genotypes. The accuracy of prediction of the indices was estimated with the correlation (r) of the selection coefficients and the breeding values.

Table 15 Narrow band spectral indices for leaf pigments and light use efficiency.

NAME		FORMULA	REFERENCE
	LEAF PIGMENTS		
Carotenoid Reflectance Index-1	CRI-1	$\frac{1}{\rho_{510}} - \frac{1}{\rho_{550}}$	(Gitelson, Zur, et al. 2002)
Carotenoid Reflectance Index-2	CRI-2	$\frac{1}{\rho_{510}} - \frac{1}{\rho_{700}}$	(Gitelson, Zur, et al. 2002)
Anthocyanin Reflectance Index	ARI	$\frac{1}{\rho_{550}} - \frac{1}{\rho_{700}}$	(Gitelson, Merzlyak, and Chivkunova 2001)
Blue Green Pigment Index	BGPI	$\frac{\rho_{450}}{\rho_{550}}$	(Zarco-Tejada et al. 2005)
Blue Red Pigment Index	BRPI	$\frac{\rho_{450}}{\rho_{690}}$	(Zarco-Tejada et al. 2005)
Normalized Phaeophytinization Index	NPI	$\frac{\rho_{415} - \rho_{435}}{\rho_{415} + \rho_{435}}$	(Barnes et al. 1992)
	LIGHT USE EFFICIENCY		
Photochemical Reflectance Index	PRI	$\frac{\rho_{531} - \rho_{570}}{\rho_{531} + \rho_{570}}$	(Gamon, Serrano, and Surfus 1997)
Structure Insensitive Pigment Index	SIPI	$\frac{\rho_{800} - \rho_{450}}{\rho_{800} + \rho_{650}}$	(Panuelas et al. 1995)
Red Green Ratio Index	RGRI	$\frac{\sum_{i=600}^{699} R_i}{\sum_{i=500}^{599} R_j}$	(Gamon and Surfus 1999)

Table 16 Narrow band vegetation indices for leaf area and plant water content.

NAME		FORMULA	REFERENCE
	LEAF AREA		
Modified Triangular Vegetation Index	MTVI	$1.2[1.2(\rho_{800}-\rho_{550})-2.5(\rho_{670}-\rho_{550})]$	(Haboudane et al. 2004)
	RED-EDGE INDICES		
Red-edge position	ReP	$700+40\left[\frac{\rho_{670}+\rho_{780}}{2}-\rho_{700}\right]/(\rho_{740}-\rho_{700})$	(Gayout, Baret, and Major 1988)
Vogelmann Index-1	VGI-1	$^{740}/_{720}$	(Vogelmann, Rock, and Moss 1993)
Vogelmann Index-2	VGI-2	$\frac{\rho_{734}-\rho_{747}}{\rho_{715}-\rho_{726}}$	(Zarco-Tejada et al. 2003)
Vegetation Stress Ratio	VSR	$^{725}/_{702}$	(White, Williams, and Barr 2008)
Modified Red-edge Normalized Difference Vegetation Index	MRENDVI	$\frac{\rho_{750}-\rho_{705}}{\rho_{750}+\rho_{705}-2*\rho_{455}}$	(Datt 1999)
	PLANT WATER CONTENT		
Water Index	WI	$^{970}/_{900}$	(Penuelas et al. 1993)
Moisture Stress Index	MSI	$\frac{\rho_{1599}}{\rho_{819}}$	(Hunt and Rock 1989)
Simple Ratio Water Index	SRWI	$\frac{\rho_{860}}{\rho_{1240}}$	(Zarco-Tejada, Rueda, and Ustin 2003)

Table 17 Narrow band vegetation indices for plant greenest.

NAME		FORMULA	REFERENCE
	PLANT GREENEST		
Normalized Difference Vegetation Index	NDVI	$\frac{\rho_{800} - \rho_{640}}{\rho_{800} + \rho_{640}}$	(Rouse et al. 1974)
Plant Scenecense Reflectance Index	PSRI	$\frac{\rho_{680} - \rho_{500}}{\rho_{750}}$	(Merzlyak et al. 1999)
Reg-green Ratio Index	RGI	$\frac{\rho_{690}}{\rho_{550}}$	(Gamon and Surfus 1999)
Greenest Index	GI	$\frac{\rho_{554}}{\rho_{677}}$	(Zarco-Tejada et al. 2005)
Normalize Difference Nitrogen Index	NDNI	$\frac{\log\left(\frac{1}{\rho_{1510}}\right) - \log(\frac{1}{\rho_{1680}})}{\log\left(\frac{1}{\rho_{1510}}\right) + \log(\frac{1}{\rho_{1680}})}$	(Serrano, Penuelas, and Ustin 2002)
Normalized Pigment Chlorophyll Index	NPCI	$\frac{\rho_{680} - \rho_{430}}{\rho_{680} + \rho_{430}}$	(Penuelas et al. 1994)
Pigment Specific Simple Ratio for Chlorophyll *a*	PSI-*a*	$\frac{\rho_{800}}{\rho_{675}}$	(Blackburn 1998)
Pigment Specific Simple Ratio for Chlorophyll *b*	PSI-*b*	$\frac{\rho_{800}}{\rho_{650}}$	(Blackburn 1998)
Transformed Chlorophyll Absorption Ratio Index	TCARI	$3[(\rho_{700} - \rho_{670}) - 0.2(\rho_{700} - \rho_{550})(\rho_{700}/\rho_{670})]$	(Haboudane et al. 2002)

Table 18 Broad spectral indices for leaf pigments, leaf area and plant water content.

NAME		FORMULA	REFERENCE
	LEAF PIGMENTS		
Modified Anthocyanin Reflectance Index	mARI	$\left[\left(\frac{1}{\rho_{\text{Green}}}\right) - \left(\frac{1}{\rho_{\text{Red edge}}}\right)\right] * \rho_{\text{NIR}}$	(Gitelson, Keydan, and Merzlyak 2006)
Anthocyanin Reflectance Index	ARI	$\frac{\rho_{\text{GREEN}}}{\rho_{\text{NIR}}}$	(Berg and Perkins 2005)
	LEAF AREA		
Enhanced Vegetation Index	EVI	$2.5 * \frac{(\rho_{NIR} - \rho_{Red})}{(\rho_{NIR} + 6\rho_{Red} - 7.5\rho_{Blue} + 1)}$	(Huete et al. 1997)
Leaf Area Index	LAI	$3.618 * EVI - 0.118$	(Boegh and Soe 2002)
	PLANT WATER CONTENT		
Normalized Difference Infrared Index	NDII	$\frac{(\rho_{\text{NIR}} - \rho_{\text{SWIR}})}{(\rho_{\text{NIR}} + \rho_{\text{SWIR}})}$	(Kim et al. 2015)
Moisture Stress Index	MSI	$\frac{\rho_{\text{SWIR}}}{\rho_{\text{NIR}}}$	(Kim et al. 2015)

Table 19 Broad band vegetation indices for plant greenest.

NAME		FORMULA	REFERENCE
	PLANT GREENEST		
Soil Adjusted Vegetation Index	SAVI	$\frac{(\rho_{NIR} - \rho_{Red})}{(\rho_{NIR} + \rho_{Red} + L)} * (1 + L)$	(Huete 1988)
Normalized Difference Vegetation index	NDVI	$\frac{(\rho_{NIR} - \rho_{Red})}{(\rho_{NIR} + \rho_{Red})}$	(White, Williams, and Barr 2008)
Simple Ratio	SR	$\frac{\rho_{NIR}}{\rho_{Red}}$	(Birth and McVey 1968)
Green Normalized Difference Vegetation Index	GNDVI	$\frac{(\rho_{NIR} - \rho_{Green})}{(\rho_{NIR} + \rho_{Green})}$	(Gitelson, Kaufman, and Merzlyak 1996)
Green Difference Vegetation Index	GDVI	$\rho_{NIR} - \rho_{Green}$	(Sripada et al. 2006)
Difference Vegetation Index	DVI	$\rho_{NIR} - \rho_{Red}$	(Tucker 1979)
Red Green Ratio Index	RGRI	$\rho_{Red} - \rho_{Green}$	(Gamon and Surfus 1999)
Green Ratio Vegetation Index	GRVI	$\frac{\rho_{NIR}}{\rho_{Green}}$	(Sripada et al. 2006)
Transformed Difference Vegetation Index	TDVI	$\sqrt{0.5 + \frac{(\rho_{NIR} - \rho_{Reed})}{(\rho_{NIR} + \rho_{Reed})}}$	(Bannari, Asalhi, and Teillet 2002)
Visible Atmospherically Resistant Index	VARI	$\frac{\rho_{Green} - \rho_{Reed}}{\rho_{Green} + \rho_{Reed} - \rho_{Blue}}$	(Gitelson, Stark, et al. 2002)

4.3 Results

4.3.1 Analysis of variance and correlation of GY and components of GY

Significant differences were detected for GY (Table 14). Relative high heritability estimates were constant across environments, with close to 90% efficiency detecting the variation of the additive genetic effect of the genotypes. The SNO, GNO and TGW also had significant differences at 1% of probability, but their estimates of heritability were lower than GY per se.

All phenotypic and genotypic correlations of the components of GY with GY were statistically associated at 1% of probability (Table 14). As expected, genotypic correlations were considerably high for all three components of GY, except for TGW in the trial I, where a low correlation coefficient of 0.25 was detected. A correlated response to selection larger than 1.0 was determined for SNO and GNO with GY, but not for TGW. SNO was the only component with which indirect selection is as efficient as direct selection of GY. The strong correlation between BIO and GY suggests the potential application of BIO for indirect selection. However, h^2 estimates of BIO are significantly lower that GY, leading to a low selection efficiency of indirect selection.

Table 20 Analysis of variance, and broad sense heritability estimates for the GY (grain yield in g/m^2), SNO (spike number/m^2), GNO (grain number/m^2), TGW (thousand grain weight in g), HI (harvest index), and BIO (biomass in g/m^2).

		HS-I	HS-II	HS-III
GY	Genotype	5.36**	6.74**	14.46**
	Mean	97.06	44.18	94.75
	CV (%)	9.62	14.13	12.92
	h^2 (%)	87	88	89
SNO	Genotype	0.021**	5.89**	-
	Mean	175.94	103.19	-
	CV (%)	4.26	15.26	-
	h^2 (%)	63	61	-
GNO	Genotype	165.76**	1511025.9 **	497.78**
	Mean	3400	1854	3846
	CV (%)	9.19	25.40	13.58
	h^2 (%)	86	83	86
TGW	Genotype	18.17**	21.99**	0.0078**
	Mean	28.58	23.35	24.29
	CV (%)	6.15	7.41	3.38
	h^2 (%)	85	86	73
HI	Genotype	0.002**	0.0058**	0.006**
	Mean	0.22	0.32	0.32
	CV (%)	12.88	24.7	16.58
	h^2 (%)	72	65	79
BIO	Genotype	11178.4**	2453.25**	8327.47**
	Mean	444.48	137.53	290.84
	CV (%)	18.24	31.87	43.0
	h^2 (%)	77	72	52

CV: general coefficient of determination; h^2: broad sense heritability;
^{ns} Not significant by F-test, and * and ** Significant at 5% and 1% probability by F-test respectively.

Table 21 Phenotypic (r_p) and genotypic (r_g) correlation of components of GY with GY, response to selection (RS), correlated response (CR) and selection efficiency (SE) of indirect selection for GY, harvest index (HI), biomass in g/m^2 (BM) and spike number/m^2 (SNO).

Trait		r_p	r_g	R	CR	SE
GY	I	-	-	2.11	-	-
	II	-	-	2.81	-	-
	III	-	-	5.99	-	-
SNO	I	0.71**	0.77**	0.87	1.02	1.17
	II	0.73**	0.83**	1.41	1.12	0.79
	III	-	-	-	-	-
GNO	I	0.96**	0.96**	77.2	1.48	0.019
	II	0.96**	0.97**	745.13	1.55	0.003
	III	0.97**	0.98**	200.56	2.31	0.011
TGW	I	0.25**	0.27**	2.76	0.42	0.15
	II	0.53**	0.57**	2.84	0.92	0.32
	III	0.48**	0.60**	1.21	1.31	1.09
HI	I	0.66**	0.74**	0.03	1.04	37.80
	II	0.54**	0.74**	0.06	1.03	16.64
	III	0.77**	0.85**	0.07	1.93	29.05
BM	I	0.88**	0.94**	92.78	1.37	0.015
	II	0.87**	0.95**	42.03	1.39	0.034
	III	0.73**	0.96**	65.81	1.77	0.027

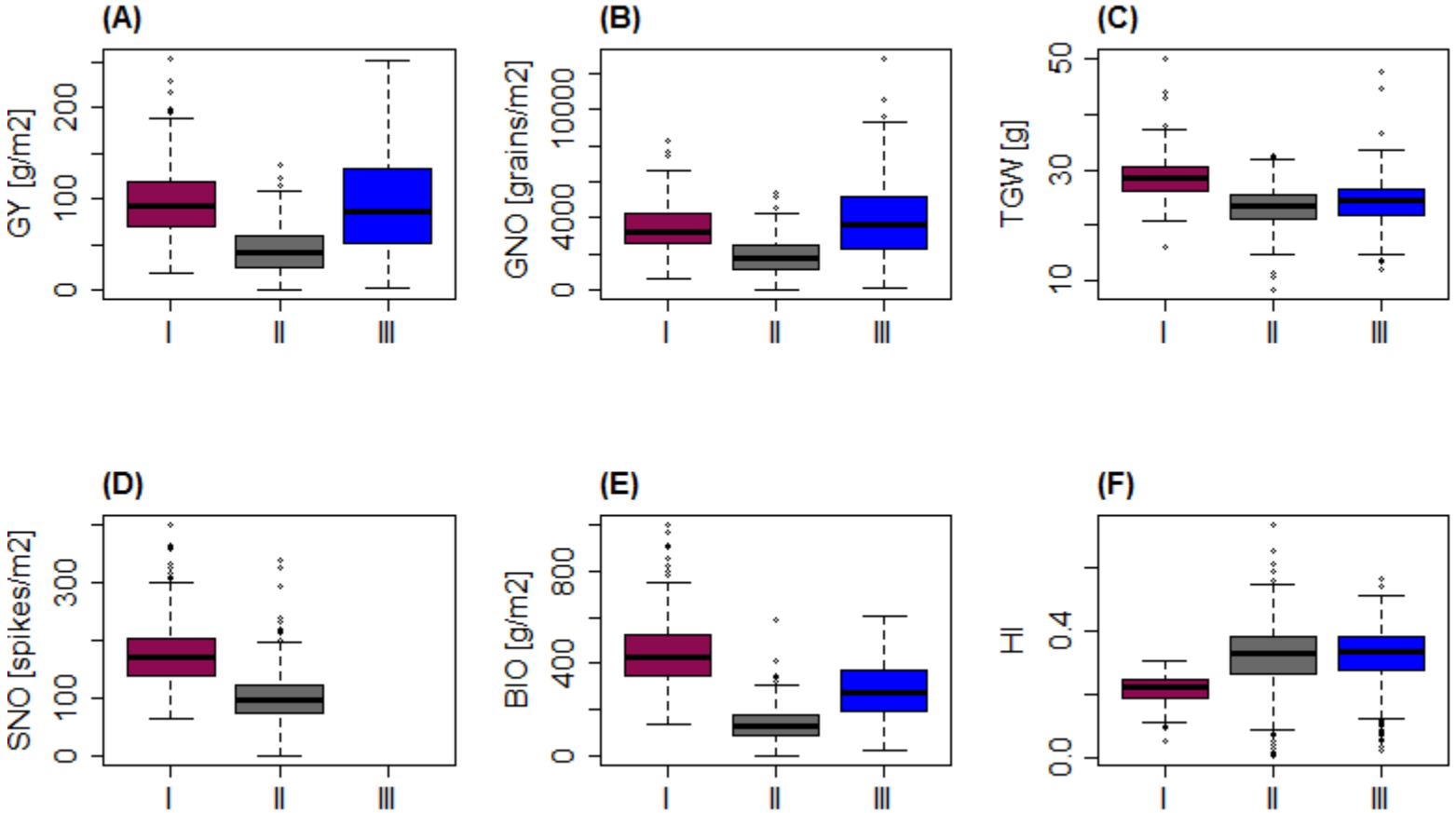

Fig. 21 Boxplot for GY (grain yield in g/m^2), GNO (grain number/m^2), TGW (thousand grain weight in g), SNO (spike number/m^2), BIO (biomass in g/m^2) and HI (harvest index) of the genotypes evaluated in 2013 (trial I) and 2014 (trial II and III).

4.3.2 Spectral features associated to GY

The light reflectance of genotypes with high GY was statistically different to the average reflectance of genotypes with low GY (Table 16). These differences were detected at the NIR and SWIR of the spectrum. The NIR region directly interacts with the spongy mesophylls cells, healthy vegetation tends to have a higher reflectance, and the SWIR is associated with absorption of water. For the visible and red-edge, no statistical differences were detected.

Table 22 Two samples t-test of the average light reflectance (LR) for the spectral signatures within 1 +/- SD from the mean of GY.

Average LR (%)						
	Wavelengths	**+1SD**	**-1SD**	**T-value**	**95% CI**	**p-value**
HI-I	Visible	0.112	0.118	-0.067	-0.023/0.022	0.94
SD=37.93	Red-edge	0.217	0.214	0.101	-0.056/0.062	0.91
	NIR	0.568	0.511	13.06	0.049/0.066	<0.01
	SWIR	0.242	0.250	-1.5132	-0.018/0.002	0.13
HI-II	Visible	0.073	0.087	-1.82	-0.029/0.0011	0.07
SD=24.07	Red-edge	0.129	0.154	-1.28	-0.064/0.014	0.21
	NIR	0.344	0.358	-4.37	-0.020/-0.008	<0.01
	SWIR	-0.039	-0.025	-9.287	-0.039/-0.025	<0.01
HI-III	Visible	0.081	0.087	-1.012	-0.018/0.006	0.31
SD=52.67	Red-edge	0.138	0.148	-0.831	-0.035/0.015	0.41
	NIR	0.287	0.276	0.643	-0.002/0.005	0.05
	SWIR	0.151	0.178	-9.69	-0.03/-0.021	<0.01

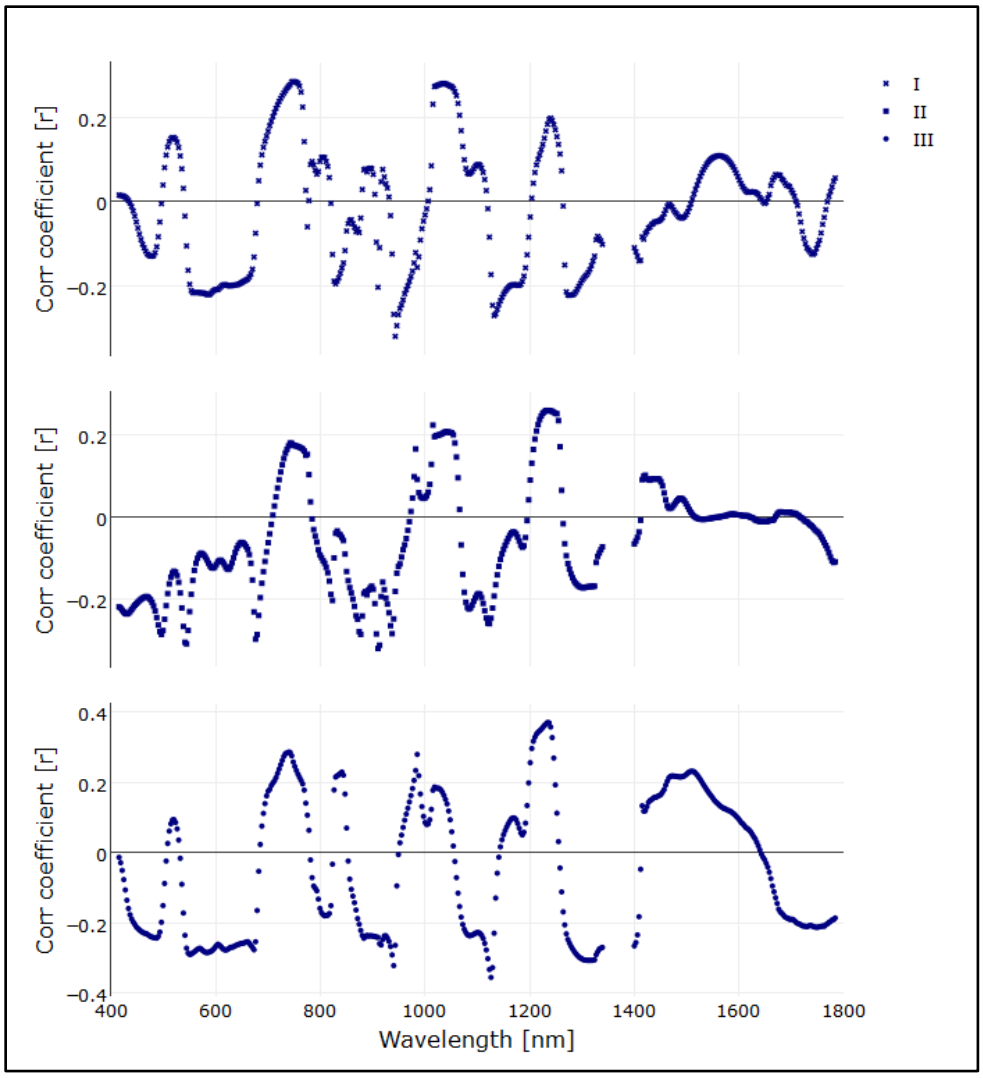

Fig. 22 Pearson correlation coefficients of the first derivative of the reflectance and GY for the trials I) HS-II, II) HS-II and III) HS-III.

The results of the derivative analysis were consistent across the environments, narrow areas of the spectrum were associated with the variation of GY (Fig. 23). Although, no differences were detected in the reflectance of the VIS region for genotypes with high and low GY, the derivative reflectance associated five VIS regions (Table 17).

Table 23 Correlation coefficients of the first derivative of the spectrum and GY.

	ID	Spectral range (nm)	Number of bands*	I	II	III
Visible	SR-D1	460-487	27	-0.12	-0.21	-0.24
	SR-D2	547-556	9	-0.20	-0.22	-0.29
	SR-D3	592-631	38	-0.21	-0.12	-0.28
	SR-D4	670-673	3	-0.15	-0.19	-0.28
	SR-D5	736-748	18	0.28	0.18	0.28
NIR	SR-D6	910-913	3	-0.15	-0.32	-0.26
	SR-D7	937-943	6	-0.24	-0.24	-0.30
SWIR	SR-D8	1015-1057	42	0.27	0.21	0.17
	SR-D9	1126-1135	9	-0.24	-0.21	-0.26
	SR-D10	1228-1252	24	0.18	0.26	0.31
	SR-D11	1267-1318	51	-0.20	-0.15	-0.29

The sparse linear combinations of the predictors are presented in Fig. 24. Coefficients equal to cero are statistically not associated with the variability of GY. The canopy reflectance of fourteen spectral regions across the spectrum were associated with GY. Overall, spectral regions detected with the derivative analysis were very similar to the detected with the PLSR, except for the spectral regions detected after the 1.3 µm.

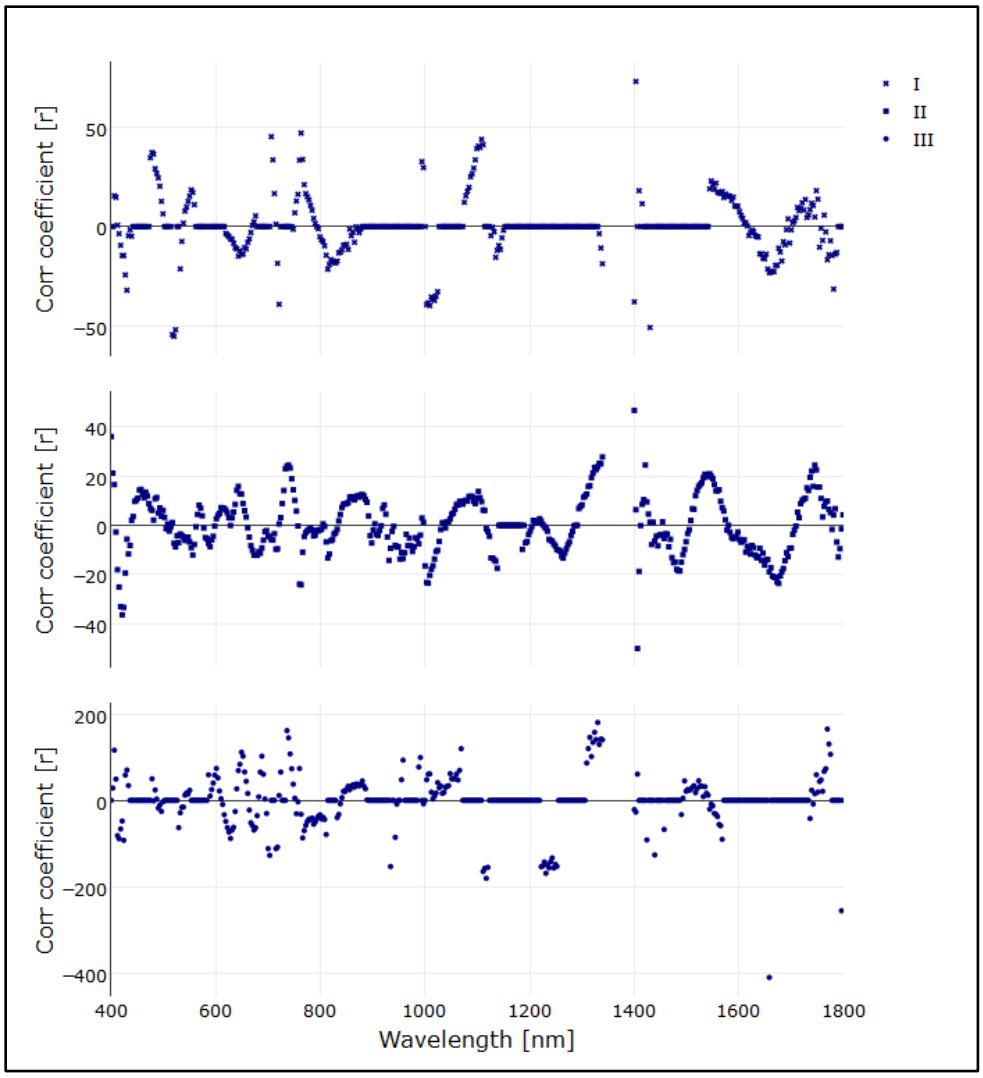

Fig. 23 Coefficient estimated in the SPLSR analysis for prediction of GY incorporating the canopy reflectance from the 0.4 to 1.8µm.

Table 24 Spectral band identified with the SPLSR analysis.

	ID	Spectral range (nm)	Number of bands*
Visible	SR-P1	406-433	27
	SR-P2	478-499	21
	SR-P3	532-550	18
	SR-P4	619-676	57
NIR	SR-P6	748-811	63
	SR-P7	832-877	45
SWIR	SR-P8	994-997	3
	SR-P9	1003-1024	21
	SR-P10	1111	1
	SR-P11	1333-1339	6
	SR-P12	1400-1403	3
	SR-P13	1544-1568	24
	SR-P14	1736-1775	39

The phenotypic correlations (r_p) of the spectral regions (SR's) and the GY were significant with 1% and 5% of probability (Table 19). The genotypic correlations (r_g), were high, but the heritability estimates were considerable lower that GY. In all cases, indirect selection of GY with the SR's is more efficient that direct selection. The negative response of the selection efficiency (SE) suggest selection towards decrease of the light reflectance of these SR's to increase GY.

Table 25 Broad sense heritability estimates, correlated response (CR), response to selection (R), and phenotypic and genotypic correlations of the selected spectral regions and GY.

Data Set	**I**	**II**	**IIII**	**I**	**II**	**III**	**I**	**II**	**III**
Vegetation index	***SR-1*** *406-433*			***SR-2*** *460-499*			***SR-4*** *592-676*		
r_p	-0.14	-0.19	-0.22	-0.14	-0.22	-0.21	-0.17	-0.24	-0.24
r_g	-0.43	-0.21	-0.57	-0.41	-0.24	-0.52	-0.52	-0.26	-0.44
h^2	0.37	0.51	0.31	0.39	0.57	0.36	0.23	0.72	0.55
R	0.0019	0.004	0.001	0.003	0.005	0.003	0.009	0.016	0.009
CR	-0.43	-0.26	-0.81	-0.43	-0.32	-0.80	-0.41	-00.38	-0.83
SE	-227.01	-75.31	-548.71	-143.3	-58.92	-331.53	-105.45	-25.31	-89.52
	SR-17 *1544-1568*			***SR-18*** *1736-1775*					
r_p	-0.15	-0.31	-0.15	-0.13	-0.31	-0.13			
r_g	-0.39	-0.46	-0.98	-0.36	-0.53	-			
h^2	0.28	0.39	0.08	0.27	0.30	-			
R	0.008	0.011	0.002	0.008	0.008	-			
CR	-0.34	-0.49	-0.71	-0.31	-0.51	-			
SE	-42.03	-44.41	-364.75	-36.94	-60.65	-			
All r_p and r_g are significant at 5% of probability or less.									

4.3.3 Vegetation indices for indirect selection of GY

Vegetation indices (VI's) were strongly associated with GY. The solid bars represent the correlation coefficients of the GY with the narrow (Fig. 25) and broad (Fig. 26) indices. Narrow band indices related to light use efficiency (PRI and SIPI), red-edge indices (VGI-2 and MRENDVI), water content (WI), and plant greenest (NDVI, PSI-a, and PSI-b) were selected to build the selection indices. Only six broad indices relevant to the leaf pigments (ARI), the red-edge indices (ReCl), plant water content (NDII) and plant greenest (SAVI, GRVI and TDVI) were chosen.

The heritability estimates of the selected VI's varied across the environments (Table 20). The lowest estimates of heritability were obtained in the trial HS-I. Genotypic correlations were all statistically significant and the response to indirect selection (RIS) was superior for all the VI's, particularly for the anthocyanin reflectance index (ARI) and the water index (WI).

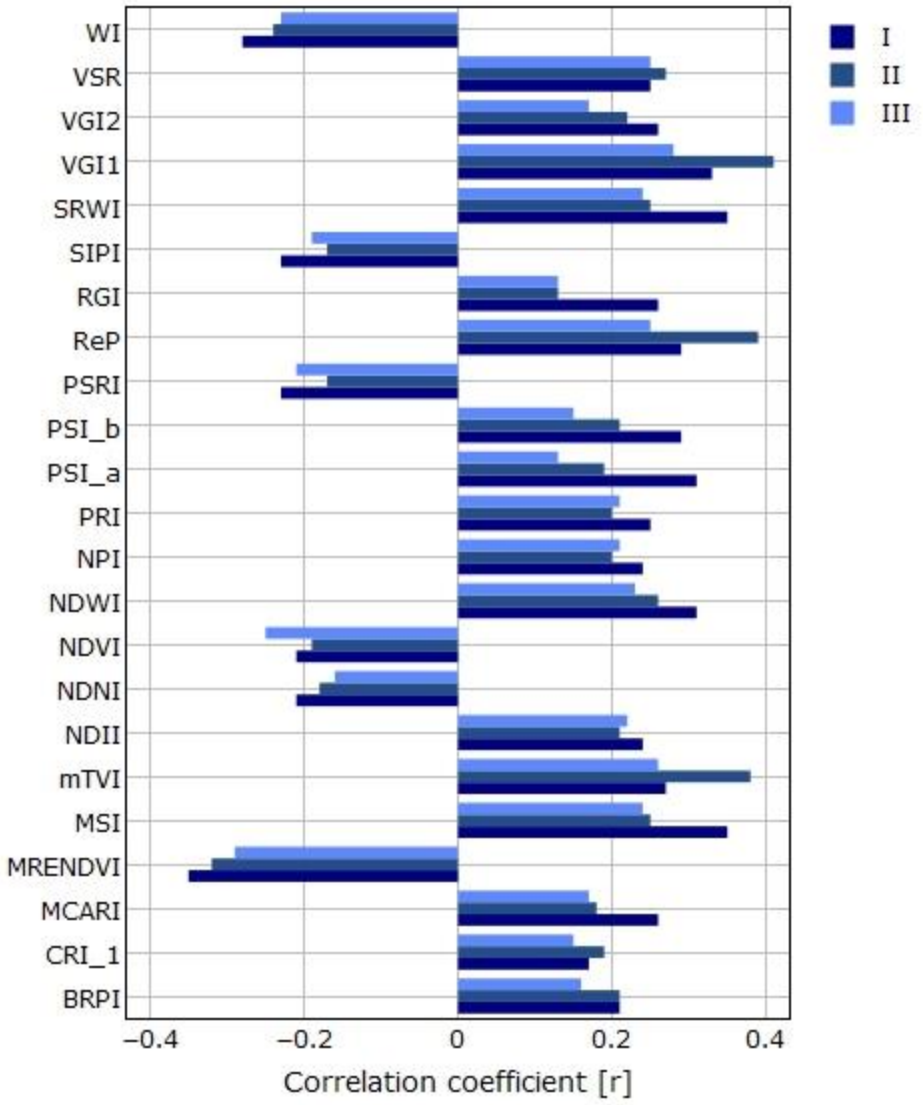

Fig. 24 Correlation coefficients of narrow band vegetation indices and GY.

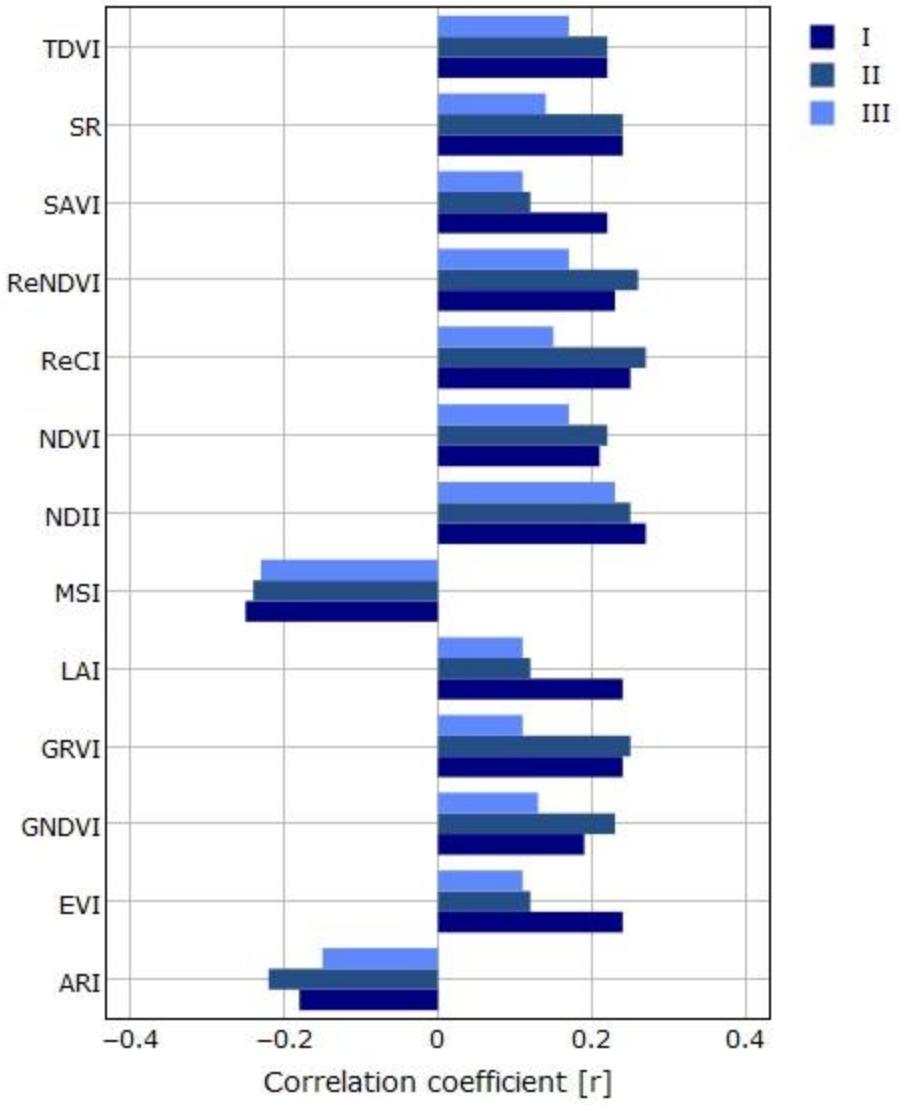

Fig. 25 Correlation coefficients of broad band indices and GY.

Table 26 Phenotypic (r_p) and genotypic (r_g) correlations of narrow and broad spectral indices, and estimates of the broad sense heritability (h^2), response to selection (R), correlated response to selection (CR) and efficiency of indirect selection.

Data Set	**HS-I**	**HS-II**	**HS-III**	**HS-I**	**HS-II**	**HS-III**	**HS-I**	**HS-II**	**HS-III**
Vegetation index	**PRI**			**SIPI**			**VGI-2**		
r_p	0.24	0.20	0.21	0.25	0.20	0.21	0.33	0.41	0.28
r_g	0.35	0.24	0.22	0.31	0.28	0.34	0.41	0.58	0.51
h^2	0.13	0.87	0.79	0.17	0.82	0.79	0.13	0.81	0.35
R	0.002	0.025	0.017	0.006	0.061	0.055	-	0.09	0.02
CR	0.21	0.39	0.50	0.22	0.44	0.77	-	0.91	0.77
RIS	97.18	15.86	29.48	34.54	7.11	14.09	-	10.15	36.28
Vegetation index	**MRENDVI**			**WI**			**NDVI**		
r_p	0.25	0.27	0.25	-0.35	-0.32	-0.29	0.24	0.21	0.22
r_g	0.32	0.36	0.31	-0.87	-0.41	-0.48	0.28	0.28	0.32
h^2	0.17	0.86	0.82	0.16	0.82	0.73	0.17	0.84	0.82
R	0.01	0.09	0.09	0.003	0.023	0.017	0.01	0.09	0.09
CR	0.22	0.58	0.72	-0.58	-0.65	-1.05	0.19	0.44	0.73
RIS	22.77	6.31	8.37	-201.38	-27.2	-62.3	19.76	4.82	8.61
Vegetation index	**PSI-a**			**PSI-b**					
r_p	0.31	0.19	0.13	0.29	0.21	0.15			
r_g	0.70	0.25	0.22	0.68	0.26	0.24			
h^2	0.11	0.84	0.72	0.11	0.84	0.73			
R	0.16	2.49	0.81	0.14	2.15	0.75			
CR	0.38	0.39	0.48	0.38	0.42	0.52			
RIS	2.34	0.16	0.59	2.61	0.19	0.69			
All r_p and r_g were significant at 1% of probability									

Table 26 Continued.

Data Set	**HS-I**	**HS-II**	**HS-III**	**HS-I**	**HS-II**	**HS-III**	**HS-I**	**HS-II**	**HS-III**
Vegetation index	**ARI**	**ReCl**	**NDII**						
r_p	-0.18	-0.22	-0.15	0.25	0.27	0.15	0.27	0.25	0.23
r_g	-0.92	-0.26	-0.40	0.47	0.36	0.30	0.43	0.37	0.31
$\mathbf{h^2}$	0.12	0.81	0.79	0.11	0.84	0.77	0.13	0.77	0.71
R	0.002	0.03	0.03	0.03	0.34	0.22	0.006	0.069	0.055
CR	-0.53	-0.41	-0.92	0.26	0.58	0.68	0.25	0.57	0.66
RIS	-265.03	-12.81	-28.59	12.25	1.72	3.18	41.98	8.12	12.18
Vegetation index	**SAVI**			**GRVI**			**TDVI**		
r_p	0.22	0.22	0.17	0.24	0.25	0.15	0.22	0.22	0.17
r_g	0.21	0.29	0.31	0.60	0.33	0.32	0.18	0.29	0.31
$\mathbf{h^2}$	0.16	0.84	0.82	0.10	0.82	0.73	0.17	0.84	0.83
R	0.006	0.06	0.053	0.07	0.85	0.49	0.003	0.029	0.029
CR	0.14	0.46	0.72	0.32	0.52	0.69	0.12	0.46	0.72
RIS	26.91	8.10	13.27	5.23	0.61	1.39	45.37	15.81	24.71
All r_p and r_g were significant at 1% of probability									

4.3.4 Selection indices with GY components, associated spectral features and vegetation indices for indirect selection of GY

The weights of the Smith-Hazel (S/H) selection index were assigned for every combination of predictors. The expected genetic gain (EGG) of GY was calculated for the top 5% of the genotypes selected with the S/H index. The relative efficiency (RE) of selection was computed considering direct selection of GY as 100% efficient. According to the results, the indirect selection with SNO and TKW is not as efficient as the direct selection with GY. The BIO and GNO both had a similar RE of close to 98%. When all these criteria were combined into the selection indices, the RE was close to ~98%, except the YCI_{11} that combines the SNO and TKW. A superior increase of 100.39 was detected when selecting with the YCI_9, that includes the GY and BIO.

The selection indices that integrate the SR's were able to predict ~40% of the RE with the direct selection. The SRI_2, SRI_5, and SRI_6 obtained the highest RE. When the SR's were combined into the selection indices, the SRI_{16}, SRI_{19}, SRI_{21}, and SRI_{24} had the highest EGG. The SRI_5, and SRI_6 correspond to water absorption band at the SWIR. The selection indices that incorporated the broad band indices all achieved a similar percentage of EGG. With these indices, not more that 37.71% EGG was obtained, except for the $BVII_{48}$ with 73.59%. The $BVII_{48}$ combines all six narrow band indices. Narrow band indices for carotenoids and water content in the plants did not reach the EGG obtained with the direct selection. However, in the case of the $NVII_6$, the index estimates 51% of the EGG. This index integrates the NDVI.

Table 27 Expected genetic gain (EGG) for the selected 5% of the genotypes, and relative efficiency of indirect selection (RE) compared with selection of GY per se incorporating the components of GY and BIO as selection indices. Biomass (BIO), and the correlation coefficient (r) of the coefficient of the index and the breeding value.

Index No.	Yield traits	EGG	*RE (%)	r
YCI_1	X_1 GY (g/m^2)	52.28	100	0.94
YCI_2	X_2 SNO/m^2	44.81	86.27	0.85
YCI_3	X_3 GNO/m^2	50.61	96.71	0.93
YCI_4	X_4 TKW(g)	21.31	44.43	0.93
YCI_5	X_5 BIO(g)	50.67	97.17	0.91
YCI_6	X1 + X2	50.42	96.51	0.91
YCI_7	X1 + X3	51.06	97.75	0.93
YCI_8	X1 + X4	52.27	99.93	0.94
YCI_9	X1 + X5	52.51	100.39	0.93
YCI_{10}	X2 + X3	50.97	97.59	0.92
YCI_{11}	X2 + X4	45.97	88.65	0.86
YCI_{12}	X2 + X5	49.71	95.41	0.89
YCI_{13}	X3 + X4	51.00	97.65	0.92
YCI_{14}	X3 + X5	51.16	97.94	0.93
YCI_{15}	X4 + X5	50.71	97.23	0.91
YCI_{16}	X1 + X2 + X3	51.05	97.74	0.93
YCI_{17}	X1 + X2 + X4	50.73	97.15	0.90
YCI_{18}	X1 + X2 + X5	50.72	97.24	0.91
YCI_{19}	X1 + X3 + X4	51.09	97.81	0.93
YCI_{20}	X1 + X3 + X5	51.23	98.08	0.93
YCI_{21}	X1 + X4 + X5	51.51	98.66	0.92
YCI_{22}	X2 + X3 + X4	51.01	97.65	0.93
YCI_{23}	X2 + X3 + X5	51.14	97.91	0.92
YCI_{24}	X2 + X4 + X5	49.85	95.70	0.89
YCI_{25}	X3 + X4+ X5	51.19	98.05	0.93
YCI_{26}	X1 + X2+ X3 + X4	51.08	97.81	0.92
YCI_{27}	X1 + X2+ X3 + X5	51.05	97.75	0.93
YCI_{28}	X2+ X3 + X4 + X5	51.17	97.96	0.93
YCI_{29}	X1 + X2+ X3 + X4 + X5	51.24	98.09	0.92
*Considering the direct selection of GY as 100% efficient				

Table 28 Expected genetic gain (EGG) for the selected 5% of the genotypes, and relative efficiency of indirect selection (RE) compared with selection of GY per se incorporating the selected spectral regions with the derivative analysis and the SPLSR in selection indices for GY, and the correlation coefficient (r) of the coefficient of the index and the breeding value.

Index No.	Yield traits	EGG	*RE (%)	r
SRI$_1$	GY (g/m^2)	60.20	100	0.86
SRI $_2$	SR1	17.64	30.38	0.73
SRI $_3$	SR2	14.74	26.81	0.59
SRI $_4$	SR4	13.67	22.43	0.52
SRI $_5$	SR17	18.76	34.01	0.58
SRI $_6$	SR18	15.48	31.11	0.59
SRI $_7$	SR1+ SR2	-60.87	-101.41	0.89
SRI $_8$	SR1+ SR4	-60.81	-101.28	0.88
SRI $_9$	SR1+ SR17	-60.81	-101.27	0.88
SRI $_{10}$	SR1+ SR18	-60.79	-101.26	0.88
SRI $_{11}$	SR2+ SR4	13.66	23.32	0.54
SRI $_{12}$	SR2+ SR17	17.08	31.22	0.58
SRI $_{13}$	SR2+ SR18	21.7	37.22	0.59
SRI $_{14}$	SR4+ SR17	16.99	29.76	0.55
SRI $_{15}$	SR4+ SR18	24.40	38.87	0.56
SRI $_{16}$	SR17+ SR18	26.42	43.37	0.55
SRI $_{17}$	SR1+ SR2+SR4	14.84	25.51	0.56
SRI $_{18}$	SR1+ SR2+SR17	17.35	31.48	0.58
SRI $_{19}$	SR1+ SR2+SR18	25.8	41.81	0.60
SRI $_{20}$	SR1+ SR4+SR17	17.35	30.39	0.55
SRI $_{21}$	SR1+ SR4+SR18	25.51	40.29	0.56
SRI $_{22}$	SR2+ SR4+SR17	16.22	28.71	0.55
SRI $_{23}$	SR2+ SR4+SR18	24.19	38.35	0.58
SRI $_{24}$	SR4+ SR17+SR18	24.94	40.28	0.56
SRI $_{25}$	SR1+ SR2+SR4+SR17	16.58	29.29	0.56
SRI $_{26}$	SR1+ SR2+SR4+SR18	23.91	38.16	0.57
SRI $_{27}$	SR-2+ SR4+SR17+SR18	22.68	37.28	0.56
SRI $_{28}$	SR1+SR-2+ SR4+SR17+SR18	-60.16	-99.91	0.88
*Considering the direct selection of GY as 100% efficient				

Table 29 Expected genetic gain (EGG) for the selected 5% of the genotypes, and relative efficiency of indirect selection (RE) compared with selection of GY per se incorporating broad band spectral indices in selection indices for GY, and the correlation coefficient (r) of the coefficient of the index and the breeding value.

Index No.	Yield traits	EGG	*RE (%)	r
BVII $_{1}$	GY (g/m^2)	185.23	100	0.92
BVII $_{2}$	X1 ARI	74.42	34.05	0.99
BVII $_{3}$	X2 ReCl	66.16	35.51	0.99
BVII $_{4}$	X3 NDII	68.11	36.31	0.84
BVII $_{5}$	X4 SAVI	78.37	37.67	0.82
BVII $_{6}$	X5 GRVI	54.39	32.22	0.99
BVII $_{7}$	X6 TDVI	76.57	37.73	0.87
BVII $_{8}$	X1 + X2	67.36	35.58	0.99
BVII $_{9}$	X1 + X3	71.28	36.26	0.95
BVII $_{10}$	X1 + X4	77.75	36.66	0.96
BVII $_{11}$	X1 + X5	55.04	32.28	0.99
BVII $_{12}$	X1 + X6	76.04	36.04	0.99
BVII $_{13}$	X2 + X3	66.82	35.83	0.97
BVII $_{14}$	X2 + X4	68.06	35.89	0.98
BVII $_{15}$	X2 + X5	57.25	33.07	0.99
BVII $_{16}$	X2 + X6	67.11	35.74	0.99
BVII $_{17}$	X3 + X4	72.87	37.09	0.83
BVII $_{18}$	X3 + X5	55.37	32.59	0.99
BVII $_{19}$	X3 + X6	70.73	36.86	0.85
BVII $_{20}$	X4 + X5	55.72	32.64	0.99
BVII $_{21}$	X4 + X6	77.83	37.71	0.83
BVII $_{22}$	X5 + X6	54.98	32.38	0.99
BVII $_{23}$	X1 + X2 + X3	67.76	35.87	0.99
BVII $_{24}$	X1 + X2 + X4	68.92	35.91	0.99
BVII $_{25}$	X1 + X2 + X5	57.71	33.11	0.99
BVII $_{26}$	X1 + X2 + X6	68.11	35.78	0.99
BVII $_{27}$	X1 + X3 + X4	73.91	36.81	0.89
BVII $_{28}$	X1 + X3 + X5	55.96	32.64	0.99
BVII $_{29}$	X1 + X3 + X6	72.47	36.61	0.93
BVII $_{30}$	X1 + X4 + X5	56.13	32.54	0.99
BVII $_{31}$	X1 + X4 + X6	77.52	36.95	0.93
BVII $_{32}$	X1 + X5 + X6	55.59	32.44	0.99
BVII $_{33}$	X2 + X3 + X4	68.31	36.11	0.95
*Considering the direct selection of GY as 100% efficient				

Table 29 Continued.

Index No.	Yield traits	EGG	*RE (%)	r
BVII $_{34}$	X2 + X3 + X5	57.87	33.31	0.99
BVII $_{35}$	X2 + X3 + X6	67.54	36.11	0.96
BVII $_{36}$	X3 + X4 + X5	56.41	32.82	0.99
BVII $_{37}$	X3 + X4 + X6	73.61	37.24	0.83
BVII $_{38}$	X4 + X5 + X6	56.08	32.63	0.99
BVII $_{39}$	X1 + X2 + X3 + X4	69.03	36.10	0.97
BVII $_{40}$	X1 + X2 + X3 + X5	58.29	33.33	0.99
BVII $_{41}$	X1 + X2 + X3 + X6	68.35	36.01	0.98
BVII $_{42}$	X2 + X3 + X4 + X5	58.62	33.45	0.99
BVII $_{43}$	X2 + X3 + X4 + X6	68.85	36.22	0.94
BVII $_{44}$	X3 + X4 + X5 + X6	56.89	32.94	0.99
BVII $_{45}$	X1 + X2 + X3 + X4 + X5	59.01	33.48	0.99
BVII $_{46}$	X1 + X2 + X3 + X4 + X6	69.49	36.21	0.96
BVII $_{47}$	X2 + X3 + X4 + X5 +X6	58.96	33.54	0.99
BVII $_{48}$	X1 + X2 + X3 + X4 + X5 + X6	152.76	73.59	0.99
*Considering the direct selection of GY as 100% efficient				

Table 30 Expected genetic gain (EGG) for the selected 5% of the genotypes, and relative efficiency of indirect selection (RE) compared with selection of GY per se incorporating narrow band spectral indices in selection indices for GY, and the correlation coefficient (r) of the coefficient of the index and the breeding value.

Index No.	Yield traits	EGG	*RE (%)	r
NVII $_{1}$	GY (g/m^2)	71.96	100	0.99
NVII $_{2}$	X1 PRI	24.43	32.74	0.81
NVII $_{3}$	X2 SIPI	19.95	27.58	0.77
NVII $_{4}$	X3 MRENDVI	24.95	39.57	0.99
NVII $_{5}$	X4 WI	21.11	30.01	0.67
NVII $_{6}$	X5 NDVI	36.62	50.48	0.99
NVII $_{7}$	X6 PSI-a	18.34	25.58	0.64
NVII $_{8}$	X7 PSI-b	22.84	30.57	0.99
NVII $_{9}$	X3 + X5	30.88	45.57	0.99
NVII $_{10}$	X1 + X5	33.28	44.71	0.95
NVII $_{11}$	X1 + X3 + X5	29.29	43.08	0.99
NVII $_{12}$	X2 + X3 + X5	27.88	40.62	0.99
NVII $_{13}$	X1 + X2 + X3 + X5	27.41	39.67	0.99
NVII $_{14}$	X3 + X4 + X5	26.53	39.03	0.99
NVII $_{15}$	X3 + X5 + X6	26.03	37.94	0.99
NVII $_{16}$	X2 + X3	25.43	37.84	0.99
NVII $_{17}$	X4 + X5	27.15	37.69	0.77
NVII $_{18}$	X1 + X3	24.29	37.51	0.99
NVII $_{19}$	X1 + X4 + X5	27.09	37.33	0.76
NVII $_{20}$	X2 + X3 + X4 +X5	25.36	36.89	0.99
NVII $_{21}$	X1 + X2 + X3	24.98	36.86	0.99
NVII $_{22}$	X1 + X2 + X5	27.27	36.84	0.85
NVII $_{23}$	X1 +X2 + X3 + X4 + X5	25.36	36.66	0.99
NVII $_{24}$	X3 + X4	23.67	35.75	0.99
NVII $_{25}$	X2 + X5	25.94	35.49	0.89
NVII $_{26}$	X3 + X4 +X5 + X6	24.38	35.44	0.99
NVII $_{27}$	X1 + X3 + X4	23.64	35.34	0.99
*Considering the direct selection of GY as 100% efficient				

4.4 Discussion

The heritability estimates of the components of GY impacted the efficiency of indirect selection. Selection efficiency with the yield components was not superior to the direct selection with GY. The concept of genetic gain is based on the change in the mean performance of a population with each cycle of selection. In this study, the selection index YCI_9 that involves the GY and BIO was the only index that provided ~1% superior gains in the mean of the selected genotypes for advance to the next generation. This index also resulted to be 37 times more efficient for selection than direct selection.

Under heat stress, the canopy reflectance at the NIR and SWIR was statistically associated to GY. Similar results have already been reported for spring wheat under reduced irrigations conditions (Babar, van Ginkel, et al. 2006). The derivative response of the spectrum facilitated the separation of the reflectance peaks of overlapping bands, and narrow regions of the spectral bands related to carotenoids, chlorophyll, and water bands at the NIR and SWIR were identified.

Incorporating the specific spectral regions into selection indices, a genetic gain of approximately 50% can be achieved. These indices integrate the water absorption band *SR17*, *SR18* in combination with the *SR1* and *SR4* wavelength. Combining the broad indices ARI, ReCl, NDII, SAVI, GRVI and TDVI in the S/H selection index estimated 74% of the genetic gain obtained with direct selection. The NDVI from the narrow band indices estimate more than 50% of the genetic gain.

4.5 Conclusions

This study demonstrated that the use of spectral reflectance as indirect selection criteria can be as efficient as selection of GY per se under sever heat stress conditions. Indirect selection based on GY component did not provide any superior improvement of the EGG. The BIO is strongly associated with GY, and selection derived from this morphological trait is 97.2% as efficient as GY per se. The best results of selection were obtained with the broad band indices ARI, ReCl, NDII, SAVI, GRVI, and TDVI, with ~74% of efficiency. Closely related with BIO, the narrow band NDVI achieved 50% of the EGG obtained with direct selection.

CHAPTER V

CONCLUSIONS

Epicuticular wax is the outermost cuticle of leaves, strongly associated to major physiological process and characteristics of the plant. The presence of these waxes on leaf surfaces provides photoprotective protection, support the regulations of water loos through the stomatal route, and dissipate excess of heat. The selection of genotypes with high EW can provide adaptation to high temperatures and water scarcity environments. The spectral bands in the visible region of the spectrum are highly associated to EW content, and variations on these specific bands provide a reliable estimation of EW. Considering the results of this study, four novel empirical based indices are proposed for phenotyping EW with a leaf clip spectroradiometer: $EWI\text{-}1_{Blue/Red}$, $EWI\text{-}2_{Blue/NIR,}$ $EWI\text{-}15_{625\ (1/736\ -\ 1/832)}$ and $EWI\text{-}16_{(625\text{-}736)\ /\ 832}$. Two linear models are also proposed, the *Model-10* and *Model-11*. Further this study, it is necessary to gain more insights into the prediction of the proposed indices/models under field conditions and with canopy reflectance.

Consistent results of the spectral response of the plant under field conditions suggest the possibility of using spectral indices/models as proxy measurements to understand the genetic and physiological basis of EW. The relative high heritability and the moderated to strong genetic correlation of the *DIB-2*, *DIB-3,* and *MB-DI-2* provides a reliable estimation of EW for selection under field conditions. The application of these indirect selection methods will facilitate the acquisition of multiple measurements

throughout the growing season and accurately capture the variation of EW. In this study, we state that spectral reflectance can be used in plant breeding platforms not only for indirect selection, but as a component in an integrative selection in the breeding pipeline.

In our third study, we demonstrated that the use of spectral reflectance as indirect selection criteria can be as efficient as selection of GY per se under sever heat stress conditions. Indirect selection based on GY component did not provide any superior improvement of the GY. The BIO is strongly associated with GY, and selection derived from this morphological trait is 97.2% as efficient as GY per se. The best results of selection were obtained with the broad band indices ARI, ReCl, NDII, SAVI, GRVI, and TDVI, with ~74% of efficiency. Closely related with BIO, the narrow band NDVI achieved 50% of the EGG obtained with direct selection.

REFERENCES

Allard, R.W. 1960. *Principles of plant breeding*. New York, USA: John Wiley and Sonc Inc. .

Alvarado, G., S. Perez-Elizalde, and J. Ceron. 2015. "SI-R Codes for computing selection indices in R http://hdl.handle.net/11529/10352." (International Maize and Wheat Improvement Center).

Andrade-Sanchez, P., M.A. Gore, J.T. Heun, K.R. Thorp, A.E. Carmo-Silva, A.N. French, M.E. Salvucci, and J.W. White. 2014. "Development and evaluation of a field-based high-throughput phenotyping platform." *Functional Plant Biology* 41:68-79.

Araus, J. L., and J. E. Cairns. 2014. "Field high-throughput phenotyping: the new crop breeding frontier." *Trends Plant Sci* 19 (1):52-61. doi: 10.1016/j.tplants.2013.09.008.

Asseng, S., F. Ewert, P. Martre, R. P. Rötter, D. B. Lobell, D. Cammarano, B. A. Kimball, M. J. Ottman, G. W. Wall, J. W. White, M. P. Reynolds, P. D. Alderman, P. V. V. Prasad, P. K. Aggarwal, J. Anothai, B. Basso, C. Biernath, A. J. Challinor, G. De Sanctis, J. Doltra, E. Fereres, M. Garcia-Vila, S. Gayler, G. Hoogenboom, L. A. Hunt, R. C. Izaurralde, M. Jabloun, C. D. Jones, K. C. Kersebaum, A. K. Koehler, C. Müller, S. Naresh Kumar, C. Nendel, G. O'Leary, J. E. Olesen, T. Palosuo, E. Priesack, E. Eyshi Rezaei, A. C. Ruane, M. A. Semenov, I. Shcherbak, C. Stöckle, P. Stratonovitch, T. Streck, I. Supit, F. Tao, P. J. Thorburn, K. Waha, E. Wang, D. Wallach, J. Wolf, Z. Zhao, and Y. Zhu. 2014. "Rising temperatures reduce global wheat production." *Nature Climate Change* 5 (2):143-147. doi: 10.1038/nclimate2470.

Asseng, Senthold, I. A. N. Foster, and Neil C. Turner. 2011. "The impact of temperature variability on wheat yields." *Global Change Biology* 17 (2):997-1012. doi: 10.1111/j.1365-2486.2010.02262.x.

Babar, M. A., M. van Ginkel, A. R. Klatt, B. Prasad, and M. P. Reynolds. 2006. "The Potential of Using Spectral Reflectance Indices to Estimate Yield in Wheat Grown Under Reduced Irrigation." *Euphytica* 150 (1-2):155-172. doi: 10.1007/s10681-006-9104-9.

Babar, M.A., M.P. Reynolds, M. van Ginkel, A.R. Klatt, W.R. Raun, and M.L. Stone. 2006. "Spectral reflectance indices as a potential indirect selection criteria for wheat yield under irrigation." *Crop Sciences* 46:578-588.

Bannari, A., H. Asalhi, and P. M. Teillet. 2002. "Transformed difference vegetation index (TDVI) for vegetation cover mapping." 5:3053-3055. doi: 10.1109/igarss.2002.1026867.

Barnes, J. D., L. Balaguer, E. Manrique, S. Elvira, and A. W. Davison. 1992. "A Reappraisal of the Use of Dmso for the Extraction and Determination of Chlorophylls-a and Chlorophylls-B in Lichens and Higher-Plants." *Environmental and Experimental Botany* 32 (2):85-100. doi: Doi 10.1016/0098-8472(92)90034-Y.

Bengtson, C., Larsson, S., Liljenberg, C. 1978. "Effects of water stress on cuticular transpiration rate and amount and composition of epicuticular wax in seedlings of six oat varieties." *Physiol. Plant.* 44:319-324.

Berg, van den A.K., and T. Perkins. 2005. "Nondestructive estimation of anthocyanin content in autumn sugar mapple leaves." *HortScience* 40(3):685-686.

Birth, G., and G.R. McVey. 1968. "Measuring the color of growing turf with a reflectance spectophometer " *Agronomy Journal* 60 (6):640-643.

Blackburn, G. A. 1998. "Spectral indices for estimating photosynthetic pigment concentrations: A test using senescent tree leaves." *International Journal of Remote Sensing* 19 (4):657-675. doi: 10.1080/014311698215919.

Blum, A. , B. Sinmena, J. Mayer, G. Golan, and L. Shpiler. 1994. "Stem reserve mobilisation support wheat-grain filling under heat stres." *Australian Journal of Plant Physiology* 21:771-81.

Blum, A., N. Klueva, and H. T. Nguyen. 2001. "Wheat cellular thermotolerance is related to yield under heat stress." *Euphytica* 117 (2):117-123. doi: Doi 10.1023/A:1004083305905.

Bromba, M.U.A., and H. Ziegler. 1981. "Application hints for Savitzky-Golay digital smoothing filters." *Analytical Chemistry* 53:1583-1586.

Buschhaus, C., and R. Jetter. 2011. "Composition differences between epicuticular and intracuticular wax substructures: how do plants seal their epidermal surfaces" *J Exp Bot* 62 (3):841-53. doi: 10.1093/jxb/erq366.

Chung, D., Chun, H., Keles, S. 2012. An introduction ot the 'spls' package, Version 1.0.

Cossani, C. M., and M. P. Reynolds. 2012. "Physiological traits for improving heat tolerance in wheat." *Plant Physiol* 160 (4):1710-8. doi: 10.1104/pp.112.207753.

Datt, B. 1999. "A new reflectance index for remote sensing of chlorophyll content in higher plants: Tests using Eucalyptus leaves." *Journal of Plant Physiology* 154 (1):30-36.

Daughtry, C.S.T. 2001. "Discriminating crop residual from soil by shortwave infrared reflectance." *Agronomy Journal* 93:128-131.

Easterling, W.; Apps, M. 2005. "Assesing the consequences of climate change for food and forest resocurces: a view fro the IPCC." *Climate Change* 70:165-189.

Ebercon, A., A. Blum, and W.R. Jordan. 1977. "A rapid colorimetric method for epicuticular wax contest of sorghum leaves." *Crop Science* 17(1):179-180.

FAO. 2013. "World Food and Agriculture. Statistical Year-book. ." *Food and Agriculture Organization of the United States, Rome.*

Foley, J. A., N. Ramankutty, K. A. Brauman, E. S. Cassidy, J. S. Gerber, M. Johnston, N. D. Mueller, C. O'Connell, D. K. Ray, P. C. West, C. Balzer, E. M. Bennett, S. R. Carpenter, J. Hill, C. Monfreda, S. Polasky, J. Rockstrom, J. Sheehan, S. Siebert, D. Tilman, and D. P. Zaks. 2011. "Solutions for a cultivated planet." *Nature* 478 (7369):337-42. doi: 10.1038/nature10452.

Fontana, G., A. Toreti, A. Ceglar, and G. De Sanctis. 2015. "Early heat waves over Italy and their impacts on durum wheat yields." *Natural Hazards and Earth System Sciences* 15 (7):1631-1637. doi: 10.5194/nhess-15-1631-2015.

Gamon, J. A., L. Serrano, and J. S. Surfus. 1997. "The photochemical reflectance index: an optical indicator of photosynthetic radiation use efficiency across species, functional types, and nutrient levels." *Oecologia* 112 (4):492-501. doi: DOI 10.1007/s004420050337.

Gamon, J. A., and J. S. Surfus. 1999. "Assessing leaf pigment content and activity with a reflectometer." *New Phytologist* 143 (1):105-117. doi: DOI 10.1046/j.1469-8137.1999.00424.x.

Gamon, J.A., C.B. Field, W. Bilger, O. Bjorkman, A.L. Fredeen, and J. Panuelas. 1990. "Remote sensing of the xanthophyll cycle and chlorophyll fluorescence in sunflower leaves and canopies." *Oecologia* 85 (1):1-7. doi: Doi 10.1007/Bf00317336.

Gayout, G., F. Baret, and D.J. Major. 1988. "High spectral resolution: determination of spectral shofts between the red and near infrared." *Int. Arch. Photogramm. Remote Sensing Spat. Inform. Sci.* 27:750-760.

Geladi, P., and B. R. Kowalski. 1986. "Partial Least-Squares Regression - a Tutorial." *Analytica Chimica Acta* 185:1-17. doi: Doi 10.1016/0003-2670(86)80028-9.

Gitelson, A. A., Y. J. Kaufman, and M. N. Merzlyak. 1996. "Use of a green channel in remote sensing of global vegetation from EOS-MODIS." *Remote Sensing of Environment* 58 (3):289-298. doi: Doi 10.1016/S0034-4257(96)00072-7.

Gitelson, A. A., G. P. Keydan, and M. N. Merzlyak. 2006. "Three-band model for noninvasive estimation of chlorophyll, carotenoids, and anthocyanin contents in higher plant leaves." *Geophysical Research Letters* 33 (11). doi: Artn L11402 10.1029/2006gl026457.

Gitelson, A. A., R. Stark, U. Grits, D. Rundquist, Y. Kaufman, and D. Derry. 2002. "Vegetation and soil lines in visible spectral space: A concept and technique for remote estimation of vegetation fraction." *International Journal of Remote Sensing* 23 (13):2537-2562. doi: 10.1080/01431160110107806.

Gitelson, A.A., Y. Zur, O.B. Chivkunova, and M.N. Merzlyak. 2002. "Assessing carotenoid content in plant leaves with reflectance spectroscopy." *Photochemistry and Photobiology* 75(3) (3):272-281.

Gitelson, Anatoly A., Mark N. Merzlyak, and Olga B. Chivkunova. 2001. "Optical Properties and Nondestructive Estimation of Anthocyanin Content in Plant Leaves¶." *Photochemistry and Photobiology* 74 (1):38. doi: 10.1562/0031-8655(2001)074<0038:opaneo>2.0.co;2.

Grant, R.H., Heisler, G.M., Gao, W., Jenks, M. 2003. "Ultraviolet leaf reflectance of common urban trees and the prediction of reflectance from leaf surface characteristics." *Agricultural and Forest Meteorology* 120:127-139.

Haboudane, D., J. R. Miller, E. Pattey, P. J. Zarco-Tejada, and I. B. Strachan. 2004. "Hyperspectral vegetation indices and novel algorithms for predicting green LAI of crop canopies: Modeling and validation in the context of precision agriculture." *Remote Sensing of Environment* 90 (3):337-352. doi: 10.1016/j.rse.2003.12.013.

Haboudane, D., J. R. Miller, N. Tremblay, P. J. Zarco-Tejada, and L. Dextraze. 2002. "Integrated narrow-band vegetation indices for prediction of crop chlorophyll content for application to precision agriculture." *Remote Sensing of Environment* 81 (2-3):416-426. doi: Pii S0034-4257(02)00018-4

Hernandez, Javier, Gustavo Lobos, Iván Matus, Alejandro del Pozo, Paola Silva, and Mauricio Galleguillos. 2015. "Using Ridge Regression Models to Estimate Grain Yield from Field Spectral Data in Bread Wheat (Triticum Aestivum L.) Grown under Three Water Regimes." *Remote Sensing* 7 (2):2109-2126. doi: 10.3390/rs70202109.

Holmes, M.G., and D.R. Keiller. 2002. "Effects of pubescence and waxes on the reflectance of leaves in the ultraviolet and photosynthetic wavebands a comparison of a range of species." *Plant, Cell and Environment* 25 (1):85-93. doi: DOI 10.1046/j.1365-3040.2002.00779.x.

Huete, A. R. 1988. "A soil-adjusted vegetation index (SAVI)." *Remote Sensing of Environment* 25 (3):295-309. doi: 10.1016/0034-4257(88)90106-x.

Huete, A. R., H. Q. Liu, K. Batchily, and W. vanLeeuwen. 1997. "A comparison of vegetation indices global set of TM images for EOS-MODIS." *Remote Sensing of Environment* 59 (3):440-451. doi: Doi 10.1016/S0034-4257(96)00112-5.

Hunt, E.R., and B.N. Rock. 1989. "Detection of changes in leaf water content using near- and middle-infrared reflectance." *Remote Sensing of Environment* 30:43-45.

Inc., SAS Institute. 2011. "Base SAS® 9.3 Procedures Guide. Cary, NC: SAS Institute Inc. "

Johnson, D.A., R.A. Richards, and N.C Turner. 1983. "Yield, water relations, gas exchange, and surface reflectances of near-isogenic wheat lines differing in glaucousness." *Crop Science* 23 (2):318-325.

Johnson, H. W., H. F. Robinson, and R. W. Comstock. 1955. "Estimates of genetic and environmental variability in Soybean." *Agronomy Journal* 43:314-318.

Kim, D. M., H. Zhang, H. Zhou, T. Du, Q. Wu, T. C. Mockler, and M. Y. Berezin. 2015. "Highly sensitive image-derived indices of water-stressed plants using hyperspectral imaging in SWIR and histogram analysis." *Sci Rep* 5:15919. doi: 10.1038/srep15919.

Knippling, E.B. 1970. "Physical and physiological basis for the reflectance of visible and near-infreared radiation from vegetation." *Remote Sensing of Environment* 1:155-159.

Lan, Y., H. Zhang, R. Lacey, W. Hoffman, and W. Wu. 2009. "Development of an integration sensor andinstrumentation system for measuring crop conditions " *Agricultural Engineering International: CIGR Journal* 11:1-16.

Maccioni, A., G. Agati, and P. Mazzinghi. 2001. "New vegetation indices for remote sensing measurements of chlorophylls based on leaf directional reflectance spectra." *Journal of Photochemistry and Photobiology B: Biology* 61:52-61.

Merzlyak, M. N., A. A. Gitelson, O. B. Chivkunova, and V. Y. Rakitin. 1999. "Non-destructive optical detection of pigment changes during leaf senescence and fruit ripening." *Physiologia Plantarum* 106 (1):135-141. doi: DOI 10.1034/j.1399-3054.1999.106119.x.

Mittler, R. 2002. "Oxidative stress, antioxidants and stress tolerance." *Trends Plant Sci* 7 (9):405-10.

Mondal, S., R.E. Mason, T. Huggins, and D.B. Hays. 2014. "QTL on wheat (Triticum aestivum L.) chromosomes 1B, 3D and 5A are associated with constitutive production of leaf cuticular wax and may contribute to lower leaf temperatures under heat stress." *Euphytica* 201 (1):123-130. doi: 10.1007/s10681-014-1193-2.

Nash, D., M. Miyaio, and N Murata. 1985. " Heat inactiation of oxygen evolution in Photosystem II particles and its acceleration by chloride depletion and exogeous manganese." *Biochemica et Biophysica*:127-133.

Ogren, W. L. 1984. "Photorespiration - Pathways, Regulation, and Modification." *Annual Review of Plant Physiology and Plant Molecular Biology* 35:415-442. doi: DOI 10.1146/annurev.pp.35.060184.002215.

Olascoaga, B., E. Juurola, P. Paulo, P. Lukes, L. Halonen, E. Nikinmaa, J. Back, and A. Porcar-Castell. 2014. "Seasonal variation in the relflectance of photosynthetically active radiation from epicuticulae waxes of Scot pine (Pinus sykvestris) needles." *Boreal Environment Researh* 19:132-141.

Panuelas, J., F. Baret, and I. Fillela. 1995. "Semi-empirical indices to assess carotenoidschlorophyll a ratio from leaf spectral reflectance." *Photosynthetica* 31:221-230.

Panuelas, J., I. Fillella, P. Lloret, F. Munoz, and M. Vilajeliu. 1995. "Reflectance assessment of mite effect on apple trees." *International Journal Remote Sensing* 16 (14):2727-2733.

Penuelas, J., I. Filella, C. Biel, L. Serrano, and R. Save. 1993. "The Reflectance at the 950-970 Nm Region as an Indicator of Plant Water Status." *International Journal of Remote Sensing* 14 (10):1887-1905.

Penuelas, J., J. A. Gamon, A. L. Fredeen, J. Merino, and C. B. Field. 1994. "Reflectance Indexes Associated with Physiological-Changes in Nitrogen-Limited and Water-Limited Sunflower Leaves." *Remote Sensing of Environment* 48 (2):135-146. doi: Doi 10.1016/0034-4257(94)90136-8.

Pietragalla, J., and A. Pasl. 2012. "Grain yield and yield components " In *Physiological Breeding II: A Field Guide to Wheat Phenotyping* edited by A.D.J. Pask, J. Pietragalla, D.M. Mullan and M.P. Reynolds. Mexico, D.F.:CIMMYT.

Porter, J. R., and M. Gawith. 1999. "Temperatures and the growth and development of wheat: a review." *European Journal of Agronomy* 10 (1):23-36. doi: Doi 10.1016/S1161-0301(98)00047-1.

Ray, D. K., N. D. Mueller, P. C. West, and J. A. Foley. 2013. "Yield Trends Are Insufficient to Double Global Crop Production by 2050." *PLoS One* 8 (6):e66428. doi: 10.1371/journal.pone.0066428.

Reynolds, M., D. Bonnett, S. C. Chapman, R. T. Furbank, Y. Manes, D. E. Mather, and M. A. Parry. 2011. "Raising yield potential of wheat. I. Overview of a consortium approach and breeding strategies." *J Exp Bot* 62 (2):439-52. doi: 10.1093/jxb/erq311.

Reynolds, M., F. Dreccer, and R. Trethowan. 2007. "Drought-adaptive traits derived from wheat wild relatives and landraces." *J Exp Bot* 58 (2):177-86. doi: 10.1093/jxb/erl250.

Reynolds, M., and P. Langridge. 2016. "Physiological breeding." *Curr Opin Plant Biol* 31:162-71. doi: 10.1016/j.pbi.2016.04.005.

Reynolds, M. P., M. Balota, M. I. B. Delgado, I. Amani, and R. A. Fischer. 1994. "Physiological and Morphological Traits Associated with Spring Wheat Yield under hot, Irrigated Conditions." *Australian Journal of Plant Physiology* 21 (6):717-730.

Reynolds, M.P., Mujeeb-Kazi, A., Sawkins, M. 2005. "Prospects for utilizing plant-adaptive mechanisms to improve wheat and other crops in drougth and salinity prone environments " *Annals of Applied Biology* 146:239-259.

Reynolds, Matthew P., Carolina Saint Pierre, Abu S. I. Saad, Mateo Vargas, and Anthony G. Condon. 2007. "Evaluating Potential Genetic Gains in Wheat Associated with Stress-Adaptive Trait Expression in Elite Genetic Resources under Drought and Heat Stress." *Crop Science* 47 (Supplement_3):S-172. doi: 10.2135/cropsci2007.10.0022IPBS.

Reynolds, Matthew, Maria Tattaris, C. Mariano Cossani, Marc Ellis, Kazuko Yamaguchi-Shinozaki, and Carolina Saint Pierre. 2015. "Exploring Genetic Resources to Increase Adaptation of Wheat to Climate Change."355-368". doi: 10.1007/978-4-431-55675-6_41.

Richards, R. A., H. M. Rawson, and D. A. Johnson. 1986. "Glacousness in wheat: Development and effect on water-use efficiency, gas exchange and photosynthetic tissue temperatures." *Plant Physiol* 13:465-473.

Robinson, S.A., Lovelock, C.E., Osmond, C.B. 1993. "Wax as a mechanism for protection against photoinhibition- A study of Cotylecon orbiculata." *Botanica Acta*:307-312.

Rosegrant, M.W., and M. Agcaoili. 2010. "Global food demand, supply, and price prospect to 2010." *Washington, DC: International Food Policy Reseatch Institute*

Rouse, J.W., R.H. Hass, J.A. Scheel, D.W. Deering, and J.C. Harlan. 1974. "Monitoring the vernal advancement and retrogradation (green wave effect) of nature vegetation." *NASA/GSFC Final Report; NASA: Greenbelt, MD, USA*

Salvucci, M. E., and S. J. Crafts-Brandner. 2004. "Relationship between the heat tolerance of photosynthesis and the thermal stability of rubisco activase in plants from contrasting thermal environments." *Plant Physiol* 134 (4):1460-70. doi: 10.1104/pp.103.038323.

Semenov, M. A., and N. G. Halford. 2009. "Identifying target traits and molecular mechanisms for wheat breeding under a changing climate." *J Exp Bot* 60 (10):2791-804. doi: 10.1093/jxb/erp164.

Serrano, L., J. Penuelas, and S. L. Ustin. 2002. "Remote sensing of nitrogen and lignin in Mediterranean vegetation from AVIRIS data: Decomposing biochemical from structural signals." *Remote Sensing of Environment* 81 (2-3):355-364. doi: Pii S0034-4257(02)00011-1. doi 10.1016/S0034-4257(02)00011-1.

Shanahan, J. F., I. B. Edwards, J. S. Quick, and J. R. Fenwick. 1990. "Membrane Thermostability and Heat Tolerance of Spring Wheat." *Crop Science* 30 (2):247-251.

Shepherd, T., and G. D. Wynne. 2006. "The effects of stress on plant cuticular waxes." *New Phytol* 171 (3):469-99. doi: 10.1111/j.1469-8137.2006.01826.x.

Smith, H.F. 1936. "A discriminant function for plant selection." *Papers on Quantitative Genetics and Related Topics* (Department of Genetics, North Carolina State College, Raleigh, NC). (7):240-250. doi: 10.1111/j.1469-1809.1936.tb02143.x.

Sripada, R. P., R. W. Heiniger, J. G. White, and A. D. Meijer. 2006. "Aerial color infrared photography for determining early in-season nitrogen requirements in corn." *Agronomy Journal* 98 (4):968-977. doi: 10.2134/agronj2005.0200.

Stevens, A., Ramirez-Lopez, L. 2014. "An introduction to the prospectr package."

Team, R Development Core. 2008. "R: A language and environment for statistical computing. R Foundation for Statistical Computing, Vienna, Austria. ISBN 3-900051-07-0, URL http://www.R-project.org.".

Tewari, A. K., and B. C. Tripathy. 1998. "Temperature-stress-induced impairment of chlorophyll biosynthetic reactions in cucumber and wheat." *Plant Physiology* 117 (3):851-858.

Tilman, D., C. Balzer, J. Hill, and B. L. Befort. 2011. "Global food demand and the sustainable intensification of agriculture." *Proc Natl Acad Sci U S A* 108 (50):20260-4. doi: 10.1073/pnas.1116437108.

Tucker, C. J. 1979. "Red and Photographic Infrared Linear Combinations for Monitoring Vegetation." *Remote Sensing of Environment* 8 (2):127-150. doi: 10.1016/0034-4257(79)90013-0.

Van den Berg, A.K., and T.D. Perkins. 2005. "Non-destructive estimation of anthocyanin content in autumn sugar maple leaves." *Horticultural Science* 40(3):685-686.

Vogelmann, J. E., B. N. Rock, and D. M. Moss. 1993. "Red Edge Spectral Measurements from Sugar Maple Leaves." *International Journal of Remote Sensing* 14 (8):1563-1575.

Walton, T. J. 1990. "Waxes, cutin and suberin." *Methods in plant biochemistry* 4:106-158.

Wardlaw, I. F. 1994. "The Effect of High-Temperature on Kernel Development in Wheat - Variability Related to Pre-Heading and Postanthesis Conditions." *Australian Journal of Plant Physiology* 21 (6):731-739.

Weber, V. S., J. L. Araus, J. E. Cairns, C. Sanchez, A. E. Melchinger, and E. Orsini. 2012. "Prediction of grain yield using reflectance spectra of canopy and leaves in maize plants grown under different water regimes." *Field Crops Research* 128:82-90. doi: 10.1016/j.fcr.2011.12.016.

Wheeler, T., and J. von Braun. 2013. "Climate change impacts on global food security." *Science* 341 (6145):508-13. doi: 10.1126/science.1239402.

White, D.C., M. Williams, and S.L. Barr. 2008. "Detectig sub-surface soil disturbance using hyperspectral first derivative band ratios of asociated vegetation stress." *The International Archives of the Photogrammetry, Remote Sensing and Spatial Information Sciences* (XXXVII):243-248.

Wollenweber, B., J. R. Porter, and J. Schellberg. 2003. "Lack of interaction between extreme high-temperature events at vegetative and reproductive growth stages in wheat." *Journal of Agronomy and Crop Science* 189 (3):142-150. doi: DOI 10.1046/j.1439-037X.2003.00025.x.

Yu, K., V. Lenz-Wiedemann, G. Leufen, M. Hunsche, G. Noga, X. Chen, and G. Bareth. 2012. "Assessing hyperspectral vegetation indices for estimating leaf chlorophyll concentration of summer barley." *Annals of the Photogrammetry, Remote Sensing and Spatial Information Science* I-7.

Zarco-Tejada, P. J., A. Berjon, R. Lopez-Lozano, J. R. Miller, P. Martin, V. Cachorro, M. R. Gonzalez, and A. de Frutos. 2005. "Assessing vineyard condition with hyperspectral indices: Leaf and canopy reflectance simulation in a row-structured discontinuous canopy." *Remote Sensing of Environment* 99 (3):271-287. doi: 10.1016/j.rse.2005.09.002.

Zarco-Tejada, P. J., J. C. Pushnik, S. Dobrowski, and S. L. Ustin. 2003. "Steady-state chlorophyll a fluorescence detection from canopy derivative reflectance and double-peak red-edge effects." *Remote Sensing of Environment* 84 (2):283-294. doi: Pii S0034-4257(02)00113-X

Zarco-Tejada, P. J., C. A. Rueda, and S. L. Ustin. 2003. "Water content estimation in vegetation with MODIS reflectance data and model inversion methods." *Remote Sensing of Environment* 85 (1):109-124. doi: 10.1016/s0034-4257(02)00197-9.